

2014

## DESIGN AND SYNTHESIS OF MULTIFUNCTIONAL POLYMERIC MICELLES FOR GENE-DIRECTED ENZYME PRODRUG THERAPY

Alicia J. Sawdon  
*Michigan Technological University*

Follow this and additional works at: <https://digitalcommons.mtu.edu/etds>

 Part of the [Chemical Engineering Commons](#)


Copyright 2014 Alicia J. Sawdon

---

### Recommended Citation

Sawdon, Alicia J., "DESIGN AND SYNTHESIS OF MULTIFUNCTIONAL POLYMERIC MICELLES FOR GENE-DIRECTED ENZYME PRODRUG THERAPY", Dissertation, Michigan Technological University, 2014.  
<https://digitalcommons.mtu.edu/etds/862>

Follow this and additional works at: <https://digitalcommons.mtu.edu/etds>

 Part of the [Chemical Engineering Commons](#)

DESIGN AND SYNTHESIS OF MULTIFUNCTIONAL POLYMERIC MICELLES  
FOR GENE-DIRECTED ENZYME PRODRUG THERAPY

By

Alicia J. Sawdon

A DISSERTATION

Submitted in partial fulfillment of the requirements for the degree of

DOCTOR OF PHILOSOPHY

In Chemical Engineering

MICHIGAN TECHNOLOGICAL UNIVERSITY

2014

© 2014 A.J. Sawdon

This dissertation has been approved in partial fulfillment of the requirements for the Degree of DOCTOR OF PHILOSOPHY in Chemical Engineering.

Department of Chemical Engineering

Dissertation Advisor: *Dr. Ching-An Peng*

Committee Member: *Dr. Lanrong Bi*

Committee Member: *Dr. Gerard T. Caneba*

Committee Member: *Dr. Michael E. Mullins*

Department Chair: *Dr. S. Komar Kawatra*

*To my family*

*"I knew who I was this morning,  
But I've changed a few times since then."*

## TABLE OF CONTENTS

<b>LIST OF FIGURES</b> .....	<b>IX</b>
<b>LIST OF TABLES</b> .....	<b>XI</b>
<b>PREFACE</b> .....	<b>XII</b>
<b>ACKNOWLEDGEMENTS</b> .....	<b>XIII</b>
<b>ABSTRACT</b> .....	<b>XIV</b>
<b>CHAPTER 1: INTRODUCTION</b> .....	<b>1</b>
1.1. GENE-DIRECTED ENZYME PRODRUG THERAPY (GDEPT).....	1
1.1.1. <i>Prodrugs for thymidine kinase (TK)</i> .....	2
1.1.2. <i>Prodrugs for thymidine phosphorylase (TP)</i> .....	3
1.2. CURRENT POSITION OF GENE THERAPY .....	4
1.3. NONVIRAL DELIVERY METHODS .....	5
1.4. COMPOSITION, FORMATION AND CHARACTERIZATION OF POLYMERIC MICELLES .....	6
1.4.1. <i>Micelle formation</i> .....	7
1.4.2. <i>Preparation of micelles</i> .....	10
1.4.3. <i>Factors affecting drug loading and drug release from micelles</i> .....	11
1.5. TARGETING SCHEMES .....	12
1.5.1. <i>Passive Targeting</i> .....	14
1.5.2. <i>Active targeting</i> .....	17
1.5.3. <i>Receptor-mediated targeting</i> .....	19
1.6. ENGINEERING ANTIPHAGOCYtic BIOMIMETIC DRUG CARRIERS .	22
1.6.1. <i>Erythrocyte-inspired therapeutic delivery</i> .....	22
1.6.2. <i>Carrier cells for therapeutic delivery</i> .....	24
1.6.3. <i>Pathogen-inspired therapeutic delivery</i> .....	25
1.6.4. <i>CD47</i> .....	26
1.7. RATIONALE AND HYPOTHESES.....	28
1.8. SPECIFIC AIMS.....	29
1.1.1. <i>Specific aim 1: Optimization of polymeric prodrug nanocarriers</i> .....	29

1.1.2.	<i>Specific aim 2: Efficacy of polymeric prodrug nanocarriers on cancer cell treatment</i>	30
1.1.3.	<i>Specific aim 3: Antiphagocytic and targeted micelle carriers</i>	30
1.9.	REFERENCES	32
<b>CHAPTER 2: POLYMERIC MICELLES FOR ACYCLOVIR DRUG DELIVERY</b>		<b>46</b>
2.1.	ABSTRACT	46
2.2.	INTRODUCTION	46
2.3.	MATERIALS AND METHODS	48
2.3.1.	<i>Materials</i>	48
2.3.2.	<i>Characterization methods</i>	49
2.3.3.	<i>Synthesis of ACV-tagged amphiphilic polymers</i>	49
2.3.4.	<i>Preparation of polymeric prodrug micelles</i>	51
2.3.5.	<i>Determination of critical micelle concentration</i>	51
2.3.6.	<i>Size and morphology of polymeric prodrug micelles</i>	51
2.3.7.	<i>Drug release kinetics</i>	52
2.3.8.	<i>Cytotoxicity test</i>	52
2.4.	RESULTS AND DISCUSSION	53
2.4.1.	<i>Synthesis and characterization of amphiphilic prodrug polymers</i>	53
2.4.2.	<i>Formation and characterization of ACV-tagged polymeric micelles</i>	59
2.4.3.	<i>In vitro release of ACV from polymeric micelles</i>	62
2.4.4.	<i>Cytotoxicity study</i>	64
2.5.	CONCLUSION	65
2.6.	REFERENCES	66
<b>CHAPTER 3: GANCICLOVIR INTEGRATED POLYMERIC NANOCARRIERS FOR SUICIDE GENE THERAPY</b>		<b>69</b>
3.1.	ABSTRACT	69
3.2.	INTRODUCTION	69
3.3.	MATERIALS AND METHODS	72

3.3.1.	<i>Materials</i> .....	72
3.3.2.	<i>Characterization methods</i> .....	72
3.3.3.	<i>Synthesis of GCV-tagged amphiphilic polymers</i> .....	73
3.3.4.	<i>Preparation of polymeric prodrug micelles</i> .....	74
3.3.5.	<i>Determination of critical micelle concentration</i> .....	74
3.3.6.	<i>Size and morphology of polymeric prodrug micelles</i> .....	74
3.3.7.	<i>Drug release kinetics</i> .....	75
3.3.8.	<i>Establishing TK-overexpressed HT29 cells</i> .....	75
3.3.9.	<i>Development of GCV-PCL-chitosan/TK nanovectors</i> .....	75
3.3.10.	<i>Cytotoxicity studies</i> .....	76
3.4.	RESULTS AND DISCUSSION.....	76
3.4.1.	<i>Synthesis and characterization of amphiphilic prodrug polymers</i> .....	76
3.4.2.	<i>Formation and characterization of GCV-tagged polymeric micelles</i> ....	80
3.4.3.	<i>In vitro release of GCV from polymeric micelles</i> .....	82
3.4.4.	<i>Cytotoxicity studies</i> .....	84
3.5.	CONCLUSION .....	89
3.6.	REFERENCES .....	90
<b>CHAPTER 4: ENHANCED ANTICANCER ACTIVITY OF 5'DFUR-PCL-MPEG POLYMERIC PRODRUG MICELLES ENCAPSULATING CHEMOTHERAPEUTIC DRUGS.....</b>		<b>93</b>
4.1.	ABSTRACT .....	93
4.2.	INTRODUCTION .....	93
4.3.	MATERIALS AND METHODS .....	95
4.3.1.	<i>Materials</i> .....	95
4.3.2.	<i>Characterization methods</i> .....	96
4.3.3.	<i>Synthesis of 5'DFUR-tagged amphiphilic polymers</i> .....	96
4.3.4.	<i>Preparation of polymeric prodrug micelles</i> .....	97
4.3.5.	<i>Determination of critical micelle concentration</i> .....	98
4.3.6.	<i>Size and morphology of polymeric prodrug micelles</i> .....	98
4.3.7.	<i>Drug loading content and entrapment efficiency</i> .....	98

4.3.8.	<i>Drug release kinetics</i> .....	99
4.3.9.	<i>Cytotoxicity studies</i> .....	99
4.4.	RESULTS AND DISCUSSION.....	100
4.4.1.	<i>Synthesis and characterization of amphiphilic prodrug polymers</i> .....	100
4.4.2.	<i>Formation and characterization of 5'DFUR-tagged polymeric micelles</i> .....	104
4.4.3.	<i>Evaluation of drug loading content and entrapment efficiency</i> .....	106
4.4.4.	<i>In vitro drug release</i> .....	106
4.4.5.	<i>Cytotoxicity of 5'DFUR-tagged polymeric micelles loaded with chemotherapeutic agents</i> .....	109
4.5.	CONCLUSION .....	114
4.6.	REFERENCES .....	115
<b>CHAPTER 5: DEVELOPMENT OF ANTIPHAGOCYtic CD47-TAGGED POLYMERIC MICELLES TO TARGET <math>\alpha_v\beta_3</math> INTEGRIN- BEARING TUMOR CELLS.....</b>		
5.1.	ABSTRACT .....	118
5.2.	INTRODUCTION .....	118
5.3.	MATERIALS AND METHODS .....	119
5.3.1.	<i>Materials</i> .....	119
5.3.2.	<i>Synthesis of MPEG-PCL-PEI</i> .....	120
5.3.3.	<i>Preparation of polymeric micelles</i> .....	121
5.3.4.	<i>Size and zeta potential measurements</i> .....	121
5.3.5.	<i>Biotinylation of polymeric micelles</i> .....	121
5.3.6.	<i>Amplification and expression of CD47-SA fusion protein</i> .....	122
5.3.7.	<i>Quantification of CD47-SA binding</i> .....	123
5.3.8.	<i>Macrophage studies</i> .....	123
5.3.9.	<i>Integrin targeting</i> .....	124
5.4.	RESULTS AND DISCUSSION.....	124
5.4.1.	<i>Characterization of polymeric micelles</i> .....	124
5.4.2.	<i>Antiphagocytic effect</i> .....	127



5.4.3. <i>Integrin targeting</i> .....	129
5.5. CONCLUSIONS.....	130
5.6. REFERENCES .....	131
<b>CHAPTER 6: SUMMARY AND FUTURE DIRECTIONS .....</b>	<b>132</b>
6.1. THESIS CONCLUSIONS AND SUMMARY OF FINDINGS.....	132
6.2. FUTURE DIRECTIONS .....	133
6.3. REFERENCES .....	135
<b>APPENDIX I: COPYRIGHT MATERIAL FOR CHAPTER 1 .....</b>	<b>136</b>
<b>APPENDIX II: COPYRIGHT MATERIAL FOR CHAPTER 2 .....</b>	<b>141</b>

## LIST OF FIGURES

<b>Figure 1.1.</b> Graphical representation of gene therapy clinical trials .....	1
<b>Figure 1.2.</b> Gene Directed Enzyme Prodrug Therapy.....	2
<b>Figure 1.3.</b> Block-copolymer micelle .....	7
<b>Figure 1.4.</b> Techniques used for the preparation of polymeric micelles .....	10
<b>Figure 1.5.</b> Mechanisms for drug delivery from micelle carriers.....	16
<b>Figure 1.6.</b> Polymeric micelles for targeted drug delivery .....	18
<b>Figure 1.7.</b> The interaction of phagocyte receptors and an opsonized particle tagged with CD47 ligand.....	27
<b>Figure 2.1.</b> Synthetic scheme of ACV-PCL-MPEG and ACV-PCL-chitosan ...	53
<b>Figure 2.2.</b> <sup>1</sup> H NMR spectra of (i) ACV and (ii) ACV-PCL.....	54
<b>Figure 2.3.</b> <sup>1</sup> H NMR spectra of (iii) MPEG and (iv) ACV-PCL-MPEG .....	57
<b>Figure 2.4.</b> FTIR spectra of ACV-PCL-MPEG.....	58
<b>Figure 2.5.</b> <sup>1</sup> H NMR spectra of (v) chitosan and (vi) ACV-PCL-chitosan .....	58
<b>Figure 2.6.</b> FTIR spectra of ACV-PCL-chitosan.....	59
<b>Figure 2.7.</b> CMC and particle size distribution .....	61
<b>Figure 2.8.</b> In vitro drug release profile of ACV-PCL-MPEG .....	62
<b>Figure 2.9.</b> In vitro drug release profile of ACV-PCL-chitosan .....	63
<b>Figure 2.10.</b> Viability of HT29 colorectal cancer cells .....	64
<b>Figure 3.1.</b> Synthetic scheme of GCV-PCL-chitosan.....	77
<b>Figure 3.2.</b> <sup>1</sup> H NMR spectra of (i) GCV and (ii) GCV-PCL.....	78
<b>Figure 3.3.</b> <sup>1</sup> H NMR spectra of (iii) chitosan and (iv) GCV-PCL-chitosan .....	79
<b>Figure 3.4.</b> FTIR spectra of GCV-PCL-chitosan .....	80
<b>Figure 3.5.</b> CMC and particle size distribution .....	81
<b>Figure 3.6.</b> In vitro drug release of GCV from GCV-PCL-chitosan in PBS at 37°C with esterase .....	83
<b>Figure 3.7.</b> In vitro drug release of GCV from GCV-PCL-chitosan in PBS.....	84
<b>Figure 3.8.</b> Cell growth kinetics profile.....	85
<b>Figure 3.9.</b> Cell viability after treatment with GCV-PCL-chitosan micelles.....	86
<b>Figure 3.10.</b> Expression of HSV-TK gene plasmid .....	87

<b>Figure 3.11.</b> One-step delivery of HSV-TK and GCV to HT29 cells.....	88
<b>Figure 4.1.</b> Synthetic scheme of 5'DFUR-PCL-MPEG.....	101
<b>Figure 4.2.</b> <sup>1</sup> H NMR spectra of (i) 5'DFUR and (ii) 5'DFUR-PCL.....	102
<b>Figure 4.3.</b> <sup>1</sup> H NMR spectra of (iii) MPEG and (iv) 5'DFUR-PCL-MPEG.....	103
<b>Figure 4.4.</b> FTIR spectra of 5'DFUR-PCL-MPEG.....	103
<b>Figure 4.5.</b> CMC and particle size distribution.....	105
<b>Figure 4.6.</b> In vitro drug release of 5'DFUR for 5'DFUR-PCL-MPEG.....	107
<b>Figure 4.7.</b> In vitro drug release profiles of DOX and SN-38.....	108
<b>Figure 4.8.</b> Cell viability after treatment with 5'DFUR-PCL-MPEG.....	110
<b>Figure 4.9.</b> Cell viability after treatment with micelles encapsulating DOX.....	112
<b>Figure 4.10.</b> Cell viability after treatment with micelles encapsulating SN-38.....	113
<b>Figure 5.1.</b> Synthetic scheme of MPEG-PCL-PEI.....	125
<b>Figure 5.2.</b> Size and zeta analysis of MPEG-PCL-MPEG.....	125
<b>Figure 5.3.</b> Synthetic scheme of biotinylation and fluorescent of micelles.....	126
<b>Figure 5.4.</b> HABA/avidin assay.....	127
<b>Figure 5.5.</b> Effect of CD47 on micelle uptake by J774A.1 cells.....	128
<b>Figure 5.6.</b> Flow cytometry analysis.....	128
<b>Figure 5.7.</b> Integrin targeting to BHK cells.....	129
<b>Figure 5.8.</b> Integrin targeting to PC3 cells.....	130
<b>Figure 6.1.</b> In vitro drug release profile of 5-FC from 5-FC-PCL-MPEG.....	134

## LIST OF TABLES

<b>Table 1.1.</b> Polymers used in the synthesis of block-copolymer micelles .....	8
<b>Table 2.1.</b> Number-averaged molecular weight and degree of polymerization of ACV-PCL .....	55
<b>Table 2.2.</b> Characterization of ACV-PCL polymers .....	56
<b>Table 3.1.</b> Characterization of GCV-PCL-chitosan.....	78
<b>Table 3.2</b> Size and charge of GCV-PCL-chitosan/TK .....	82
<b>Table 4.1.</b> Characterization of 5'DFUR-PCL-MPEG .....	104
<b>Table 4.2.</b> Characteristics and drug loading of 5'DFUR-tagged micelles .....	105

## PREFACE

Parts of chapter 1, “Introduction,” were previously published in *Nanomedicine for Drug Delivery and Therapeutics* Ch. 15, (2013) 438-469 and *Therapeutic Delivery* 4, (2013) 825-839. Alicia Sawdon was the first author and Dr. Ching-An Peng was the corresponding author of these articles. The first author was responsible for the literature review and writing of the articles. The first and corresponding authors were responsible for proofreading and editing the articles before publication. Figure 1.1 does not require copyright because the data was obtained from <http://www.abedia.com/wiley/index.html> and graphed by myself.

Chapter 2, “Polymeric micelles for acyclovir drug delivery,” was previously published in *Macromolecular Research* 20, (2012) 1-4 and *Colloids and Surfaces B: Biointerfaces* 122, (2014) 738-45. Alicia Sawdon was the first author and Dr. Ching-An Peng was the corresponding author of these articles. Alicia Sawdon conducted the experiment work, analyzed the data and wrote the paper. The first and corresponding authors were responsible for proofreading and editing the articles before publication.

Chapter 3, “Ganciclovir integrated polymeric nanocarriers for gene-directed enzyme prodrug therapy,” is planned for publication in *Molecules* and *Macromolecular Bioscience*. Alicia Sawdon will be the first author and Dr. Ching-An Peng will be the corresponding author of these articles. The first author is responsible for conducting the experimental work, analyzing the data and writing the paper. Both the first and corresponding authors will be responsible for proofreading and editing the articles before publication.

Chapter 4, “Enhanced anticancer activity of 5’DFUR-PCL-MPEG polymeric prodrug micelles encapsulating chemotherapeutic drugs,” is planned for publication in *Journal of Controlled Release*. Alicia Sawdon will be the first author and is responsible for collecting experimental work, analyzing the data and writing the paper. Jiasheng Wang and Jen-I Hsu were responsible for collecting preliminary data and contributed to the writing of the paper. Dr. Ching-An Peng will be the corresponding author, he and the first author will be responsible for proofreading and editing the article for publication.

Chapter 5, “Development of antiphagocytic CD47-tagged polymeric micelles to target  $\alpha_v\beta_3$  integrin-bearing tumor cells,” is planned for publication in *ACS Biomaterials*. Alicia Sawdon will be the first author and Dr. Ching-An Peng will be the corresponding author of this article. The first author is responsible for collecting experimental work, analyzing the data and writing the paper. The corresponding author and first author, will be responsible for proofreading and editing the article before publication.

## ACKNOWLEDGEMENTS

I would like to acknowledge my advisor, Dr. Ching-An Peng, for his guidance and support throughout my time as a Ph.D. student. He has not only presented me with a multitude of opportunities but guided me into becoming a professional. I would also like to thank my committee members, Dr. Lanrong Bi, Dr. Gerard T. Caneba, and Dr. Michael E. Mullins for their time and feedback.

I would like to thank my colleagues in the lab, Nastaran Alinezhadbalala, Nasrin Salehi, and Jun Zhang for their constant engagement and advice. But mostly, for listening to my advice and helping to manage the lab.

I would like to thank my family, without your encouragement and support none of this would have been possible. Most importantly, to my mother, Mary Sawdon, for giving me the motivation and confidence to push forward and for always being there to answer my calls when I felt the world was ending...it was not.

Lastly, I would like to thank Ethan Weydemeyer, without your help and moral support I might have given up before realizing this dream. Time for our next adventure!

## ABSTRACT

Gene-directed enzyme prodrug therapy is a form of cancer therapy in which delivery of a gene that encodes an enzyme is able to convert a prodrug, a pharmacologically inactive molecule, into a potent cytotoxin. Currently delivery of gene and prodrug is a two-step process. Here, we propose a one-step method using polymer nanocarriers to deliver prodrug, gene and cytotoxic drug simultaneously to malignant cells. Prodrugs acyclovir, ganciclovir and 5-doxifluridine were used to directly to initiate ring-opening polymerization of  $\epsilon$ -caprolactone, forming a hydrophobic prodrug-tagged poly( $\epsilon$ -caprolactone) which was further grafted with hydrophilic polymers (methoxy poly(ethylene glycol), chitosan or polyethylenimine) to form amphiphilic copolymers for micelle formation. Successful synthesis of copolymers and micelle formation was confirmed by standard analytical means. Conversion of prodrugs to their cytotoxic forms was analyzed by both two-step and one-step means i.e. by first delivering gene plasmid into cell line HT29 and then challenging the cells with the prodrug-tagged micelle carriers and secondly by complexing gene plasmid onto micelle nanocarriers and delivery gene and prodrug simultaneously to parental HT29 cells. Anticancer effectiveness of prodrug-tagged micelles was further enhanced by encapsulating chemotherapy drugs doxorubicin or SN-38. Viability of colon cancer cell line HT29 was significantly reduced. Furthermore, in an effort to develop a stealth and targeted carrier, CD47-streptavidin fusion protein was attached onto the micelle surface utilizing biotin-streptavidin affinity. CD47, a marker of self on the red blood cell surface, was used for its antiphagocytic efficacy micelles bound with CD47 showed antiphagocytic efficacy when exposed to J774A.1 macrophages. Since CD47 is not only an antiphagocytic ligand but also an integrin associated protein, it was used to target integrin  $\alpha_v\beta_3$ , which is overexpressed on tumor-activated neovascular endothelial cells. Results showed that CD47-tagged micelles had enhanced uptake when treated to PC3 cells which have high expression of  $\alpha_v\beta_3$ . The synthesized multifunctional polymeric

micelle carriers developed could offer a new platform for an innovative cancer therapy regime.



## CHAPTER 1: INTRODUCTION<sup>1</sup>

### 1.1. GENE-DIRECTED ENZYME PRODRUG THERAPY (GDEPT)

Gene therapy, is the insertion of genetic material into an individual's cell to treat a disease. The development of gene therapy began during the 1960's to early 1970's. During this time, two discoveries were made which helped establish gene therapy as a therapeutic approach—an efficient method of gene transfer and cloned forms of specific genes. The first clinical gene therapy protocol was approved in 1989 and since then, more than 1800 clinical trials have been approved world-wide, more than 60% for treatment of cancer (Figure 1.1) [1, 2].

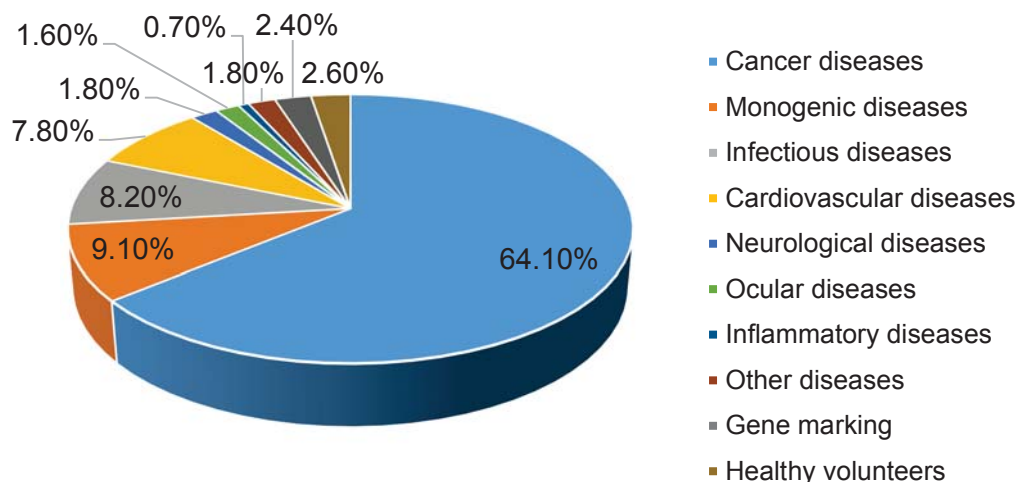


**Figure 1.1.** Graphical representation of the different indications addressed by gene therapy clinical trials. Adapted from The Journal of Gene Medicine, Wiley and Sons (<http://www.abedia.com/wiley/index.html>).

Suicide gene therapy or GDEPT, is a form of gene therapy in which genes are delivered to the targeted cells and expressed. These genes have the ability to convert inactive molecules (prodrugs) to a toxic species (Figure 1.2). Ideally, activation of a prodrug occurs by an enzyme that is either expressed in the tumor

<sup>1</sup>The material contained in this chapter was previously published in *Nanomedicine for Drug Delivery and Therapeutics* Ch. 15, (2013) 438-469, and *Therapeutic Delivery* 4 (2013) 825-839.

site in higher concentrations or unique to the tissue. Various combinations of enzyme and prodrug systems have been proposed for GDEPT, these include classical suicide gene/prodrug combinations such as cytosine deaminase/ 5-fluorocytosine, cytochrome P450/ cyclophosphamide, thymidine phosphorylase/ 5-doxifluridine, and the most well studied strategy herpes simplex virus thymidine kinase/ganciclovir [3, 4].

### 1.1.1. Prodrugs for thymidine kinase (TK)

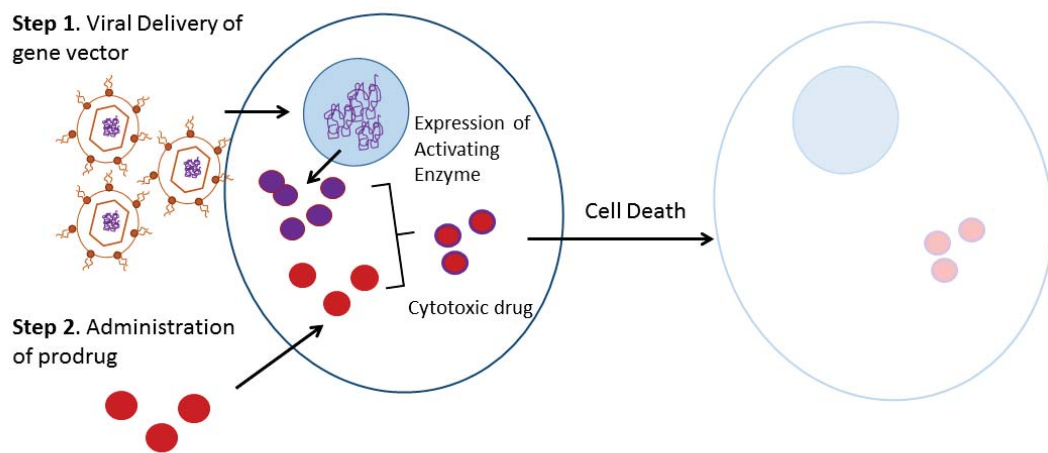


**Figure 1.2.** Gene Directed Enzyme Prodrug Therapy. Current two-step delivery of gene and prodrug for the treatment of cancer. First, the activation enzyme is delivered and expressed in the cell. Second, the prodrug is administered and activated to its cytotoxic form by the enzyme, leading to cell death.

The most prominent and well-studied enzyme/prodrug GDEPT therapy is the use of herpes simplex virus thymidine kinase (HSV-TK) in conjunction with a variety of guanosine-based prodrugs i.e. ganciclovir (GCV), penciclovir, acyclovir (ACV), valacyclovir, (E)-5-(2-bromovinyl)-2'-deoxyuridine, and 2'-exo-methanocarbothymidine [4]. Here, HSV-TK enzyme converts the prodrugs to their monophosphate, other cellular kinases (such as cellular guanylate kinase and cellular phosphoglycerate kinase) then convert the monophosphorylated form of the prodrug to the toxic triphosphate. Cell death is caused by inhibition of DNA

polymerase by the incorporation of dGTP into elongating DNA during cell division [5, 6]. However, prodrugs of HSV-TK are dependent upon the 'bystander effect' for enhanced infectivity. The bystander effect for HTV-TK system was first described in 1990 by Moolten and Wells [7]. These experiments showed that even if only 10% of cells were transfected with HTV-TK gene plasmid, treatment with GCV could lead to 100% cell death. Several mechanisms for the bystander effect have been proposed, including: apoptosis, and gap junctions [8, 9]. The most accepted mechanism of the bystander effect is that the transfer of toxic metabolic products happens through gap junction intercellular communication (GJIC) [8, 10-13]. Cells and tissues use gap junctions to pass information from one cell to the next through channels. These channels are formed from two oligomeric integral membrane proteins called connexons. Connexons regulate intracellular transfer of metabolites as well as ions [14]. It should be noted that in studies where GJIC was inhibited, the bystander effect was still observed [12, 15]. Therefore, it is commonly agreed that bystander cell death is due to multiple combinations of cellular mechanisms.

#### *1.1.2. Prodrugs for thymidine phosphorylase (TP)*

TP is an endogenous enzyme reported to occur to a greater extent in tumor cells than in normal tissue. Furthermore, TP is an angiogenic factor meaning the upregulation of TP in cells has the potential for enhanced tumor growth. 5-deoxyfluoridine (5'DFUR) is an analog of deoxyuridine and a prodrug of 5-fluorouracil (5-FU). 5'DFUR is converted to its active and toxic form, 5-FU, through cleavage by TP. TP expression in some breast, ovarian, colorectal and gastric cancers is upregulated and therefore direct use of 5'DFUR has been researched [16-18]. Similar to the HSV-TK system, TP/5'DFUR exhibits a strong bystander effect [17]. Here, it has been shown that the bystander effect for the TP/5'DFUR system does not require cell-cell contact [19] significantly enhancing TP/5'DFUR as a suicide gene pair.

## 1.2. CURRENT POSITION OF GENE THERAPY

Despite the current successes with gene therapy, there are genuine concerns regarding the safety of gene transfer in humans as well as technical issues in terms of quality and stability of transgene expression; most notably, is the use of viral vectors for delivery of genes into host cells. In 1999, gene therapy was delivered a blow when 18-year old Jesse Gelsinger took part in a gene therapy clinical trial at the University of Pennsylvania in Philadelphia. He was administered a high dose of adenovirus for treatment of ornithine-transcarbamylase. His immune system responded immediately and four days later he died due to multiorgan failure [20]. Markedly, this was the first known case in which a death could be directly linked to the viral vector used for the treatment. Despite the setback from Gelsinger's death, gene therapy is still a promising tool for cancer therapy. As such, several gene therapy products have made their way into the clinical setting outside of the United States.

Since 2000, several gene therapy based products have been approved for clinical use including Gendicine™ and Oncorine™ which received approval in China in 2003 and 2005, respectively. Gendicine™, developed by SiBiono Gene Tech Co., is an adenoviral vector in which E1 gene is replaced with a human p53 cDNA for treatment of head and neck squamous cell carcinoma [21, 22]. Oncorine™, developed by Sunway Biotech Co. Ltd, contains a deletion in the E1B 55k region which restricts virus binding to p53 protein and is approved for use in combination with chemotherapy [23]. In 2004, Ark Therapeutics Group plc, obtained a GMP Certification in the European Union for the manufacture of gene-based medicine, Cerepro® [24]. Cerepro®, is an adenoviral vector which carries the gene for HSV-TK and is intended for the treatment of malignant brain tumors through GDEPT. In 2008, Cerepro® became the first and so far the only adenoviral vector to complete a phase III clinical trial [25, 26]. Most recently, in October, 2012, the European Commission granted marketing authorization for Glybera® for treatment of severe lipoprotein lipase deficiency [27].

It should be noted that these gene therapy products still employ viral vectors for their delivery. As noted by the death of Jesse Gelsinger, viral vector delivery is notorious for causing immunogenicity and tumorigenicity. Therefore, the use of nonviral delivery methods can and are explored for cancer gene therapy.

### 1.3. NONVIRAL DELIVERY METHODS

Incorporation of chemotherapeutic agents into nanoparticle-based drug delivery systems such as, liposomes, polymeric nanoparticles, microcapsules and micelles have been studied extensively for the delivery of drugs to treat a wide range of cancers [28-31]. Due to the fact that nanoparticles can be prepared using a variety of polymers, biodegradable polymers have been studied extensively. Moreover, considerable research has been conducted in the preparation of a variety of biodegradable polymeric nanoparticles for drug delivery [29, 32-35]. For these reasons, polymeric nanocarriers are a choice delivery system for cancer gene therapy.

In particular, polymeric micelles have shown promise for their use in cancer treatment. Polymeric micelles can be prepared using a variety of biodegradable and FDA approved polymers [36, 37], which can house hydrophobic drugs enhancing bioavailability [38]. In addition, polymeric micelles possess a small size (< 200 nm) which allow them to passively target tumor cells through the enhanced permeability and retention (EPR) effect [39]. Both in the laboratory and clinically polymeric micelles are proving effective for cancer treatment [40].

Currently, six micellar systems have made their way into clinical trials. NK105, and Genexol-PM are micellar formulations used for the encapsulation of paclitaxel (PTX). PTX is known to be useful combating ovarian, breast and lung cancers [41, 42]. PTX however has very serious side effects such as neutropenia and peripheral sensory neuropathy. In addition, due to the mixture of Cremophor EL and ethanol used to solubilize PTX, 2-4% of patients report anaphylaxis and

other severe hypersensitive reactions [43]. NC6004 is a poly(ethylene glycol) (PEG) based polymeric micelle for the entrapment of cisplatin. Cisplatin (cis-dichlorodiammineplatinum[II] or CDDP) is commonly used to treat epithelial malignancies of the lung, ovarian, bladder, testis, head and neck, esophagus, gastric, colon and pancreas. However, similar to PTX, CDDP causes several serious adverse side effects such as nephrotoxicity and neurotoxicity, which lead to discontinued treatment [44]. Despite the development of platinum analogues (e.g. carboplatin and oxaliplatin) [45] to overcome CDDP related disadvantages, CDDP has higher toxicity and is the standard treatment for cancer therapy [46, 47]. NC6004 was developed to reduce side effects associated to CDDP and to improve efficacy of delivery to targeted sites. NK012 is a micelle carrier composed of PEG-*b*-poly(glutamic acid) (PGlu), SN-38 (a metabolite of irinotecan hydrochloride, CPT-11) was conjugated to PGlu by coupling agent 1,3-diisoproylcarboiimide and catalyst N-dimethylamino-phridine, causing PGlu to become more hydrophobic leading to micelle formation [48]. Both SP1049C and NK911 are micelle carriers developed for the encapsulation of doxorubicin, another widely used anticancer agent.

#### 1.4. COMPOSITION, FORMATION AND CHARACTERIZATION OF POLYMERIC MICELLES

Interest in using block copolymers for drug delivery has arisen mainly because of their self-associative characteristics. Block copolymers are macromolecules with two or more different polymer blocks arranged in a linear and/or radial arrangement. Synthesis of di- and triblock copolymers has been studied extensively [49]. Commonly, block and graft copolymers are synthesized by ring-opening polymerization [50, 51] or free radical polymerization [52, 53]. Diblock copolymers have shell and core structures. The hydrophilic shell segment protects the drug from the aqueous environment and stabilizes the micelle, while the hydrophobic core encapsulates the non-water soluble drug. In some cases, the core can be made up of a water soluble polymer caused to be hydrophobic

by chemical conjugation to a hydrophobic drug [54], or by complexation of two oppositely charged polyions [55]. In addition to diblock copolymers, multiblock copolymers i.e. triblock and graft copolymers, have been described as potential drug carrier systems [56, 57]. Generally, when the hydrophilic segment is longer than the core block, spherical micelles are formed (Figure 1.3). In contrast, rods and lamellae form when the length of the core segment is longer than the corona chain [58]. Choosing an appropriate copolymer system is essential to achieve an ideal drug carrier and every polymer combination has its own unique advantages.

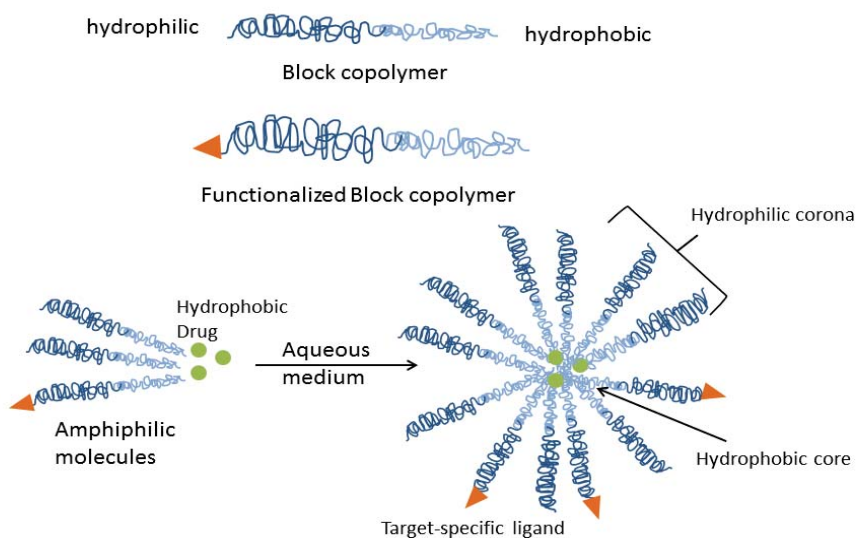


**Figure 1.3.** Block-copolymer micelle. A block-copolymer micelle loaded with a hydrophobic chemotherapeutic agent and functionalized with a target-specific ligand.

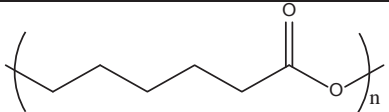
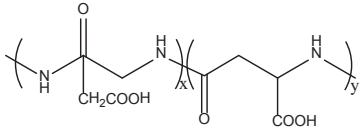
#### 1.4.1. Micelle formation

The hydrophobic corona of micellar systems is commonly made up of polyesters, polyethers and poly(amino acid) derivatives. Commonly used poly (L-amino acids) include poly(L-aspartate) and poly(L-glutamate). For these polymers to self-assemble into amphiphilic micelles, they need to be electrostatically neutral or conjugated to hydrophobic moieties [59]. FDA approved polyesters used in copolymer synthesis include poly(lactic acid) [60], poly( $\epsilon$ -caprolactone) (PCL)

[61, 62] and poly(glycolic acid) [63, 64]. A triblock copolymer of pharmaceutical interest belongs to the poloxamer family, Pluronics (BASF Corp) is a copolymer composed of poly(ethylene glycol)-*b*-poly(propylene oxide)-*b*-poly(ethylene glycol) [65]. Engineering of block copolymers affects the temporal and distribution controls of the polymeric micelles. Controlled release of the drug (temporal control) and site-specific delivery (distribution control) can be optimized through the choice of core and shell polymers.

Routinely, the hydrophilic shell segment is made up of polyethers such as poly(ethylene glycol) (PEG) [66, 67] and poly(ethylene oxide) (PEO) [68-70]. These polymers are inexpensive, have a low toxicity and serve as efficient steric protectors of various biologically active macromolecules [70, 71]. The hydrophilic shell dictates biodistribution of the micelles, and polymers such as poly(*N*-isopropylacrylamide) [52, 53] and poly(L-lactic acid) [72] impart temperature or pH-sensitivity to the polymeric micelle carrier. Natural polymers such as chitosan [73, 74] and dextran [75, 76] have also been employed as hydrophilic shell polymers due to the nontoxic and antimicrobial effects they can impart on the carrier. A list of hydrophobic and hydrophilic polymers used in micellar formation are given in Table 1.1.

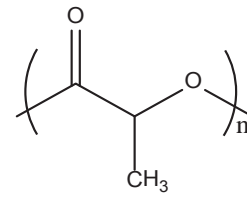
**Table 1.1.** Polymers used in the synthesis of block-copolymer micelles for drug delivery  
**Hydrophobic (Core Forming) Segment**

Poly( $\epsilon$ -caprolactone)	PCL	
Poly(L-aspartate)	PAsp	



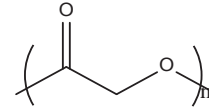
Poly(L-lactide),  
Poly(D,L-lactide)

PLA,  
PDLLA



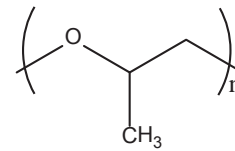
Poly(glycolic acid)

PGA



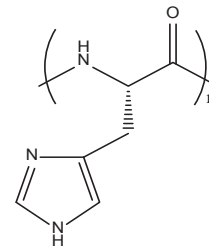
Poly(propylene oxide)

PPO



Poly(L-histidine)

PHis



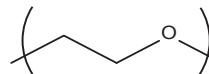
---

### Hydrophilic (Corona-forming) Segment

---

Poly(ethylene glycol)

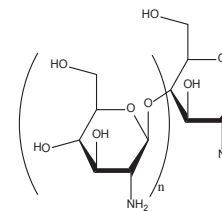
PEG



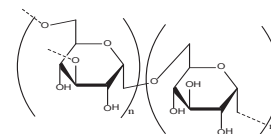
Poly(ethylene oxide)

PEO

Chitosan

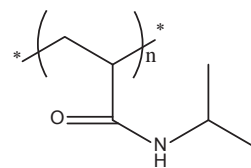


Dextran



Poly(N-isopropyl  
acrylamide)

PNIPAM,  
NIPAM



### 1.4.2. Preparation of micelles

There are various techniques used for the self-assembly of polymers into micellar structures. Selection of appropriate preparation technique is largely based on the solubility of copolymer and drug solution. These methods are direct dissolution method, evaporation method and nanoprecipitation/dialysis method (Figure 1.4).

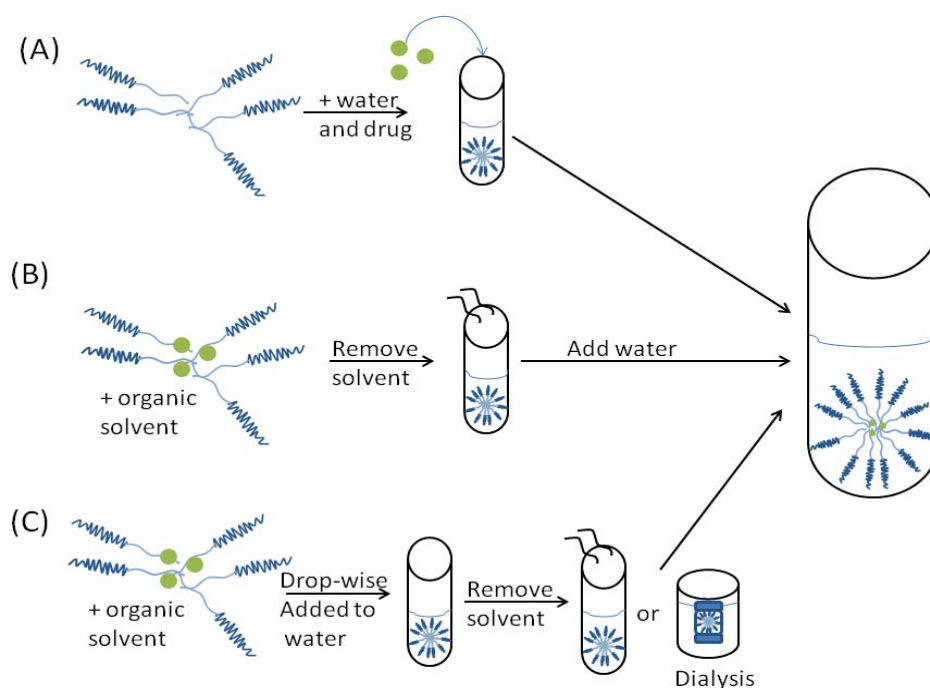


**Figure 1.4.** Techniques used for the preparation of polymeric micelles. (A) Direct Dissolution method: drug and copolymer are dissolved in water. (B) Evaporation method: drug and polymer are dissolved in an organic solvent, solvent is removed and polymer + drug are re-suspended in an aqueous solvent. (C) Dialysis method: drug and polymer are dissolved in an organic solvent that is miscible with water, the solvent mixture is slowly added to the water and then the solvent is removed by solvent-evaporation method or dialysis.

Direct dissolution involves dissolving the block copolymer along with the drug in an aqueous solvent [77]. In contrast, the evaporation method is used for drugs and copolymers with limited water solubility [78]. The most commonly used method for the preparation of micellar carriers is the dialysis method which requires two steps. First, the amphiphilic copolymer and drug are dissolved in an organic solvent (acetone, ethanol or methanol) both have an affinity toward [79]. Micelle formation then proceeds by a solvent-evaporation method [80]. There are various types of solvent-evaporation methods. If the copolymer mixture is slightly water-soluble, it can be dialyzed against water to slowly remove the organic phase and trigger micellization [81]. The oil-in-water emulsion process both drug and polymer are dissolved in a water-miscible organic solvent such as tetrahydrofuran [82] or acetone [83]. This solution is slowly added to water under vigorous stirring/sonication, rearranging the polymer to form micelles. Micelle preparation varies with copolymer composition. Vangeyte et al. demonstrated that the dialysis procedure alone did not offer adequate size control of PEG-b-PCL micelles, where as stable assemblies were formed by first dissolving the polymer in an organic solvent and then dialyzing against water [84].

#### *1.4.3. Factors affecting drug loading and drug release from polymeric micelles*

Drug loading into the micelle cores is achieved through either chemical conjugation or physical entrapment. Drug loading efficiency is calculated using the Flory-Huggins equation [85]. The partition coefficient ( $K_v$ ) is used to calculate the extent to which a drug selectively partitions into the micelle core. The partitioning behavior of drugs in the core controls the amount of drug that can be solubilized in block copolymer micelle carriers. Drug loading efficiency is dependent on many factors including the size of both the core and corona-forming blocks, specific interaction between the drug and core and the method of micelle preparation. A larger hydrophobic block leaves a bigger core structure and therefore increases the ability to entrap the drug [86]. Drug release from polymeric micelles is dependent on the type of encapsulation process used to

load the drug. For a chemically conjugated drug, bulk degradation or surface erosion of the polymer slowly releases the drug. Conversely, for a physically entrapped drug, diffusion is the main mechanism for drug release. It had been shown that drugs incorporated into micelles have superior properties compared to the free drug [87]. Micelles have also been shown to decrease toxicity of a drug compared to the free form [88]. More recently, prodrugs of doxifluridine (5'-DFUR) [89] and acyclovir [90] have been used directly in the ring-opening polymerization of  $\epsilon$ -caprolactone. Our lab has studied the toxicity of 5'-DFUR converted to 5-fluorouracil by endogenous thymidine phosphorylase in colorectal cancer cells. Due to the fact that the prodrug is directly attached to the polymer micelle, another chemotherapy drug 7-ethyl-10-hydroxy-camptothecin (SN-38) was encapsulated in the hydrophobic core of the polymeric drug micelle which drastically increased cell death [91].

#### 1.5. TARGETING SCHEMES

Development of a good drug delivery system relies heavily on the selection of appropriate design parameters such as physiochemical limitations of the drug and/or route of administration. The development of nanoparticles has evolved substantially over the last few decades and there are several key strategies in the design of nanoparticles for therapeutic applications [92]. Although there are quite a few modes of drug administration with their own biological barriers for drug carriers to overcome, systemic delivery remains the most desired mode (e.g., treating metastatic cancer where tumor nodules are spread widely around the body).

Systemic delivery of drug carriers is categorized into two classes: enteral and parenteral routes. Administration of a drug carrier in the enteral route is characterized by absorption of the drug through the gastrointestinal tract and includes oral or rectal administration. In contrast, parenteral drug administration does not pass through the gastrointestinal tract but is administered directly into

the bloodstream. The success of therapeutic carriers is dependent upon the mode of administration and thereby influences synthesis of the carrier. For example, oral administration must address carrier stability in the gastrointestinal tract, whereas intravenous injection must overcome the mononuclear phagocyte system (MPS) if prolonged blood circulation is desired. Additionally, the carrier must be designed to specifically target the site for entry [93, 94]. While each route of delivery has its own pros and cons, intravascular injection due to its precise and almost immediate onset of action is widely employed for drug delivery.

Polymeric micelles are required to exhibit a sufficient half-life in the blood compartment in which solid tumors are normally located outside of. The critical micelle concentration (CMC) is the concentration at which the single chain polymers (unimers) begin to associate to form micelles. Polymeric micelles have a low CMC ( $10^{-4}$ - $10^{-7}$  M). CMC is affected by various properties including size of core block length. An increase in hydrophobic core length corresponds with a decrease in the CMC [95]. A longer hydrophobic core is also correlated with increasing micellar stability [96], increasing in vivo performance. The low CMC of micelles is advantageous for drug delivery because the carrier will not dissociate instantly upon intravenous injection to patients.

The size, shape and surface characteristics all play a role in the biodistribution of particles used for drug delivery. The effect of size and shape on a particle has been studied extensively [97, 98]. Moreover, it is known that non-biocompatible nanoparticles are easily recognized by the MPS [99]. Ideal carriers should be between 10-200 nm to avoid removal by the MPS [98]. If however, the carrier is larger than 200 nm several strategies have been developed by researchers to prolong circulation times of particles. The first is to pre-inject decoy carriers followed by injection of carriers containing therapeutic agents [100]. As a result, phagocytes of the MPS are saturated with decoy carriers, allowing therapeutic carriers to escape and reach the desired sites. Secondly, alterations

to the carrier surface can reduce the rate of protein opsonization or avoid complement activation.

#### 1.5.1. *Passive targeting*

Another key problem for micelle carriers—or any drug carrier is developing an effective delivery method to and inside tumor cells. Many tumors exhibit a unique vasculature which possesses hyperpermeability and impaired lymphatic clearance from the interstitial space. Studies have established a phenomenon in which long-circulating polymeric carriers can effectively accumulate inside of solid tumors. The passive accumulation of drugs into tumors is termed the enhanced permeability and retention (EPR) effect. The EPR effect was first reported by Matsumura and Maeda in 1986 [101], since then, research into the EPR effect has grown considerably [39, 102, 103]. Solid tumors, generally possess a defective vascular architecture, high vascular density and/or active angiogenesis which can cause enhanced vascular permeability, as a result, particles ranging from 10-500 nm in size are able to penetrate the endothelial lining of tumor blood vessels and accumulate inside the interstitial space of tumors [104]. It is known that extensive production of vascular mediators such as bradykinin, nitric oxide, vascular permeability factor/vascular endothelial growth factor, prostaglandin, collagenase and peroxynitrite increase hyperpermeability of tumor blood vessels and increase the EPR effect [39, 105-111]. For the EPR effect to be useful in drug delivery, carriers must be long-circulating so that a sufficient amount of drug can be released into the target cells. One way to increase blood circulation time is through PEGylation.

PEGylation is the process by which PEG chains are attached to a molecule or carrier, and the stealth properties of PEG lent to them. Since PEGylation was first described, several conjugation strategies have been developed. The variety of modification procedures offered allows for the PEGylation of a wide variety of carriers and molecules [112]. PEGylated

dendrimers [113], liposomes [114, 115] and micelles [91, 116] have been developed as viable therapeutic agents for cancer therapy. Moreover, PEGylation of chemotherapy drugs [117, 118], protein molecules [119] or monoclonal antibodies [120], has been employed to increase circulation half-life time and reduce immunogenicity, without decreasing activity. Chemical conjugation of adenovirus vectors with PEG has also emerged as a viable strategy to improve the safety and efficiency of viral gene-delivery vectors [121]. Polymers based on N-(2-hydroxypropyl)methacrylamide have shown particular promise not only as drug carriers, but for surface coating of viruses or targeted drug carriers [122, 123]. While PEGylation has improved the pharmacokinetic properties of the aforementioned systems, overcoming immune clearance and cell entry across the endothelial lining and into the tissue itself is still something which needs to be addressed [124]. Furthermore, PEG has several drawbacks such as hypersensitivity reactions, non-biodegradability, instability under stress and toxicity of side products [124]. These disadvantages have prompted interest into the investigation of alternatives to PEG. There have been several alternatives to PEG suggested which reduce opsonization of drug carriers and increase blood circulation time [125-127]. Once the cells have reached the tumor site, several mechanisms have been proposed for the delivery of the drugs into the cells [128-130]. Figure 1.5 illustrates a few of the proposed passive targeting mechanisms.

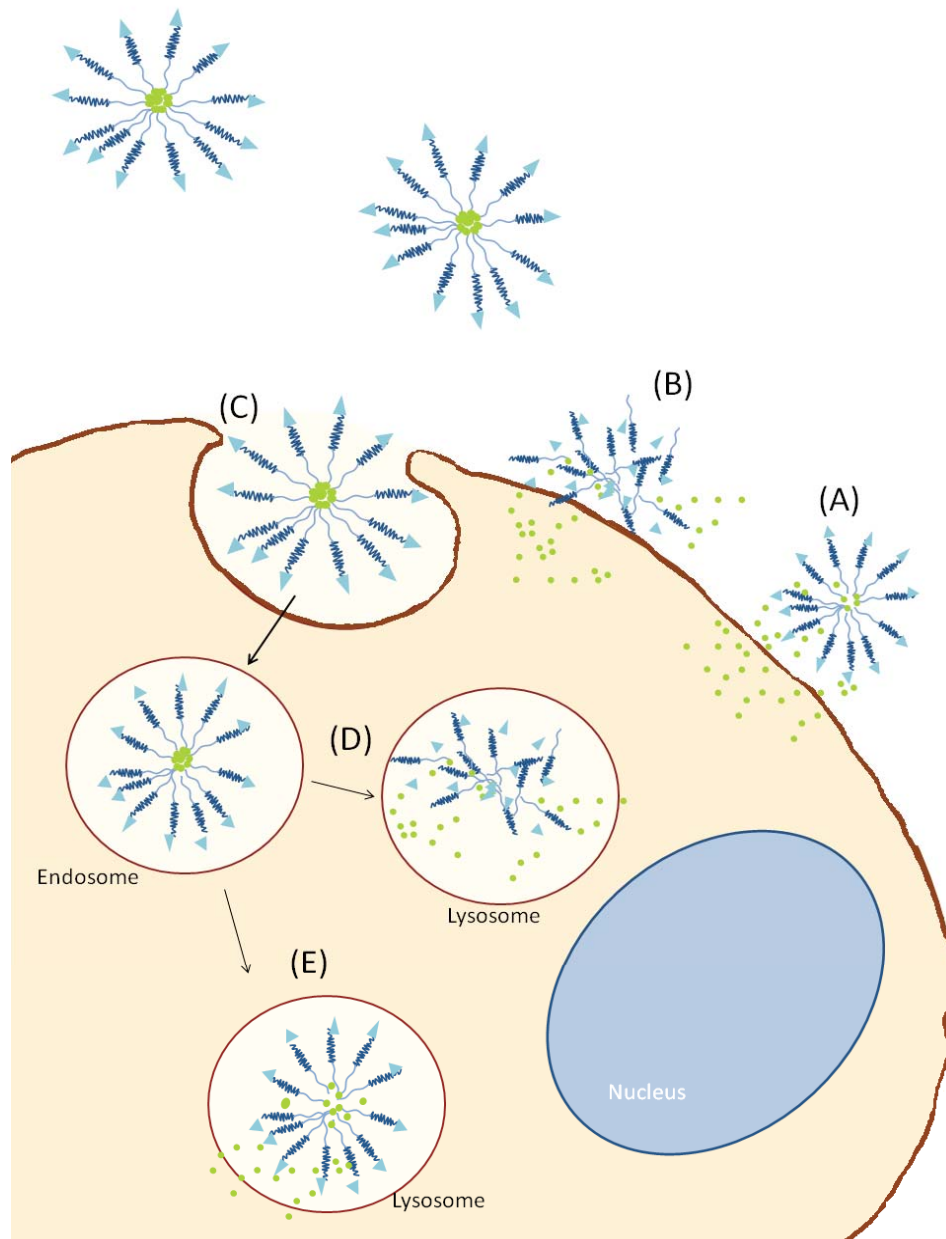


**Figure 1.5.** Mechanisms of drug delivery from micelle carriers. (A) Drug is release from micelle carrier and diffuses into the cell. (B) The micelle carrier disassembles in extracellular space and the drug is released and diffuses into the cell. (C) Drug-loaded micelles are taken up into the cell by endocytosis. The internalized drug-loaded micelle reaches the lysosome where the drug is released by either (D) degradation of polymeric micelles or (E) diffusion.



### 1.5.2. Active targeting

While passive targeting is achieved by exploiting the EPR effect, active targeting aims to increase drug delivery efficiency by taking advantage of the specific biological interactions between the tumor cell and carrier. Through conjugation of a tissue or cell-specific ligand to the carrier system (Figure 1.6), active targeting has been shown to enhance in vitro cytotoxicity against target cells [131]. Ligands can target tumor cells in several ways, two of which are through the neovasculature of angiogenesis and targeting uncontrolled cell growth. Active targeting also makes use of stimuli sensitivity such as pH and temperature sensitivity to target increased accumulation of drug into the target tissue. Kabanov *et al.* was one of the first groups to apply active targeting on a micellar drug delivery system. They conjugated  $\alpha_2$ -glycoprotein, which targets brain glial cells, to pluronic micelles containing FITC. Their results showed that  $\alpha_2$ -glycoprotein micelles had increased delivery to the brain and decreased clearance to the lung when compared to non-ligand conjugated pluronic micelles [132, 133]. Even though many believe active targeting is key for increased biodistribution, recent reviews suggest that the benefit of active targeting lies not with its ability to increase the number of carries to the tumor but with its ability to facilitate in vivo cellular uptake through passive targeting [134].

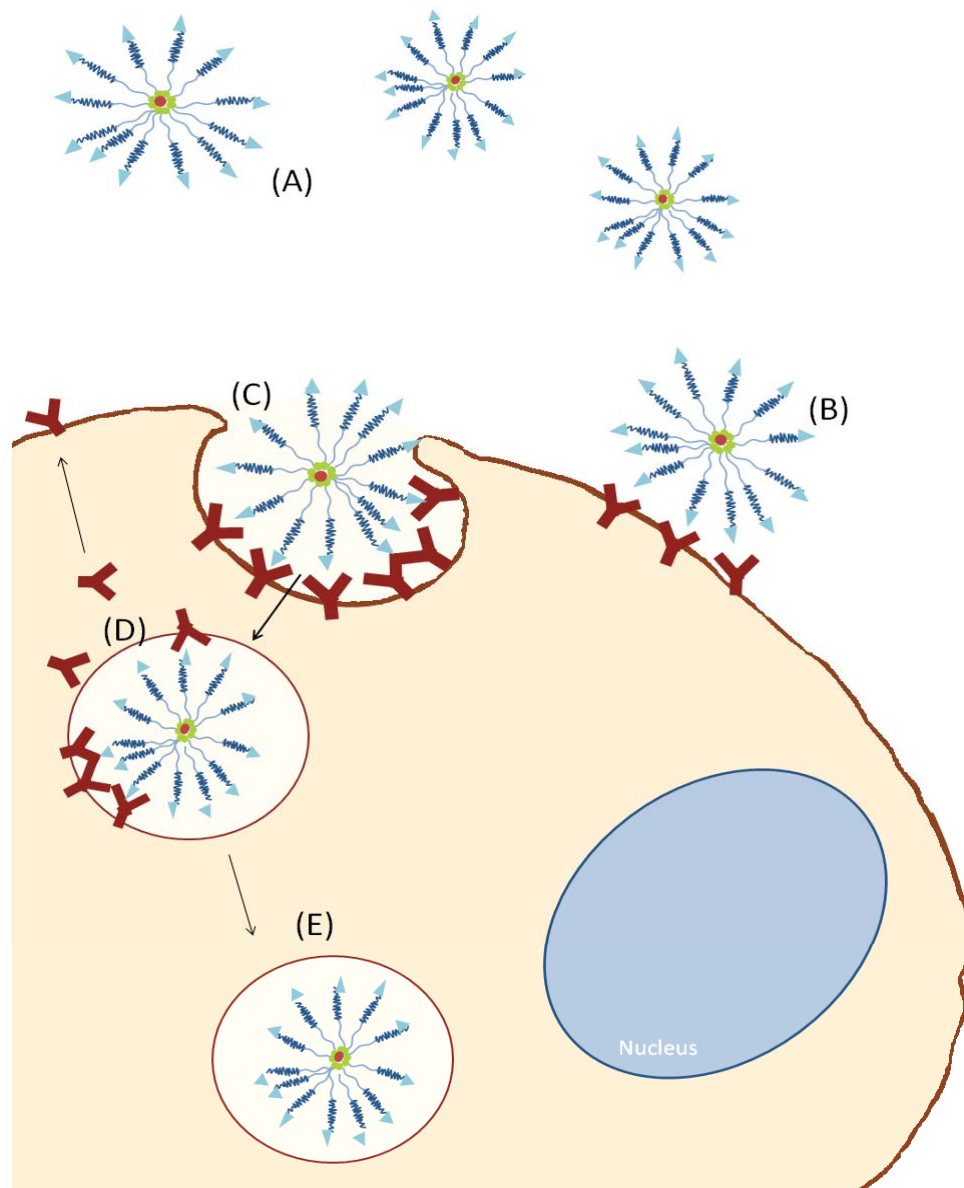


**Figure 1.6.** Polymeric micelles for targeted drug delivery. Surface modification allows for site-specific delivery of the drug to the tumor cells through receptor-mediated endocytosis. (A) Ligand-coupled micelle approaches cancer cells (B) and bind to the cell surface receptors. (C) The micelles are internalized through receptor-mediated endocytosis. (D) In early endosomes, the micelle and receptors undergo sorting where the receptor returns to the cell surface and (E) then micelles enter the late endosome which later fuses with the lysosome.

### 1.5.3. *Receptor-mediated targeting*

Cell proliferation markers can be overexpressed on certain tumor cells making them a good target for cancer therapeutics. Folate, human epidermal and transferrin receptors are the most commonly used ligand targets for cancer therapy. These targets are overexpressed in a wide range of tumor cells and their biological functions as well as internalization pathways have been studied extensively [135-137]. Ligand-mediated targeting of anticancer drugs to overexpressed receptors is increasingly becoming an effective strategy for improving therapeutic effect of cancer drugs [138]. Targeting cell proliferation receptors exploits tumor's reliance on continued stimulation by growth factors and can ensure elimination by stemming the growth of highly malignant tumors and metastatic cells.

Folic acid is one of the most highly researched targets for cancer therapy due to the fact that it is an essential vitamin for biosynthesis of nucleotide bases and is largely consumed by proliferating cells. The receptor for folic acid is overexpressed on epithelial tumors of various organs such as the colon, lung, prostate, ovaries, breast and brain [139]. After intercellular transport of folate-equipped micelles, the drug is released intracellularly due to the slightly acidic (pH 5-6) conditions of endosomes. Moreover, folate conjugates have been shown to escape cancer cells multidrug efflux pumps and remain in recycling endosomes or escape into the cytoplasm [139]. Folate ligands are nontoxic, inexpensive, have a high binding affinity ( $10^{-10}$  M), low immunogenicity, can easily be conjugated to various drug carrier systems and can be stored stably [140].

The human epidermal receptor (HER) family of receptor tyrosine kinases consists of four closely related receptors. Of these receptor tyrosine kinases epidermal growth factor receptor (EGFR) and human epidermal receptor-2 (HER-2) are known to mediate cell signaling pathways involved in growth and proliferation in response to the binding of a variety of growth factor ligands [137].

EGFR is overexpressed in one-third of all solid tumors including breast [141], lung [142], colorectal [143], head and neck [144], esophageal [145], renal cell [146], and prostate cancers [147]. There are six known endogenous ligands for EGFR: EGF, transforming growth factor- $\alpha$  (TGF- $\alpha$ ), amphiregulin, betacellulin, heparin-binding EFG (HB-EFG) and epiregulin [148]. The most commonly detected in humans and therefore best studied are TGF- $\alpha$  and EGF. The presence of EGFR is frequently associated with metastatic spread [149] however it has also demonstrated to have pro-angiogenic properties [150]. Targeting EGFR as an anticancer strategy was first proposed in the 1980's [151], there are now 13 anti-EGFR agents undergoing clinical trials either as monotherapy or in combination with standard treatment [137]. Several EGFR inhibitors mainly Iressa and Erbitux have even made their way to clinical trials with limited success [137] and are now FDA-approved [152, 153]. Reilly's group is now undergoing phase 1 clinical trials with radiopharmaceutical  $^{111}\text{In}$ -DTPA-hEGF for treatment of EGFR-overexpressing breast cancer cells [154].

Transferrin (Tf) is an iron-binding blood plasma glycoprotein that binds to transferrin receptors (TfR) which are over expressed in malignant cells due to an increased iron requirement. Tf binds to endogenous iron in plasma, once bound to TfR, it is endocytosed into acidic compartments and the bound iron dissociates. TfRs are overexpressed in certain body tissues such as liver, epidermis, intestinal epithelium, vascular endothelium of the brain capillary and certain blood cells in the bone marrow. Tf-TfR mediated drug delivery has been studied for the treatment of breast cancer, prostate cancer and myeloid leukemia [136, 155, 156]. Use of Tf has been given specific attention with regards to brain cancer because it can facilitate the transcytosis of drug carriers across the blood brain barrier. Yue's group has used active targeting with several targeting moieties [157, 158]. Recently, the Tf-TfR interaction was studied because of the small amount of Tf needed to conjugate on the micelle and its higher endocytosis efficiency. Their results showed that Tf conjugation significantly increased cellular

uptake of Tf-micelles in MCF-7 and SGC-7901 cell lines. In vivo studies also confirmed antitumor effectiveness [159].

Angiogenesis is the physiological process involving the growth of new blood vessels from pre-existing blood vessels. Most mammalian cells retain a blood vessel size of 100 to 200  $\mu\text{m}$ , to surpass this size, new blood vessels must be formed [160]. It is known that for a tumor cell to grow beyond its critical size or metastasize to another organ, new blood vessels must be formed. Therefore, in 1971, it was proposed that one way to stop tumor growth could be to block angiogenesis [161]. It is widely accepted that tumor angiogenesis happens by the activation of the 'angiogenic switch'. When pro-angiogenic molecules and anti-angiogenic molecules are in balance the switch is off but when that balance is turned, the switch is turned on [162]. There are now more than 30 known activators and inhibitors of angiogenesis of these, vascular endothelial growth factor receptors (VEGFR), integrins, matrix metalloproteinase receptors and vascular cell adhesion molecule-1 are the most common angiogenic targets studied by nanoscale drug delivery systems [140].

VEGFR is one of the most commonly studied tumor angiogenesis inducers studied. VEGF ligands bind to and active three different type III receptor tyrosine kinases: VEGFR-1, VEGFR-2 and VEGFR-3. VEGFR-2 expression is restricted to the vasculature and therefore has been studied as an inducer of tumor angiogenesis [163]. Integrins  $\alpha_v\beta_3$  is an arginine-glycine-aspartic acid (RGD) containing molecule that is responsible for anchoring cells to the extracellular matrix. Several studies have found that  $\alpha_v\beta_3$  has a key role in endothelial cell survival and migration during angiogenesis [164, 165]. In a recent study, PEG-*b*-poly(lysine) micelles were complexed with cyclic RGD peptide and targeted to integrin expressing HeLa cells. Uptake of the micelles was viewed by comparing fluorescently labeled, targeted and untargeted micelles in live-cell imaging experiments through fluorescence microscopy and flow cytometry. Their results showed that RGD ligand accelerated the internalization of micelles [166].

## 1.6. ENGINEERING ANTIPHAGOCYtic BIOMIMETIC DRUG CARRIERS

While synthetic biomaterials for therapeutic delivery have been significantly advanced in terms of functionality and diversity, they still lack in the complexity of natural particulates. For example, red blood cells (RBCs) exhibit a complex biological functionality: they possess a small size, flexibility and chemical composition which allow them to complete complex tasks flawlessly in the human body without being recognized as foreign particles for up to 4 months [167]. Pathogens such as bacteria and viruses have developed immune escaping mechanisms which allow them to infect tissues with maximum efficacy [168]. Recently, researchers' understanding of immune surveillance has been growing greatly [169-171] and several immune system components have been implicated in the identification and elimination of cancer cells [172, 173]. To this end, the remarkable properties cells in the body possess are being exploited for the delivery of therapeutic and/or diagnostic agents. Due to the increased understanding of circulating body cells as carriers, surface biochemistry of blood cells, and the immune escaping mechanisms pathogens and tumor cells employ, researchers are taking a lead from nature in the design of drug carriers. Aided by advances in nanotechnology and biology, researchers are able to design delivery vehicles which mimic natural cells. These novel biomimetic strategies have been proposed to camouflage drug carriers in order to bypass immune surveillance. These systems prolong the circulation time in bloodstream and lead to effective delivery of theranostic agents.

### 1.6.1. *Erythrocyte-inspired therapeutic delivery*

To develop a RBC carrier, a multitude of techniques have been established for the loading of therapeutic agents without changing RBC's physiological survival properties [174]. Of the erythrocyte ghost preparation methods available, hypotonic treatment is the standard preparation which retains the physiochemical characteristics of erythrocyte membranes [175, 176]. RBCs are placed in a

hypotonic solution where osmotic pressure releases the intracellular contents within the RBC membrane. Meanwhile, the therapeutic agent of interest in the solution can then passively diffuse into RBCs and retain inside the cells via isotonic buffer resealing. Due to the pioneering studies using RBCs to deliver  $\beta$ -glucosidase and  $\beta$ -galactosidase for the treatment of Gaucher's disease [177], several enzyme replacement therapeutics have been developed, some of which have entered long-term clinical trials [178-181]. Furthermore, erythrocyte ghosts have been harnessed for the delivery of oligonucleotides [182] and plasmid DNA [183]. RBC carriers have also been used to entrap small drug molecules [184], increasing biodistribution of the drug. Likewise, the encapsulation of multiple drugs have been studied [185]. Erythrocyte ghosts engineered to contain hemagglutinin fusion protein found on lipid membranes and for encapsulation of superparamagnetic nanoparticles and anti-cancer drug decitabine has been made for sustained and targeted delivery [186].

RBC membrane-derived liposomes, termed nano-erythroosomes, were first reported by Lejeune *et al.* [187]. Recently, Hu *et al.* used the plasma membrane of erythrocyte ghosts to cloak biodegradable polymeric nanoparticles via membrane extrusion and demonstrated extended blood circulation half-life time of RBC membrane-camouflaged polymeric nanoparticles [188]. Compared to PEG-coated nanoparticles, which had an elimination half-life of 15.8 hours, the RBC-membrane-coated nanoparticles had an elimination half-life of 39.6 hours nearly double that of the control. Another way in which researchers are taking advantage of the properties of RBCs is through the coupling of therapeutic agents onto the outer surface of RBCs by covalent conjugation [189]. Taking advantage of ligands on the RBC surface, such as the complement receptor 1, drugs can be conjugated and their circulation time increased. A "hitchhiking" strategy was employed to attach therapeutic polymeric nanoparticles on the surface of RBCs through physical means and showed a drastic improvement in blood circulation time [190].

### 1.6.2. *Carrier cells for therapeutic delivery*

Natural carrier cells such as cytokine-induced killer (CIK cells), T cells and mesenchymal stem cells (MSCs) have all been exploited for the delivery of various therapeutic agents and for the delivery of oncolytic viruses. An advantage of using these cells is for their tumor-homing or tumor targeting abilities. Moreover, addition of therapeutic agents into these cells does not affect the integrity of the natural particulates. CIK cells have demonstrated the ability to localize into leukemia tissue and become toxic to them [191]. CIK cells have shown effective in the treatment of several solid malignancies including those of the lungs and ovaries [192, 193]. Success of CIK treatment *in vivo* has led to clinical studies of the treatment for solid tumors with encouraging results [194].

Similar to CIK cells, T-cell based immunotherapies have shown successful in tumor immunotherapy by increasing the numbers of endogenous NK and CD8<sup>+</sup> T cells which are potent mediators of antitumor immunity [195, 196]. Recently, T cells co-transduced with prostate tumor antigens to target tumor cells were successfully used for tumor treatment by Kloss *et al.* [197]. In the study, T cells were rendered tumor specific and elicited complete tumor remission without sacrificing T cell reactivity.

MSCs exhibit migratory properties which make them attractive candidates for targeted delivery of genes and viruses. Recent studies have shown that MSCs are not only able to migrate to and incorporate within the connective tissue of tumors, but actively seek out metastases far removed from the primary tumor site [198-200]. MSCs have been utilized as delivery vehicles of interleukins in order to improve the anticancer immune surveillance by activating cytotoxic lymphocytes and NK cells [201]. MSCs have also been used as delivery agents for gene-directed enzyme prodrug therapy. Several prodrug-enzyme activation schemes are available for killing tumor cells and are being evaluated in clinical trials [202]. The approach of using MSCs to deliver a gene to a prodrug was first



explored by Aboody *et al.* through delivery of cytosine deaminase (CD) which can be used for activation of prodrug 5-fluorocytosine to 5-fluorouracil [203]. Kosaka *et al.* evaluated the effect of MSC transfection with adenovirus carrying CD followed by treatment of 5-fluorocytosine *in vivo* [204]. Their results showed that delivery of MSCs transfected with CD resulted in significant prolongation of survival of rats with glioma cells. Fei *et al.* transfected MSCs with lentiviral vectors expressing CD with similar success in decreased tumor viability [205]. Other prodrug-gene combinations have been studied in conjunction with MSCs. Mori *et al.* transfected HSV-TK into MSCs then treated glioma cells with the MSCs/TK followed by treatment with ganciclovir [206]. Their results showed that significant cell death occurred in glioma cells treated with MSCs/TK compared to non-transfected MSCs. The use of MSCs for GDEPT and as targeting vehicles is proving very promising for treatment of various cancer types.

### 1.6.3. *Pathogen-inspired therapeutic delivery*

As our understanding of the methods by which pathogens evade the immune system has grown, the ability to apply the immune evasion capabilities of pathogens to material design has been developed. One of the earliest attempts to exploit a naturally derived polysaccharide was through the coating of liposomes with linear dextran [207]. Bacterial dextran is produced by the fermentation of sucrose with *Leuconostoc mesenteroides* [208]. After ethanol precipitation from the culture medium, acid hydrolysis is used to reduce the overall molecular weight of dextran. Dextran with an average molecular weight of 70 kD has been used as a plasma volume expander [209]. Dextran coating enhances the circulation time of drug molecules [210] and stability of micelle carriers [75]. Coating of poly(lactic acid) nanoparticles with dextran induced a diminished protein adsorption [211]. Dextran coating prolonged the blood circulation time of carriers made of poly(methyl methacrylate) polymer [212] and contrast agents [213]. Hyaluronan covalently attached to the surface of lipid nanoparticles has been demonstrated to endow the carriers with extended

circulation and active targeting towards hyaluronan receptor CD44, which is highly expressed on tumors [214].

Heparin is known to modulate the action of several systems including viral entry [215] and angiogenesis [216]. Heparin is a member of the glycosaminoglycan family of carbohydrates and found on the surface of cells and in the extracellular matrix [217]. It is known that heparin-like polysaccharides can be obtained from microorganisms such as *Escherichia coli* and resembles a type II glycosaminoglycuronan chain [218]. Due to its biological and pharmacological activities heparin has been used to surface-functionalized a variety of nanoparticles [219]. Heparin-coated poly(methyl methacrylate) nanoparticles exhibited a prolonged blood circulation time for 2 days, because host factor H can bind to heparin and inhibit complement activation [212]. Recently, a heparin-mimicking polymer conjugate was synthesized by Nguyen *et al.* [220]. The synthesized heparin was far more stable under stress than the control without sacrificing the native activity of heparin.

#### 1.6.4. CD47

In 2000, Oldenborg *et al.* reported that CD47 functioned as a “marker of self” on murine RBCs [221]. Murine RBCs deficient in CD47 were rapidly cleared from the bloodstream by macrophages compared to wild-type mice. Indeed, as a RBC ages, CD47 expression levels decrease (30% lower expression of CD47) on the oldest RBCs compared to the youngest RBCs, clearly supporting the role of CD47 in long-term circulation of RBCs in the bloodstream [222]. CD47 is widely expressed on a majority of normal tissues in humans and other mammals and leads to the phagocytosis of aged or damaged cells [223]. CD47 regulates phagocytosis by its interaction with signal regulatory protein alpha (SIRP $\alpha$ ) on macrophages [224]. Through CD47 ligation with SIRP $\alpha$ , tyrosine phosphatase is activated and myosin accumulation at the phagocytic synapse is repressed, leading to inhibition of Fc $\gamma$  and complement receptor mediated phagocytosis

[225]. If the inhibitory signals generated by CD47-SIRP $\alpha$  association are sufficient to counteract the phagocytic signals mediated through F $\gamma$  and the complement receptors, ingestion of particles (e.g., RBCs or CD47-tagged drug carriers) is reduced or inhibited (Figure 1.7).

Moghimi *et al.*, suggested that CD47 could represent a viable solution in the design of macrophage-evading therapeutic carriers [218]. Hsu *et al.* first demonstrated the antiphagocytic effect of soluble CD47-streptavidin (CD47-SA:

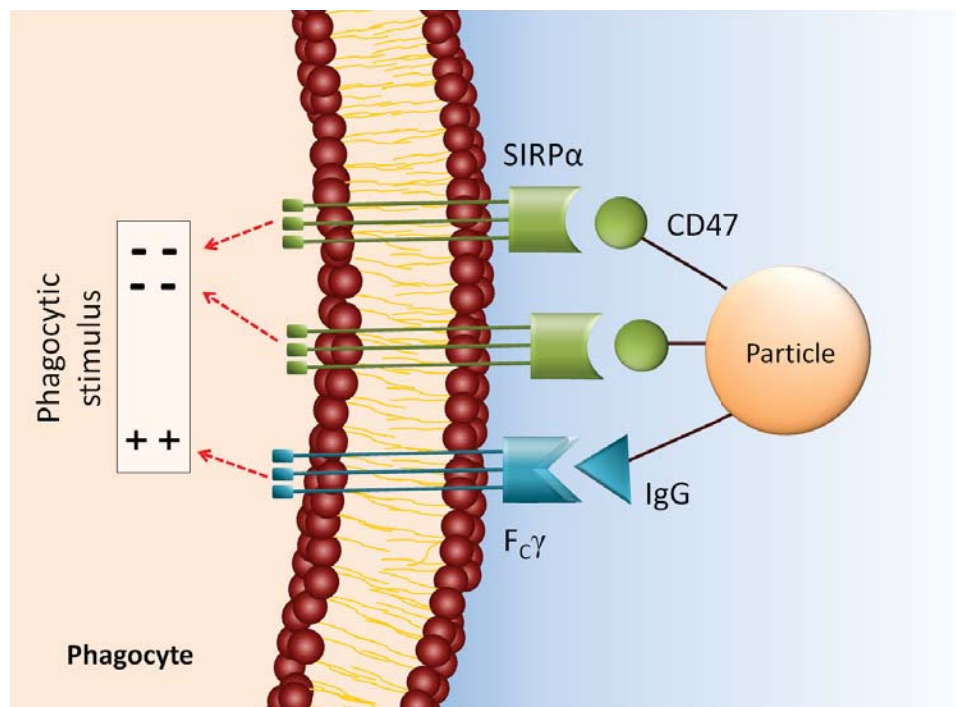


**Figure 1.7.** The interaction of phagocyte receptors and an opsonized particle tagged with CD47 ligand. The interaction of SIRP $\alpha$  and CD47 generates an antiphagocytic signal onto the particle and competes against the phagocytic signal triggered by F $\gamma$ -IgG binding. If the negative signal dominates in this tug of war, the particle gets the chance to avoid phagocytic internalization.

containing only the extracellular domain of CD47) fusion protein, expressed in BL21 bacteria and then purified by biotinylated agarose column, on macrophage cells [226]. In the study, it was shown that perfluorocarbon-based oxygen carriers

were able to avoid being engulfed by J774A.1 macrophage cells for up to 2 hours after cells were pretreated with soluble CD47-SA for 1 hour.

Tsai *et al.* employed mammalian CHO cells transfected with CD47-encoding plasmid (containing only extracellular domain sequence of CD47) to produce and biotinylate extracellular domain of CD47 ligand [227]. Streptavidin-coated polystyrene microbeads of 2.1  $\mu\text{m}$  in diameter were tagged with biotinylated CD47 with a density comparable to that on RBCs and exhibited significant phagocytosis resistance with THP-1 macrophages. Recently, Rodriguez *et al.* has led to the development of a man-made “Self” peptide which can inhibit phagocytosis and enhance delivery of nanoparticles [228]. Through structure biology and computer simulation, a 21-amino acid “Self” peptide fragment (shortened from the 117-amino acid extracellular domain of CD47). This peptide was then put onto fluorescent polystyrene nanobeads of size 160 nm. Within half an hour, the beads tagged with the peptide showed 4 times as many beads still in circulation compared to the control beads. Additionally, delivery of paclitaxel to tumor bearing mice with the peptide-tagged polystyrene nanobeads showed similar tumor size reduction as delivery by the standard paclitaxel carrier (i.e., Cremophor) without similar toxic side effects.

## 1.7. RATIONALE AND HYPOTHESIS

Cancer is a leading cause of death worldwide and was the cause of 8.2 million deaths in 2012. It is expected that the number of cancer cases will rise from 14 million in 2012 to 22 million within the next two decades [229]. Despite considerable advances in surgical and adjuvant therapies, many forms of cancer still show resistance to treatment. One way researchers are combating cancer is through gene therapy, which is the insertion of genetic material into an individual’s cell to treat a disease. One approach scientists are using gene therapy to treat cancer is through GDEPT. In such an approach, a prodrug, a pharmacologically inactive molecule that requires enzymatic and/or chemical

transformation to release a cytotoxic drug, is given to the patient. The prodrug contains the drug which will be used to destroy the targeted cancer cells. The gene for a foreign enzyme and the prodrug are administered in a two-step process. That is, first the foreign gene is introduced into the targeted cancer cells, expressed and released into the cytoplasm and then the prodrug is administered. The prodrug is activated by the gene-expressed exogenous enzyme and converted to its cytotoxic form.

My thesis examines the potential of multifunctional polymeric prodrug micelles for cancer gene therapy. I hypothesize that (i) prodrugs ACV, GCV or 5'DFUR can be used as initiators directly in ring-opening polymerization of  $\epsilon$ -caprolactone to form a hydrophobic prodrug-tagged poly( $\epsilon$ -caprolactone) (PCL), (ii) the prodrugs released from PCL by acid hydrolysis and/or intracellular esterase can be converted to their active and toxic forms, via overexpressed enzyme (either HSV-TK or TP) in cancer cells, (iii) through design and synthesis of polymeric drug/gene nanocarriers, the releasing profile of the prodrug-activating enzyme system will be optimized to achieve maximum anticancer effectiveness in both the classical two-step and a proposed one-step approach, and (iv) CD47-streptavidin bound to the micelle surface can endow antiphagocytic and targeting properties to the micelle nanocarrier.

## 1.8. SPECIFIC AIMS

### 1.8.1. *Specific aim 1: Optimization of polymeric prodrug nanocarriers*

The anticancer prodrugs ACV, GCV and 5'DFUR will be utilized as initiators in the ring-opening polymerization of  $\epsilon$ -caprolactone to form hydrophobic prodrug-tagged PCL, which will be grafted with hydrophilic polymers (methoxy poly(ethylene glycol), polyethyleneimine, or chitosan) to form amphiphilic copolymers for the preparation of stable micellar nanoparticles. The synthesized prodrug-containing amphiphilic copolymers will be characterized accordingly using analytical tools. Experiments including self-assembly morphology, particle

size and charge, and critical micelle concentration will be used to determine the optimal parameters for polymeric nanocarrier formation. I will examine the degree of the prodrug released from synthesized amphiphilic polymers by using hydrolysis and esterase. Toxicity of the micelles will be determined against HT29 colorectal cancer cell lines.

*1.8.2. Specific aim 2: Efficacy of polymeric prodrug nanocarriers on cancer cell treatment*

Polymeric micelles with promising features will be employed for both two-step and one-step toxicity studies. HT29 colorectal cells have been chosen as the biological model for cytotoxic studies. Because HT29 cells have endogenous TP, micelles formed with 5'DFUR will be used to encapsulate DOX or SN-38. 5'DFUR and chemotherapy drugs loaded into my most desirable polymeric nanocarriers will both be slowly released within the malignant cells possibly extensively enhancing the effectiveness of anticancer therapy by synergistic or additive activity. Micelles formed from ACV or GCV will be studied by two-step toxicity by delivering HSV-TK gene plasmid to cells. The one-step approach will be achieved by synthesizing polymeric nanocarriers containing prodrug and gene encoded plasmids and culturing with cancer cells. To achieve maximal anticancer effectiveness of my one-step approach using multifunctional polymeric nanocarriers, the releasing profile of prodrug-activating enzyme will be modulated in line with the prodrug releasing window.

*1.8.3. Specific aim 3: Antiphagocytic and targeted micelle carriers*

CD47-streptavidin fusion protein can be easily attached to biotinylated substrates utilizing the biotin-streptavidin affinity, revealing antiphagocytic function. Furthermore, since CD47 is an integrin associated protein, it has the potential to be employed to target integrin  $\alpha_v\beta_3$ , which is overexpressed on tumor-activated neovascular endothelial cells and unexpressed on mature quiescent

ones lined in blood vessels. Because the affinity of biotin to streptavidin is so high and the micelle surface does not have other proteins, the crude protein can be used for CD47 functionalization on the micelle surface. Here, micelles will be biotinylated and then bound with CD47-streptavidin crude protein. The CD47 coated micelle will then be treated to macrophages and the antiphagocytic effect studied. Moreover, PC3 cells, which over express  $\alpha_v\beta_3$  integrin, will be treated with CD47 tagged micelles and the targeting ability followed.

## 1.9. REFERENCES

1. Rosenberg SA, Aebbersold P, Cornetta K *et al.* Gene transfer into humans — Immunotherapy of patients with advanced melanoma, using tumor-infiltrating lymphocytes modified by retroviral gene transduction. *New England Journal of Medicine* 323(9), 570-578 (1990).
2. Wirth T, Parker N, Ylä-Herttuala S. History of gene therapy. *Gene* 525(2), 162-169 (2013).
3. Greco O, Dachs GU. Gene directed enzyme/prodrug therapy of cancer: Historical appraisal and future perspectives. *Journal of Cellular Physiology* 187(1), 22-36 (2001).
4. Denny WA. Prodrugs for gene-directed enzyme-prodrug therapy (suicide gene therapy). *Journal of Biomedicine and Biotechnology* 2003(1), 48-70 (2003).
5. Elion GB. The biochemistry and mechanism of action of acyclovir. *The Journal of antimicrobial chemotherapy* 12 Suppl B(9-17) (1983).
6. Mar E, Chiou J, Cheng Y *et al.* Human cytomegalovirus-induced DNA polymerase and its interaction with the triphosphates of 1-(2'-deoxy-2'-fluoro-beta-D-arabinofuranosyl)-5-methyluracil, -5-iodocytosine, and -5-methylcytosine. *Journal of Virology* 56(3), 846-851 (1985).
7. Moolten FL, Wells JM. Curability of tumors bearing herpes thymidine kinase genes transferred by retroviral vectors. *Journal of the National Cancer Institute* 82(4), 297-300 (1990).
8. Freeman SM, Abboud CN, Whartenby KA *et al.* The "bystander effect": Tumor regression when a fraction of the tumor mass is genetically modified. *Cancer Research* 53(21), 5274-5283 (1993).
9. Li Bi W, Parysek LM, Warnick R *et al.* In vitro evidence that metabolic cooperation is responsible for the bystander effect observed with HSV-tk retroviral gene therapy. *Human Gene Therapy* 4(6), 725-731 (1993).
10. Fick J, Barker FG, Dazin P *et al.* The extent of heterocellular communication mediated by gap junctions is predictive of bystander tumor cytotoxicity in vitro. *Proceedings of the National Academy of Sciences* 92(24), 11071-11075 (1995).
11. Mesnil M, Piccoli C, Tiraby G *et al.* Bystander killing of cancer cells by herpes simplex virus thymidine kinase gene is mediated by connexins. *Proceedings of the National Academy of Sciences* 93(5), 1831-1835 (1996).
12. Princen F, Robe P, Lechanteur C *et al.* A cell type-specific and gap junction-independent mechanism for the herpes simplex virus-1 thymidine kinase gene/ganciclovir-mediated bystander effect. *Clinical Cancer Research* 5(11), 3639-3644 (1999).
13. Tanaka T, Yamasaki H, Mesnil M. Stimulation of intercellular communication of poor-communicating cells by gap-junction-competent cells enhances the HSV-TK/GCV bystander effect in vitro. *International Journal of Cancer* 91(4), 538-542 (2001).
14. Goodenough DA, Goliger JA, Paul DL. Connexins, connexons, and intercellular communication. *Annual Review of Biochemistry* 65(1), 475-502 (1996).
15. Imaizumi K, Hasegawa Y, Kawabe T *et al.* Bystander tumoricidal effect and gap junctional communication in lung cancer cell lines. *American Journal of Respiratory Cell and Molecular Biology* 18(2), 205-212 (1998).



16. Bronckaers A, Gago F, Balzarini J *et al.* The dual role of thymidine phosphorylase in cancer development and chemotherapy. *Medicinal Research Reviews* 29(6), 903-953 (2009).
17. Patterson AV, Zhang H, Moghaddam A *et al.* Increased sensitivity to the prodrug 5'-deoxy-5-fluorouridine and modulation of 5-fluoro-2'-deoxyuridine sensitivity in MCF-7 cells transfected with thymidine phosphorylase. *British Journal of Cancer* 72(3), 669-675 (1995).
18. Haraguchi M, Furukawa T, Sumizawa T *et al.* Sensitivity of human KB cells expressing platelet-derived endothelial cell growth factor to pyrimidine antimetabolites. *Cancer Research* 53(23), 5680-5682 (1993).
19. Evrard A, Cuq P, Ciccolini J *et al.* Increased cytotoxicity and bystander effect of 5-fluorouracil and 5-deoxy-5-fluorouridine in human colorectal cancer cells transfected with thymidine phosphorylase. *British Journal of Cancer* 80(11), 1726-1733 (1999).
20. Stolberg SG. The biotech death of Jesse Gelsinger. *New York Times Magazine* 28, 136-140 (1999).
21. Peng Z. Current status of gendicine in China: Recombinant human Ad-p53 agent for treatment of cancers. *Human gene therapy* 16(9), 1016-1027 (2005).
22. Wilson JM. Gendicine: The first commercial gene therapy product. *Human Gene Therapy* 16(9), 1014-1015 (2005).
23. Liang M. Clinical development of oncolytic viruses in China. *Current Pharmaceutical Biotechnology* 13(9), 1852-1857 (2012).
24. Mitchell P. Ark's gene therapy stumbles at the finish line. *Nature Biotechnology* 28(3), 183-184 (2010).
25. Muhammad AKMG, Puntel M, Candolfi M *et al.* Study of the efficacy, biodistribution, and safety profile of therapeutic gutless adenovirus vectors as a prelude to a phase I clinical trial for glioblastoma. *Clinical Pharmacology and Therapeutics* 88(2), 204-213 (2010).
26. Wirth T, Hedman M, Makinen K *et al.* Safety profile of plasmid/liposomes and virus vectors in clinical gene therapy. *Current Drug Safety* 1(3), 253-257 (2006).
27. Wierzbicki AS, Viljoen A. Alipogene tiparvovec: Gene therapy for lipoprotein lipase deficiency. *Expert Opinion on Biological Therapy* 13(1), 7-10 (2013).
28. Müller Rh, Mäder K, Gohla S. Solid lipid nanoparticles (SLN) for controlled drug delivery - A review of the state of the art. *European Journal of Pharmaceutics and Biopharmaceutics* 50(1), 161-177 (2000).
29. Kalachandra S, Takamata T, Lin D *et al.* Stability and release of antiviral drugs from ethylene vinyl acetate (EVA) copolymer. *Journal of Materials Science: Materials in Medicine* 17(12), 1227-1236 (2006).
30. Duncan R. Polymer conjugates as anticancer nanomedicines. *Nature Reviews Cancer* 6(9), 688-701 (2006).
31. Duncan R, Vicent MJ. Polymer therapeutics-prospects for 21st century: The end of the beginning. *Advanced Drug Delivery Reviews* 65(1), 60-70 (2013).
32. Corden TJ, Jones IA, Rudd CD *et al.* Physical and biocompatibility properties of poly-ε-caprolactone produced using in situ polymerisation: a novel manufacturing technique for long-fibre composite materials. *Biomaterials* 21(7), 713-724 (2000).
33. Jones MC, Leroux JC. Polymeric micelles – a new generation of colloidal drug carriers. *European Journal of Pharmaceutics and Biopharmaceutics* 48(2), 101-111 (1999).

34. Guan X, Quan D, Shuai X *et al.* Chitosan-graft-poly( $\epsilon$ -caprolactone)s: An optimized chemical approach leading to a controllable structure and enhanced properties. *Journal of Polymer Science Part A: Polymer Chemistry* 45(12), 2556-2568 (2007).
35. Soppimath KS, Aminabhavi TM, Kulkarni AR *et al.* Biodegradable polymeric nanoparticles as drug delivery devices. *Journal of Controlled Release* 70(1-2), 1-20 (2001).
36. Park J, Ye M, Park K. Biodegradable polymers for microencapsulation of drugs. *Molecules* 10(1), 146-161 (2005).
37. Mansour HM, Sohn M, Al-Ghananeem A *et al.* Materials for pharmaceutical dosage forms: Molecular pharmaceuticals and controlled release drug delivery aspects. *International Journal of Molecular Sciences* 11(9), 3298-3322 (2010).
38. Oerlemans C, Bult W, Bos M *et al.* Polymeric micelles in anticancer therapy: Targeting, imaging and triggered release. *Pharmaceutical Research* 27(12), 2569-2589 (2010).
39. Maeda H, Wu J, Sawa T *et al.* Tumor vascular permeability and the EPR effect in macromolecular therapeutics: A review. *Journal of Controlled Release* 65(1-2), 271-284 (2000).
40. Matsumura Y, Kataoka K. Preclinical and clinical studies of anticancer agent-incorporating polymer micelles. *Cancer Science* 100(4), 572-579 (2009).
41. Carney DN. Chemotherapy in the management of patients with inoperable non-small cell lung cancer. *Seminars in Oncology* 23(6), 71-75 (1996).
42. Khayat D, Antoine EC, Coeffic D. Taxol in the management of cancers of the breast and the ovary. *Cancer Investigation* 18(3), 242-260 (2000).
43. Weiss RB, Donehower RC, Wiernik PH *et al.* Hypersensitivity reactions from taxol. *Journal of Clinical Oncology* 8(7), 1263-1268 (1990).
44. Arany I, Safirstein RL. Cisplatin nephrotoxicity. *Seminars in Nephrology* 23(5), 460-464 (2003).
45. Cleare MJ, Hydes PC, Malerbi BW *et al.* Anti-tumour platinum complexes : Relationships between chemical properties and activity. *Biochimie* 60(9), 835-850 (1978).
46. Jin Y, Cai XY, Shi YX *et al.* Comparison of five cisplatin-based regimens frequently used as the first-line protocols in metastatic nasopharyngeal carcinoma. *Journal of Cancer Research in Clinical Oncology* 10(10) (2012).
47. Bellmunt J, Ribas A, Eres N *et al.* Carboplatin-based versus cisplatin-based chemotherapy in the treatment of surgically incurable advanced bladder carcinoma. *Cancer* 80(10), 1966-1972 (1997).
48. Koizumi F, Kitagawa M, Negishi T *et al.* Novel SN-38-Incorporating polymeric micelles, NK012, eradicate vascular endothelial growth factor-secreting bulky tumors. *Cancer Research* 66(20), 10048-10056 (2006).
49. Alexandridis P, Lindman B. Amphiphilic block copolymers: Self-assembly and applications. Elsevier. (2000).
50. Liu L, Li C, Li X *et al.* Biodegradable polylactide/poly(ethylene glycol)/polylactide triblock copolymer micelles as anticancer drug carriers. *Journal of Applied Polymer Science* 80(11), 1976-1982 (2001).
51. Lo CL, Huang CK, Lin KM *et al.* Mixed micelles formed from graft and diblock copolymers for application in intracellular drug delivery. *Biomaterials* 28(6), 1225-1235 (2007).

52. Li YY, Zhang XZ, Cheng H *et al.* Self-assembled, thermosensitive PCL-g-P(NIPAAm-co-HEMA) micelles for drug delivery. *Macromolecular Rapid Communications* 27(22), 1913-1919 (2006).
53. Changyong Choi SYC, Nah JW. Thermosensitive poly(N-isopropylacrylamide)-b-poly( $\epsilon$ -caprolactone) nanoparticles for efficient drug delivery system. *Polymer* 47(4571-4580) (2006).
54. Yokoyama M, Okano T, Sakurai Y *et al.* Introduction of cisplatin into polymeric micelle. *Journal of Controlled Release* 39(2-3), 351-356 (1996).
55. Kataoka K, Togawa H, Harada A *et al.* Spontaneous formation of polyion complex micelles with narrow distribution from antisense oligonucleotide and cationic block copolymer in physiological saline. *Macromolecules* 29(26), 8556-8557 (1996).
56. Nishiyama N, Kataoka K. Current state, achievements, and future prospects of polymeric micelles as nanocarriers for drug and gene delivery. *Pharmacology & Therapeutics* 112(3), 630-648 (2006).
57. Malmsten M, Lindman B. Self-assembly in aqueous block copolymer solutions. *Macromolecules* 25(20), 5440-5445 (1992).
58. Riess G. Micellization of block copolymers. *Progress in Polymer Science* 28(7), 1107-1170 (2003).
59. Lavasanifar A, Samuel J, Kwon GS. Poly(ethylene oxide)-block-poly(l-amino acid) micelles for drug delivery. *Advanced Drug Delivery Reviews* 54(2), 169-190 (2002).
60. Quellec P, Gref R, Dellacherie E *et al.* Protein encapsulation within poly(ethylene glycol)-coated nanospheres. II. Controlled release properties. *Journal of Biomedical Materials Research* 47(3), 388-395 (1999).
61. Xue B, Wang Y, Tang X *et al.* Biodegradable self-assembled MPEG-PCL micelles for hydrophobic oridonin delivery in vitro. *Journal of Biomedical Nanotechnology* 8(1), 80-89 (2012).
62. Xiong MP, Yáñez JA, Remsberg CM *et al.* Formulation of a geldanamycin prodrug in mPEG-b-PCL micelles greatly enhances tolerability and pharmacokinetics in rats. *Journal of Controlled Release* 129(1), 33-40 (2008).
63. Ouchi T, Miyazaki H, Arimura H *et al.* Formation of polymeric micelles with amino surfaces from amphiphilic AB-type diblock copolymers composed of poly(glycolic acid lysine) segments and polylactide segments. *Journal of Polymer Science Part A: Polymer Chemistry* 40(10), 1426-1432 (2002).
64. Mishra D, Kang HC, Bae YH. Reconstitutable charged polymeric (PLGA)2-b-PEI micelles for gene therapeutics delivery. *Biomaterials* 32(15), 3845-3854 (2011).
65. Kabanov AV, Batrakova EV, Alakhov VY. Pluronic® block copolymers as novel polymer therapeutics for drug and gene delivery. *Journal of Controlled Release* 82(2-3), 189-212 (2002).
66. Wang F, Bronich TK, Kabanov AV *et al.* Synthesis and evaluation of a star amphiphilic block copolymer from poly( $\epsilon$ -caprolactone) and poly(ethylene glycol) as a potential drug delivery carrier. *Bioconjugate Chemistry* 16(2), 397-405 (2005).
67. Zhang Y, Li X, Zhou Y *et al.* Preparation and evaluation of poly(ethylene glycol)-poly(lactide) micelles as nanocarriers for oral delivery of cyclosporine a. *Nanoscale Research Letters* 5(6), 917 - 925 (2010).

68. Hu Y, Jiang X, Ding Y *et al.* Preparation and drug release behaviors of nimodipine-loaded poly(caprolactone)–poly(ethylene oxide)–polylactide amphiphilic copolymer nanoparticles. *Biomaterials* 24(13), 2395-2404 (2003).
69. Xiong X-B, Mahmud A, Uludag H *et al.* Conjugation of arginine-glycine-aspartic acid peptides to poly(ethylene oxide)-b-poly( $\epsilon$ -caprolactone) micelles for enhanced intracellular drug delivery to metastatic tumor cells. *Biomacromolecules* 8(3), 874-884 (2007).
70. Li Y, Kwon GS. Methotrexate esters of poly(ethylene oxide)-block-poly(2-hydroxyethyl-L-aspartamide). Part I: Effects of the level of methotrexate conjugation on the stability of micelles and on drug release. *Pharmaceutical Research* 17(5), 607-611 (2000).
71. Veronese F, Harris J. Introduction and overview of peptide and protein pegylation. *Advanced Drug Delivery Reviews* 54(4), 453-456 (2002).
72. Lee ES, Na K, Bae YH. Super pH-sensitive multifunctional polymeric micelle. *Nano Letters* 5(2), 325-329 (2005).
73. Zhang C, Ding Y, Ping Q *et al.* Novel chitosan-derived nanomaterials and their micelle-forming properties. *Journal of Agricultural and Food Chemistry* 54(22), 8409-8416 (2006).
74. Qu G, Yao Z, Zhang C *et al.* PEG conjugated N-octyl-O-sulfate chitosan micelles for delivery of paclitaxel: In vitro characterization and in vivo evaluation. *European Journal of Pharmaceutical Sciences* 37(2), 98-105 (2009).
75. Houga CM, Giermanska J, Lecommandoux SB *et al.* Micelles and polymersomes obtained by self-assembly of dextran and polystyrene based block copolymers. *Biomacromolecules* 10(1), 32-40 (2008).
76. Du YZ, Weng Q, Yuan H *et al.* Synthesis and antitumor activity of stearate-g-dextran micelles for intracellular doxorubicin delivery. *ACS nano* 4(11), 6894-6902 (2010).
77. Alakhov VY, Moskaleva EY, Batrakova EV *et al.* Hypersensitization of multidrug resistant human ovarian carcinoma cells by pluronic P85 block copolymer. *Bioconjugate Chemistry* 7(2), 209-216 (1996).
78. Lu XY, Wu DC, Li ZJ *et al.* Polymer nanoparticles. *Progress in Molecular Biology and Translational Science* 104(299-323 (2011).
79. Fessi H, Puisieux F, Devissaguet JP *et al.* Nanocapsule formation by interfacial polymer deposition following solvent displacement. *International Journal of Pharmaceutics* 55(1), R1-R4 (1989).
80. Yokoyama M, Kwon GS, Okano T *et al.* Preparation of micelle-forming polymer-drug conjugates. *Bioconjugate Chemistry* 3(4), 295-301 (1992).
81. Kim JH, Emoto K, Iijima M *et al.* Core-stabilized polymeric micelle as potential drug carrier: increased solubilization of taxol. *Polymers for Advanced Technologies* 10(11), 647-654 (1999).
82. Wang YC, Liu XQ, Sun TM *et al.* Functionalized micelles from block copolymer of polyphosphoester and poly( $\epsilon$ -caprolactone) for receptor-mediated drug delivery. *Journal of Controlled Release* 128(1), 32-40 (2008).
83. Hawley AE, Illum L, Davis SS. Preparation of biodegradable, surface engineered PLGA nanospheres with enhanced lymphatic drainage and lymph node uptake. *Pharmaceutical Research* 14(5), 657-661 (1997).
84. Vangeyte P, Gautier S, Jérôme R. About the methods of preparation of poly(ethylene oxide)-b-poly( $\epsilon$ -caprolactone) nanoparticles in water: Analysis by

- dynamic light scattering. *Colloids and Surfaces A: Physicochemical and Engineering Aspects* 242(1–3), 203-211 (2004).
85. Patel S, Lavasanifar A, Choi P. Application of molecular dynamics simulation to predict the compatibility between water-insoluble drugs and self-associating poly(ethylene oxide)-b-poly( $\epsilon$ -caprolactone) block copolymers. *Biomacromolecules* 9(11), 3014-3023 (2008).
  86. Allen C, Maysinger D, Eisenberg A. Nano-engineering block copolymer aggregates for drug delivery. *Colloids and Surfaces B: Biointerfaces* 16(1–4), 3-27 (1999).
  87. Alakhov VY, Kabanov AV. Block copolymeric biotransport carriers as versatile vehicles for drug delivery. *Expert Opinion on Investigational Drugs* 7(9), 1453-1473 (1998).
  88. Kwon GS, Yokoyama M, Okano T *et al.* Biodistribution of micelle-forming polymer–drug conjugates. *Pharmaceutical Research* 10(7), 970-974 (1993).
  89. Chang KY, Lin CC, Ho GH *et al.* Synthesis and self-assembly of comb-like amphiphilic Doxifluridine–poly( $\epsilon$ -caprolactone)-graft-poly( $\gamma$ -glutamic acid) copolymer. *Polymer* 50(7), 1755-1763 (2009).
  90. Sawdon A, Peng CA. Guanosine-based antiviral acyclovir incorporated in ring-opening polymerization of  $\epsilon$ -caprolactone. *Macromolecular Research* 1-5 (2012).
  91. Wang J, Peng CA. Anticancer effectiveness of polymeric drug nanocarriers on colorectal cancer cells. *IEEE Engineering in Medicine & Biology Society* 52(10), 6090883 (2011).
  92. Petros RA, Desimone JM. Strategies in the design of nanoparticles for therapeutic applications. *Nature Reviews Drug Discovery* 9(8), 615-627 (2010).
  93. Roger E, Lagarce F, Garcion E *et al.* Biopharmaceutical parameters to consider in order to alter the fate of nanocarriers after oral delivery. *Nanomedicine* 5(2), 287-306 (2010).
  94. Brannon-Peppas L, Blanchette JO. Nanoparticle and targeted systems for cancer therapy. *Advanced Drug Delivery Reviews* 56(11), 1649-1659 (2012).
  95. Zeng F, Lee H, Chidiac M *et al.* Synthesis and characterization of six-arm star poly( $\delta$ -valerolactone)-block-methoxy poly(ethylene glycol) copolymers. *Biomacromolecules* 6(4), 2140-2149 (2005).
  96. Jette K, Law D, Schmitt E *et al.* Preparation and drug loading of poly(ethylene glycol)-block-poly( $\epsilon$ -caprolactone) micelles through the evaporation of a cosolvent azeotrope. *Pharmaceutical Research* 21(7), 1184-1191 (2004).
  97. Champion JA, Katare YK, Mitragotri S. Particle shape: A new design parameter for micro- and nanoscale drug delivery carriers. *Journal of Controlled Release* 121(1–2), 3-9 (2007).
  98. Liu Y, Tan J, Thomas A *et al.* The shape of things to come: Importance of design in nanotechnology for drug delivery. *Therapeutic Delivery* 3(2), 181-194 (2012).
  99. Stolnik S, Illum L, Davis SS. Long circulating microparticulate drug carriers. *Advanced Drug Delivery Reviews* 16(2–3), 195-214 (1995).
  100. Abra RM, Bosworth ME, Hunt CA. Liposome disposition in vivo: Effects of pre-dosing with liposomes. *Research Communications in Chemical Pathology and Pharmacology* 29(2), 349-360 (1980).
  101. Matsumura Y, Maeda H. A new concept for macromolecular therapeutics in cancer chemotherapy: Mechanism of tumoritropic accumulation of proteins and the antitumor agent SMANCS. *Cancer Research* 46, 6387-6392 (1986).

102. Maeda H, Sawa T, Konno T. Mechanism of tumor-targeted delivery of macromolecular drugs, including the EPR effect in solid tumor and clinical overview of the prototype polymeric drug SMANCS. *Journal of Controlled Release* 74(1–3), 47-61 (2001).
103. Maeda H, Greish K, Fang J. *The EPR effect and polymeric drugs: A paradigm shift for cancer chemotherapy in the 21st century*. In: *Polymer Therapeutics II*, Satchi-Fainaro R, Duncan R (Eds). Springer Berlin / Heidelberg, 103-121 (2006).
104. Hobbs SK, Monsky WL, Yuan F *et al*. Regulation of transport pathways in tumor vessels: Role of tumor type and microenvironment. *Proceedings of the National Academy of Sciences* 95(8), 4607-4612 (1998).
105. Seki T, Fang J, Maeda H. *Tumor-targeted macromolecular drug delivery based on the enhanced permeability and retention effect in solid tumor*. In: *Pharmaceutical Perspectives of Cancer Therapeutics*, Lu Y, Mahato RI (Eds). Springer US, 93-120 (2009).
106. Wu J, Akaike T, Maeda H. Modulation of enhanced vascular permeability in tumors by a bradykinin antagonist, a cyclooxygenase inhibitor, and a nitric oxide scavenger. *Cancer Research* 58(1), 159-165 (1998).
107. Wu J, Akaike T, Hayashida K *et al*. Enhanced vascular permeability in solid tumor involving peroxynitrite and matrix metalloproteinases. *Cancer Science* 92(4), 439-451 (2001).
108. Tanaka S, Akaike T, Wu J *et al*. Modulation of tumor-selective vascular blood flow and extravasation by the stable prostaglandin I<sub>2</sub> analogue beraprost sodium. *Journal of Drug Targeting* 11(1), 45-52 (2003).
109. Senger D, Galli S, Dvorak A *et al*. Tumor cells secrete a vascular permeability factor that promotes accumulation of ascites fluid. *Science* 219(4587), 983-985 (1983).
110. Dvorak HF, Brown LF, Detmar M *et al*. Vascular permeability factor/vascular endothelial growth factor, microvascular hyperpermeability, and angiogenesis. *American Journal of Pathology* 146(5), 1029-1039 (1995).
111. Fang J, Nakamura H, Maeda H. The EPR effect: Unique features of tumor blood vessels for drug delivery, factors involved, and limitations and augmentation of the effect. *Advanced Drug Delivery Reviews* 63(3), 136-151 (2011).
112. Veronese FM, Pasut G. PEGylation, successful approach to drug delivery. *Drug Discovery Today* 10(21), 1451-1458 (2005).
113. Singh P, Gupta U, Asthana A *et al*. Folate and folate-PEG-PAMAM dendrimers: Synthesis, characterization, and targeted anticancer drug delivery potential in tumor bearing mice. *Bioconjugate Chemistry* 19(11), 2239-2252 (2008).
114. Chow TH, Lin YY, Hwang JJ *et al*. Improvement of biodistribution and therapeutic index via increase of polyethylene glycol on drug-carrying liposomes in an HT-29/luc xenografted mouse model. *Anticancer Research* 29(6), 2111-2120 (2009).
115. Bohl Kullberg E, Bergstrand N, Carlsson J *et al*. Development of EGF-conjugated liposomes for targeted delivery of boronated DNA-binding agents. *Bioconjugate Chemistry* 13(4), 737-743 (2002).
116. Koo AN, Min KH, Lee HJ *et al*. Tumor accumulation and antitumor efficacy of docetaxel-loaded core-shell-corona micelles with shell-specific redox-responsive cross-links. *Biomaterials* 33(5), 1489-1499 (2012).
117. Kang JS, Deluca PP, Lee KC. Emerging PEGylated drugs. *Expert Opinon Emerging Drugs* 14(2), 363-380 (2009).

118. Greco F, Vicent MJ. Combination therapy: Opportunities and challenges for polymer–drug conjugates as anticancer nanomedicines. *Advanced Drug Delivery Reviews* 61(13), 1203-1213 (2009).
119. Yang C, Lu D, Liu Z. How PEGylation enhances the stability and potency of insulin: A molecular dynamics simulation. *Biochemistry* 50(13), 2585-2593 (2011).
120. Chapman AP. PEGylated antibodies and antibody fragments for improved therapy: A review. *Advanced Drug Delivery Reviews* 54(4), 531-545 (2002).
121. Eto Y, Yoshioka Y, Mukai Y *et al.* Development of PEGylated adenovirus vector with targeting ligand. *International Journal of Pharmacy* 354(1–2), 3-8 (2008).
122. Fisher KD, Seymour LW. HPMA copolymers for masking and retargeting of therapeutic viruses. *Advanced Drug Delivery Reviews* 62(2), 240-245 (2010).
123. Pike DB, Ghandehari H. HPMA copolymer–cyclic RGD conjugates for tumor targeting. *Advanced Drug Delivery Reviews* 62(2), 167-183 (2010).
124. Knop K, Hoogenboom R, Fischer D *et al.* Poly(ethylene glycol) in drug delivery: Pros and cons as well as potential alternatives. *Angewandte Chemie* 49(36), 6288-6308 (2010).
125. Duncan R. Polymer conjugates as anticancer nanomedicines. *Nature Reviews Cancer* 6(9), 688-701 (2006).
126. Lammers T, Ulbrich K. HPMA copolymers: 30 years of advances. *Advanced Drug Delivery Reviews* 62(2), 119-121 (2010).
127. Kopeček J, Kopečková P. HPMA copolymers: Origins, early developments, present, and future. *Advanced Drug Delivery Reviews* 62(2), 122-149 (2010).
128. Maysinger D, Berezovska O, Savic R *et al.* Block copolymers modify the internalization of micelle-incorporated probes into neural cells. *Biochimica et Biophysica Acta (BBA) - Molecular Cell Research* 1539(3), 205-217 (2001).
129. Allen C, Yu Y, Eisenberg A *et al.* Cellular internalization of PCL20-b-PEO44 block copolymer micelles. *Biochimica et Biophysica Acta (BBA) - Biomembranes* 1421(1), 32-38 (1999).
130. Luo L, Tam J, Maysinger D *et al.* Cellular internalization of poly(ethylene oxide)-b-poly( $\epsilon$ -caprolactone) diblock copolymer micelles. *Bioconjugate Chemistry* 13(6), 1259-1265 (2002).
131. Singh R, Lillard Jr JW. Nanoparticle-based targeted drug delivery. *Experimental and Molecular Pathology* 86(3), 215-223 (2009).
132. Kabanov AV, Batrakova EV, Melik-Nubarov NS *et al.* A new class of drug carriers: Micelles of poly(oxyethylene)-poly(oxypropylene) block copolymers as microcontainers for drug targeting from blood in brain. *Journal of Controlled Release* 22(2), 141-157 (1992).
133. Kabanov AV, Batrakova EV. New technologies for drug delivery across the blood brain barrier. *Current Pharmaceutical Design* 10(12), 1355-1363 (2004).
134. Pirollo KF, Chang EH. Does a targeting ligand influence nanoparticle tumor localization or uptake? *TRENDS in Biotechnology* 26(10), 552-558 (2008).
135. Lu Y, Segal E, Leamon CP *et al.* Folate receptor-targeted immunotherapy of cancer: mechanism and therapeutic potential. *Advanced Drug Delivery Reviews* 56(8), 1161-1176 (2004).
136. Qian ZM, Li H, Sun H *et al.* Targeted drug delivery via the transferrin receptor-mediated endocytosis pathway. *Pharmacological Reviews* 54(4), 561-587 (2002).

137. Laskin JJ, Sandler AB. Epidermal growth factor receptor: A promising target in solid tumours. *Cancer treatment reviews* 30(1), 1-17 (2004).
138. Vyas SP, Singh A, Sihorkar V. Ligand-receptor-mediated drug delivery: An emerging paradigm in cellular drug targeting. *Critical Reviews in Therapeutic Drug Carrier Systems* 18(1), 1-76 (2001).
139. Sudimack J, Lee RJ. Targeted drug delivery via the folate receptor. *Advanced Drug Delivery Reviews* 41(2), 147-162 (2000).
140. Byrne JD, Betancourt T, Brannon-Peppas L. Active targeting schemes for nanoparticle systems in cancer therapeutics. *Advanced Drug Delivery Reviews* 60(15), 1615-1626 (2008).
141. Klijn JGM, Berns PMJJ, Schmitz PIM *et al.* The clinical significance of epidermal growth factor receptor (EGF-R) in human breast cancer: A review on 5232 patients. *Endocrine Reviews* 13(1), 3-17 (1992).
142. Pavelic K, Banjac Z, Pavelic J *et al.* Evidence for a role of EGF receptor in the progression of human lung carcinoma. *Anticancer Research* 13(4), 1133-1137 (1993).
143. Messa C, Russo F, Caruso MG *et al.* EGF, TGF-alpha, and EGF-R in human colorectal adenocarcinoma. *Acta Oncology* 37(3), 285-289 (1998).
144. Rubin Grandis J, Melhem MF, Barnes EL *et al.* Quantitative immunohistochemical analysis of transforming growth factor-alpha and epidermal growth factor receptor in patients with squamous cell carcinoma of the head and neck. *Cancer* 78(6), 1284-1292 (1996).
145. Itakura Y, Sasano H, Shiga C *et al.* Epidermal growth factor receptor overexpression in esophageal carcinoma. An immunohistochemical study correlated with clinicopathologic findings and DNA amplification. *Cancer* 74(3), 795-804 (1994).
146. Glynn-Jones E, Goddard L, Harper ME. Comparative analysis of mrna and protein expression for epidermal growth factor receptor and ligands relative to the proliferative index in human prostate tissue. *Human Pathology* 27(7), 688-694 (1996).
147. Stumm G, Eberwein S, Rostock-Wolf S *et al.* Concomitant overexpression of the EGFR and erbB-2 genes in renal cell carcinoma (RCC) is correlated with dedifferentiation and metastasis. *International Journal of Cancer* 69(1), 17-22 (1996).
148. Yarden Y. The EGFR family and its ligands in human cancer: signalling mechanisms and therapeutic opportunities. *European Journal of Cancer* 37, Supplement 4(0), 3-8 (2001).
149. Eccles SA. Cell biology of lymphatic metastasis. The potential role of c-erbB oncogene signalling. *Recent Results Cancer Research* 157(41-54) (2000).
150. Schreiber A, Winkler M, Derynck R. Transforming growth factor-alpha: a more potent angiogenic mediator than epidermal growth factor. *Science* 232(4755), 1250-1253 (1986).
151. Sato JD, Kawamoto T, Le AD *et al.* Biological effects in vitro of monoclonal antibodies to human epidermal growth factor receptors. *Molecular Biology in Medicine* 1(5), 511-529 (1983).
152. Sebastian S, Settleman J, Reshkin SJ *et al.* The complexity of targeting EGFR signalling in cancer: From expression to turnover. *Biochimica et Biophysica Acta (BBA) - Reviews on Cancer* 1766(1), 120-139 (2006).



153. Kamath S, Buolamwini JK. Targeting EGFR and HER-2 receptor tyrosine kinases for cancer drug discovery and development. *Medicinal Research Reviews* 26(5), 569-594 (2006).
154. Chen P, Cameron R, Wang J *et al.* Antitumor effects and normal tissue toxicity of <sup>111</sup>In-labeled epidermal growth factor administered to athymic mice bearing epidermal growth factor receptor-positive human breast cancer xenografts. *Journal of Nuclear Medicine* 44(9), 1469-1478 (2003).
155. Sahoo SK, Labhasetwar V. Enhanced antiproliferative activity of transferrin-conjugated paclitaxel-loaded nanoparticles is mediated via sustained intracellular drug retention. *Molecular Pharmacology* 2(5), 373-383 (2005).
156. Mendonça LS, Firmino F, Moreira JN *et al.* Transferrin receptor-targeted liposomes encapsulating anti-BCR-ABL siRNA or asODN for chronic myeloid leukemia treatment. *Bioconjugate Chemistry* 21(1), 157-168 (2009).
157. Lu T, Sun J, Chen X *et al.* Folate-conjugated micelles and their folate-receptor-mediated endocytosis. *Macromolecular Bioscience* 9(11), 1059-1068 (2009).
158. Wan Y, Zheng Y, Song X *et al.* Anti-tumor activity of biodegradable polymer-paclitaxel conjugate micelles on Lewis lung cancer mice models. *Journal of Biomaterials Science, Polymer Edition* 30(30) (2010).
159. Yue J, Liu S, Wang R *et al.* Transferrin-conjugated micelles: Enhanced accumulation and antitumor effect for transferrin-receptor-overexpressing cancer models. *Molecular Pharmaceutics* (2012).
160. Carmeliet P, Jain RK. Angiogenesis in cancer and other diseases. *Nature* 407(6801), 249-257 (2000).
161. Folkman J. Tumor angiogenesis: Therapeutic implications. *New England Journal of Medicine* 285(21), 1182-1186 (1971).
162. Bouck N, Stellmach V, Hsu SC. How tumors become angiogenic. *Advanced Cancer Research* 69(135-174) (1996).
163. Ellis LM, Hicklin DJ. VEGF-targeted therapy: Mechanisms of anti-tumour activity. *Nature Reviews Cancer* 8(8), 579-591 (2008).
164. Brooks PC, Clark RA, Cheresh DA. Requirement of vascular integrin alpha v beta 3 for angiogenesis. *Science* 264(5158), 569-571 (1994).
165. Brooks PC, Montgomery AM, Rosenfeld M *et al.* Integrin alpha v beta 3 antagonists promote tumor regression by inducing apoptosis of angiogenic blood vessels. *Cell* 79(7), 1157-1164 (1994).
166. Mickler FM, Vachutinsky Y, Oba M *et al.* Effect of integrin targeting and PEG shielding on polyplex micelle internalization studied by live-cell imaging. *Journal of Controlled Release* 156(3), 364-373 (2011).
167. Evans EA. *Structure and deformation properties of red blood cells: Concepts and quantitative methods*. In: *Methods Enzymol.*, Sidney Fleischer BF (Ed.). Academic Press, 3-35 (1989).
168. Finlay BB, Mcfadden G. Anti-immunology: Evasion of the host immune system by bacterial and viral pathogens. *Cell* 124(4), 767-782 (2006).
169. Swann JB, Smyth MJ. Immune surveillance of tumors. *Journal of Clinical Investigation* 117(5), 1137-1146 (2007).
170. Ricklin D, Hajishengallis G, Yang K *et al.* Complement: A key system for immune surveillance and homeostasis. *Nature Immunology* 11(9), 785-797 (2010).
171. Klein G. Immune and non-immune surveillance in cancer. *Atlas of Genetics and Cytogenetics in Oncology and Haematology* 17, 114-147 (2013).

172. Chen K, Xu W, Wilson M *et al.* Immunoglobulin D enhances immune surveillance by activating antimicrobial, proinflammatory and B cell-stimulating programs in basophils. *Nature Immunology* 10(8), 889-898 (2009).
173. Chin AI, Miyahira AK, Covarrubias A *et al.* Toll-like receptor 3-mediated suppression of TRAMP prostate cancer shows the critical role of type I interferons in tumor immune surveillance. *Cancer Research* 70(7), 2595-2603 (2010).
174. Hu C-MJ, Fang RH, Zhang L. Erythrocyte-inspired delivery systems. *Advanced Healthcare Materials* 1(5), 537-547 (2012).
175. Sprandel U, Hubbard AR, Chalmers RA. In vitro studies on resealed erythrocyte ghosts as protein carriers. *Research in Experimental Medicine* 175(3), 239-245 (1979).
176. Bax BE, Bain MD, Talbot PJ *et al.* Survival of human carrier erythrocytes in vivo. *Clinical Science* 96(2), 171-178 (1999).
177. Ihler GM, Glew RH, Schnure FW. Enzyme loading of erythrocytes. *Proceedings of the National Academy of Sciences* 70(9), 2663-2666 (1973).
178. Godfrin Y, Horand F, Franco R *et al.* International seminar on the red blood cells as vehicles for drugs. *Expert Opinion on Biological Therapy* 12(1), 127-133 (2012).
179. Magnani M. Erythrocytes as carriers for drugs: The transition from the laboratory to the clinic is approaching. *Expert Opinion on Biological Therapy* 12(2), 137-138 (2012).
180. Domenech C, Thomas X, Chabaud S *et al.* L-asparaginase loaded red blood cells in refractory or relapsing acute lymphoblastic leukaemia in children and adults: results of the GRASPALL 2005-01 randomized trial. *British Journal Haematology* 153(1), 58-65 (2011).
181. Moran NF, Bain MD, Muqit MM *et al.* Carrier erythrocyte entrapped thymidine phosphorylase therapy for MNGIE. *Neurology* 71(9), 686-688 (2008).
182. Kim SH, Kim EJ, Hou JH *et al.* Opsonized erythrocyte ghosts for liver-targeted delivery of antisense oligodeoxynucleotides. *Biomaterials* 30(5), 959-967 (2009).
183. Byun HM, Suh D, Yoon H *et al.* Erythrocyte ghost-mediated gene delivery for prolonged and blood-targeted expression. *Gene Therapy* 11(5), 492-496 (2004).
184. Kwon YM, Chung HS, Moon C *et al.* L-asparaginase encapsulated intact erythrocytes for treatment of acute lymphoblastic leukemia (ALL). *Journal of Controlled Release* 139(3), 182-189 (2009).
185. Delcea M, Sternberg N, Yashchenok AM *et al.* Nanoplasmonics for dual-molecule release through nanopores in the membrane of red blood cells. *ACS Nano* 6(5), 4169-4180 (2012).
186. Cinti C, Taranta M, Naldi I *et al.* Newly engineered magnetic erythrocytes for sustained and targeted delivery of anti-cancer therapeutic compounds. *PloS one* 6(2), 0017132 (2011).
187. Lejeune A, Poyet P, Gaudreault RC *et al.* Nanoerythrocytes, a new derivative of erythrocyte ghost: III. Is phagocytosis involved in the mechanism of action? *Anticancer Research* 17(5A), 3599-3603 (1997).
188. Hu C-MJ, Zhang L, Aryal S *et al.* Erythrocyte membrane-camouflaged polymeric nanoparticles as a biomimetic delivery platform. *Proceedings of the National Academy of Sciences* 108(27), 10980-10985 (2011).

189. Zaitsev S, Danielyan K, Murciano JC *et al.* Human complement receptor type 1–directed loading of tissue plasminogen activator on circulating erythrocytes for prophylactic fibrinolysis. *Blood* 108(6), 1895-1902 (2006).
190. Chambers E, Mitragotri S. Long circulating nanoparticles via adhesion on red blood cells: Mechanism and extended circulation. *Experimental Biology and Medicine* 232(7), 958-966 (2007).
191. Marin V, Dander E, Biagi E *et al.* Characterization of in vitro migratory properties of anti-CD19 chimeric receptor-redirected CIK cells for their potential use in B-ALL immunotherapy. *Experimental Hematology* 34(9), 1218-1228 (2006).
192. Chan JK, Hamilton CA, Cheung MK *et al.* Enhanced killing of primary ovarian cancer by retargeting autologous cytokine-induced killer cells with bispecific antibodies: A preclinical study. *Clinical Cancer Research* 12(6), 1859-1867 (2006).
193. Mesiano G, Todorovic M, Gammaitoni L *et al.* Cytokine-induced killer (CIK) cells as feasible and effective adoptive immunotherapy for the treatment of solid tumors. *Expert Opinion on Biological Therapy* 12(6), 673-684 (2012).
194. Koh MBC, Ching Linn Y. Clinical expansion of cytokine induced killer (CIK) cells. *ISBT Science Series* 7(1), 154-156 (2012).
195. Verneris MR, Baker J, Edinger M *et al.* Studies of ex vivo activated and expanded CD8<sup>+</sup> NK-T cells in humans and mice. *Journal of Clinical Immunology* 22(3), 131-136 (2002).
196. Kerkar SP, Muranski P, Kaiser A *et al.* Tumor-specific CD8<sup>+</sup> T cells expressing interleukin-12 eradicate established cancers in lymphodepleted hosts. *Cancer Research* 70(17), 6725-6734 (2010).
197. Kloss CC, Condomines M, Cartellieri M *et al.* Combinatorial antigen recognition with balanced signaling promotes selective tumor eradication by engineered T cells. *Nature Biotechnology* 31(1), 71-75 (2013).
198. Qiao L, Xu Z, Zhao T *et al.* Suppression of tumorigenesis by human mesenchymal stem cells in a hepatoma model. *Cell Research* 18(4), 500-507 (2008).
199. Menon LG, Picinich S, Koneru R *et al.* Differential gene expression associated with migration of mesenchymal stem cells to conditioned medium from tumor cells or bone marrow cells. *Stem Cells* 25(2), 520-528 (2007).
200. Chen X, Lin X, Zhao J *et al.* A tumor-selective biotherapy with prolonged impact on established metastases based on cytokine gene-engineered MSCs. *Molecular Therapy* 16(4), 749-756 (2008).
201. Okada H, Pollack IF. Cytokine gene therapy for malignant glioma. *Expert Opinion on Biological Therapy* 4(10), 1609-1620 (2004).
202. Danks MK, Yoon KJ, Bush RA *et al.* Tumor-targeted enzyme/prodrug therapy mediates long-term disease-free survival of mice bearing disseminated neuroblastoma. *Cancer Research* 67(1), 22-25 (2007).
203. Aboody KS, Brown A, Rainov NG *et al.* Neural stem cells display extensive tropism for pathology in adult brain: Evidence from intracranial gliomas. *Proceedings of the National Academy of Sciences* 97(23), 12846-12851 (2000).
204. Kosaka H, Ichikawa T, Kurozumi K *et al.* Therapeutic effect of suicide gene-transferred mesenchymal stem cells in a rat model of glioma. *Cancer Gene Therapy* 19(8), 572-578 (2012).

205. Fei S, Qi X, Kedong S *et al.* The antitumor effect of mesenchymal stem cells transduced with a lentiviral vector expressing cytosine deaminase in a rat glioma model. *Journal of Cancer Research and Clinical Oncology* 138(2), 347-357 (2012).
206. Mori K, Iwata J, Miyazaki M *et al.* Bystander killing effect of thymidine kinase gene-transduced adult bone marrow stromal cells with ganciclovir on malignant glioma cells. *Neurologia Medico-chirurgica* 50(7), 545-553 (2010).
207. Pain D, Das PK, Ghosh P *et al.* Increased circulatory half-life of liposomes after conjunction with dextran. *Journal of Biosciences* 6(6), 811-816 (1984).
208. Sarwat F, Ul Qader SA, Aman A *et al.* Production & characterization of a unique dextran from an indigenous *Leuconostoc mesenteroides* CMG713. *International Journal of Biological Sciences* 4(6), 379-386 (2008).
209. Mccahon R, Hardman J. Pharmacology of plasma expanders. *Anaesthesia and Intensive Care Journal* 11(2), 75-77 (2010).
210. Tu J, Zhong S, Li P. Studies on Acyclovir–dextran conjugate: Synthesis and pharmacokinetics. *Drug Development and Industrial Pharmacy* 30(9), 959-965 (2004).
211. Ma WJ, Yuan XB, Kang CS *et al.* Evaluation of blood circulation of polysaccharide surface-decorated PLA nanoparticles. *Carbohydrate Polymers* 72(1), 75-81 (2008).
212. Passirani C, Barratt G, Devissaguet JP *et al.* Long-circulating nanoparticles bearing heparin or dextran covalently bound to poly(methyl methacrylate). *Pharmaceutical Research* 15(7), 1046-1050 (1998).
213. Chao Y, Makale M, Karmali PP *et al.* Recognition of dextran–superparamagnetic iron oxide nanoparticle conjugates (Feridex) via macrophage scavenger receptor charged domains. *Bioconjugate Chemistry* 23(5), 1003-1009 (2012).
214. Peer D, Margalit R. Loading mitomycin C inside long circulating hyaluronan targeted nano-liposomes increases its antitumor activity in three mice tumor models. *International Journal of Cancer* 108(5), 780-789 (2004).
215. Alcami A, Koszinowski UH. Viral mechanisms of immune evasion. *Immunology Today* 21(9), 447-455 (2000).
216. Rema RB, Rajendran K, Ragnathan M. Angiogenic efficacy of Heparin on chick chorioallantoic membrane. *Vascular Cell* 4(1), 4-8 (2012).
217. Berry D, Shriver Z, Natke B *et al.* Heparan sulphate glycosaminoglycans derived from endothelial cells and smooth muscle cells differentially modulate fibroblast growth factor-2 biological activity through fibroblast growth factor receptor-1. *Biochemical Journal* 373(241-249 (2003).
218. Moghimi SM, Hunter AC, Murray JC. Long-circulating and target-specific nanoparticles: Theory to practice. *Pharmacological Reviews* 53(2), 283-318 (2001).
219. Kemp MM, Linhardt RJ. Heparin-based nanoparticles. *Wiley Interdisciplinary Reviews Nanomedicine and Nanobiotechnology* 2(1), 77-87 (2010).
220. Nguyen TH, Kim SH, Decker CG *et al.* A heparin-mimicking polymer conjugate stabilizes basic fibroblast growth factor. *Nature Chemistry* 5(3), 221-227 (2013).
221. Oldenborg PA, Zheleznyak A, Fang YF *et al.* Role of CD47 as a marker of self on red blood cells. *Science* 288(5473), 2051-2054 (2000).

222. Khandelwal S, Van Rooijen N, Saxena Rajiv k. Reduced expression of CD47 during murine red blood cell (RBC) senescence and its role in RBC clearance from the circulation. *Transfusion* 47(9), 1725-1732 (2007).
223. Soto-Pantoja DR, Stein EV, Rogers NM *et al.* Therapeutic opportunities for targeting the ubiquitous cell surface receptor CD47. *Expert Opinion Therapeutic Targets* 17(1), 89-103 (2013).
224. Brown EJ, Frazier WA. Integrin-associated protein (CD47) and its ligands. *Trends in Cell Biology* 11(3), 130-135 (2001).
225. Oldenborg PA. CD47: A cell surface glycoprotein which regulates multiple functions of hematopoietic cells in health and disease. *ISRN Hematology* 2013(1-19 (2013).
226. Hsu YC, Acuña M, Tahara S *et al.* Reduced phagocytosis of colloidal carriers using soluble CD47. *Pharmaceutical Research* 20(10), 1539-1542 (2003).
227. Tsai RK, Discher DE. Inhibition of "self" engulfment through deactivation of myosin-II at the phagocytic synapse between human cells. *Journal of Cell Biology* 180(5), 989-1003 (2008).
228. Rodriguez PL, Harada T, Christian DA *et al.* Minimal "Self" peptides that inhibit phagocytic clearance and enhance delivery of nanoparticles. *Science* 339(6122), 971-975 (2013).
229. Who. Cancer Fact Sheet. *Cancer* 2011(November 3, 2014), (2014).

## CHAPTER 2: POLYMERIC MICELLES FOR ACYCLOVIR DRUG DELIVERY<sup>2</sup>

### 2.1. ABSTRACT

Polymeric prodrug micelles for delivery of acyclovir (ACV) were synthesized. First, ACV was used directly to initiate ring-opening polymerization of  $\epsilon$ -caprolactone to form ACV-polycaprolactone (ACV-PCL). Through conjugation of hydrophobic ACV-PCL with hydrophilic methoxy poly(ethylene glycol) (MPEG) or chitosan, polymeric micelles for drug delivery were formed. <sup>1</sup>H NMR, FTIR, and gel permeation chromatography were employed to show successful conjugation of MPEG or chitosan to hydrophobic ACV-PCL. Through dynamic light scattering, zeta potential analysis, transmission electron microscopy, and critical micelle concentration (CMC), the synthesized ACV-tagged polymeric micelles were characterized. It was found that the average size of the polymeric micelles was under 200 nm and the CMCs of ACV-PCL-MPEG and ACV-PCL-chitosan were 2.0 mg L<sup>-1</sup> and 6.6 mg L<sup>-1</sup>, respectively. The drug release kinetics of ACV was investigated and cytotoxicity assay demonstrates that ACV-tagged polymeric micelles were non-toxic.

### 2.2. INTRODUCTION

Due to the fact that nanoparticles can be prepared using a variety of polymers, biodegradable polymers have been extensively studied for the field of polymer therapeutics [1-3]. While there have been many biodegradable polymeric nanoparticles synthesized for drug delivery, polymeric micelles have numerous advantages over other proposed colloidal delivery systems [4-7]. Many studies have shown the promise micelles have for drug delivery because they can be tailored for prolonged blood circulation time, cellular selectivity, and for their

<sup>2</sup>The material contained in this chapter was previously published in *Macromolecular Research* 20, (2012) 1-4, and *Colloids and Surfaces B: Biointerfaces* 122 (2014) 738-45.

controlled release capabilities [8-10]. In addition, micelles can be specifically synthesized to increase a drug's solubility and bioavailability [11-14].

Acyclovir (ACV) is a guanosine-based prodrug most commonly used for the treatment of infections caused by herpes simplex virus (HSV) type 1 and 2, varicella zoster virus and, to a lesser extent, cytomegalovirus and Epstein-Barr virus [15]. Moreover, prodrug ACV can be converted to its cytotoxic phosphorylated form by herpes simplex virus thymidine kinase (HSV-TK) gene for cancer therapy [16]. That is, if the HSV-TK gene is delivered to actively dividing cancer cells, and ACV is subsequently administered to the cells, the TK enzyme phosphorylates ACV, yielding toxic metabolites which cause death in prodrug treated HSV-TK expressing cells [17-19]. However, due to ACV's poor water solubility and ensuing low bioavailability, alternative delivery approaches are required to increase the therapeutic potential of ACV. Several methods reported are to couple ACV to biocompatible hydrophilic polymers [20-22] or encapsulation into drug carriers [23-25]. Although these processes increase the bioavailability of ACV as well as offer a practical treatment for patients, they are labor-intensive and cost-ineffective. As a first step towards the formation of ACV-tagged polymeric micelles, we developed a novel technique for direct synthesis of ACV-PCL through the ring-opening polymerization of  $\epsilon$ -caprolactone ( $\epsilon$ -CL).

Polymeric micelles consist of an inner core made of a hydrophobic block copolymer and an outer corona made of the hydrophilic block of the copolymer. PCL, having been widely used as the core-forming hydrophobic segment of nanoparticles, was selected as the model polymer for this study. PCL is a semi-crystalline, linear resorbable aliphatic polyester. It has been commonly used in drug delivery systems because it is biodegradable and biocompatible. [26-28] PCL is commonly synthesized by ring-opening polymerization of  $\epsilon$ -CL using an alcohol as an initiator and stannous (II) octoate ( $\text{Sn}(\text{Oct})_2$ ) as a catalyst [29, 30]. In addition to using alcohol as the initiator, methoxy-poly(ethylene oxide) and starch have been employed as macroinitiators to form amphiphilic polymers. [31,

32]. In this study, prodrug ACV possessing hydroxyl groups was used as the initiator to obtain prodrug-PCL. Then, a hydrophilic compound (MPEG or chitosan) was grafted on the hydrophobic prodrug-PCL to form the amphiphilic block copolymer which already has the drug attached started from the ring-opening polymerization. These synthesized ACV-tagged amphiphilic polymers can self-assemble in aqueous medium to form polymeric prodrug micelles for use as nanocarriers in drug delivery.

Individual conjugation of ACV-PCL to a wide array of biocompatible hydrophilic polymers to form polymeric micelles each has their own advantages for drug delivery. With this in mind, we choose to assess the successful conjugation of two model hydrophilic polymers, MPEG and chitosan, to hydrophobic ACV-PCL. Chitosan is a natural polysaccharide derived from deacetylation of chitin. Chitosan's biocompatible and biodegradable features have attracted much attention in biomedical and pharmaceutical research [27, 33]. Similarly, MPEG is a biocompatible hydrophilic polymer commonly used in polymeric micelle formation. MPEG is inexpensive, non-toxic and is widely used to covalently modify biological macromolecules and surfaces [10, 34, 35]. Hence, ACV-PCL-MPEG and ACV-PCL-chitosan copolymers were synthesized. The chemical structure and physical properties of the copolymers were characterized and micelle formation investigated. The drug release profiles of ACV from polymeric prodrug micelles and the biocompatibility of polymeric prodrug micelles were investigated in this study.

## 2.3. MATERIALS AND METHODS

### 2.3.1. *Materials*

ACV was purchased from TCI (Tokyo, Japan). N,N'-dicyclohexyl carbodiimide (DCC),  $\epsilon$ -CL, pyrene, and succinic anhydride were purchased from Acros Organics (Geel, Belgium). Sn(Oct)<sub>2</sub>, CDCl<sub>3</sub> with 1% tetramethylsilane (TMS), deuterated dimethyl sulfoxide (DMSO-d<sub>6</sub>), dimethyl sulfoxide (DMSO), tetrahydrofuran (THF), dichloromethane (DCM), methanol, 2-propanol, hexane,



toluene, methoxypolyethylene glycol amine (MPEG-NH<sub>2</sub>; MW = 5,000), and chitosan oligosaccharide lactate (MW = 5,000) were all purchased from Sigma-Aldrich (St. Louis, MO). Ethyl ether was purchased from J.T. Baker (Austin, TX). N-Hydroxysuccinimide (NHS) was purchased from Alfa Aesar (Ward Hill, MA). Acetone was purchased from Pharmco-AAPER (Shelbyville, KY). Pyridine and hydrochloric acid (HCl) were purchased from EMD (Philadelphia, PA). Sodium chloride (NaCl) and magnesium sulfate were purchased from Showa (Tokyo, Japan). All reagents were used as received without further purification.

### 2.3.2. *Characterization methods*

Gel permeation chromatography (GPC) analyses were performed on a Waters 1525 binary HPLC pump equipped with a Waters 2414 refractive index detector (Milford, MA). Waters styragel HR 3 (MW = 500 – 30,000) and HR 4E (MW = 50 – 100,000) columns were equipped. Molecular weight calibration was performed with polystyrene standards that covered a MW range of 400 –  $4.3 \times 10^4$ . GPC analyses were performed in THF at a flow rate of 1 mL min<sup>-1</sup> with an injected volume of 50  $\mu$ l. <sup>1</sup>H NMR spectra were obtained from a Varian Unity/Inova 400 MHz instrument (Sparta, NJ). To obtain FTIR spectra by a Jasco FTIR-4200 spectrometer (Tokyo, Japan), a small amount of polymeric sample was loaded onto a silicon wafer and THF was added dropwise to dissolve the sample and evaporated afterwards. This was repeated until the entire sample was dissolved and a film had formed.

### 2.3.3. *Synthesis of ACV-tagged amphiphilic polymers*

ACV (50 mg) was weighed and mixed with  $\epsilon$ -CL (2.25 mL) under a sonication bath for 5 min at room temperature. Sn(Oct)<sub>2</sub> (0.5 wt% of  $\epsilon$ -CL) was then added into the mixture. The entire solution was placed into a 3-necked round-bottom flask. The system was purged with nitrogen and immersed in an oil bath at 140°C for 24 h. The crude product was cooled to room temperature, dissolved in DCM,

and precipitated by cold methanol. The product was then vacuum dried by a rotary evaporator at 40°C.

ACV-PCL (0.5 mmol) and succinic anhydride (1 mmol) were weighed and dissolved in toluene in a 3-necked round-bottom flask. One mmol pyridine was added and the solution was reacted under nitrogen at 70°C for 48 h. The product was then precipitated by cold hexane, and spun down. The pellet was re-dissolved in DCM and washed twice each with 10% (v/v) HCl and saturated NaCl solution. The organic phase was isolated and dried with magnesium sulfate then filtered. The carboxylated ACV-PCL was recovered by precipitation in cold hexane and then vacuum dried by rotary evaporation at 40°C.

ACV-PCL-COOH (0.54 mmol) and NHS (2.7 mmol) were weighed and mixed in 15 mL DCM, and then DCC (2.7 mmol) was added. The reaction was run under a nitrogen environment at room temperature for 24 h. The precipitated byproduct 1,3-dicyclohexylurea was removed by vacuum filtration. The filtrate was added into 35 mL diethyl ether and cooled to 4°C for 4 h to precipitate ACV-PCL-NHS. The precipitate was collected by centrifugation at 3,500 rpm for 5 min, washed with 2-propanol and solvent removed by rotary evaporation at 40°C.

ACV-PCL-NHS (10 mg) and MPEG-NH<sub>2</sub> (10 mg) were weighed and dissolved by 20 mL DCM in a round-bottom flask. The flask was purged with nitrogen and the solution was stirred for 24 h. The solution was then dialyzed (MWCO = 6-8 kD, Spectra/Por, Rancho Dominguez, CA) against pure DCM to remove remaining MPEG-NH<sub>2</sub>. ACV-PCL-MPEG was recovered by rotary evaporation at 40°C.

ACV-PCL-NHS (10 mg) was dissolved in 5 mL acetone and slowly added to chitosan solution (20 mg chitosan oligosaccharide lactate dissolved in 25 mL deionized water). The mixture, purged with nitrogen, was stirred in a round-bottom flask for 24 h. The reacted solution was vacuum dried to remove acetone and then lyophilized. The amphiphilic polymer was then dissolved in DCM and

dialyzed (MWCO = 6-8 kD, Spectra/Por) against pure DCM to remove unreacted chitosan. ACV-PCL-chitosan was recovered by rotary evaporation at 40°C.

#### 2.3.4. *Preparation of polymeric prodrug micelles*

ACV-PCL-MPEG and ACV-PCL-chitosan micelles were formed similarly. Briefly, 10 mg of ACV-tagged amphiphilic polymer was dissolved in 2 mL acetone. The solution was then added dropwise to 10 mL deionized water under sonication. Acetone was removed by rotary evaporation and the final solution was collected by filtering through a 0.45 µm filter.

#### 2.3.5. *Determination of critical micelle concentration*

The CMC was estimated by using pyrene as a fluorescent probe [36]. Briefly, 1 mg mL<sup>-1</sup> of polymeric prodrug micelle was formed. Various amounts of deionized water and micellar solution were added respectively to glass vials to obtain micellar concentrations ranging from 5 × 10<sup>-7</sup> to 1 mg mL<sup>-1</sup>. Pyrene in acetone was then added separately to the prepared vials to get a final concentration of pyrene in water of 6.0 × 10<sup>-7</sup> mg mL<sup>-1</sup>, slightly lower than the saturation solubility of pyrene in water [37]. The solutions were then allowed to equilibrate for 8 h. Fluorescent spectra were determined by a plate reader (Synergy MX, BioTek, Winooski, VT) with an excitation wavelength of 334 nm.

#### 2.3.6. *Size and morphology of polymeric prodrug micelles*

The average particle size of polymeric prodrug micelles was determined by a dynamic light scattering (DLS) instrument (Zetasizer Nano ZS, Malvern Instruments, United Kingdom) equipped with a red laser at a wavelength of 633 nm and scattering angle of 90° at 25°C. The zeta potential of the micelles dispersed in deionized water was determined with a zeta potential analyzer (Zetasizer Nano ZS). Transmission electron microscopy (TEM) image of micelles was performed on a JEM-4000FX (JEOL, Tokyo, Japan) at 80 kV. The TEM

samples were prepared by adding 10  $\mu\text{L}$  of micellar solution ( $1 \text{ mg mL}^{-1}$ ) onto a Formvar grid for 5 min and wicking away solution in excess. The samples were negatively stained with 10  $\mu\text{L}$  phosphotungstic acid solution (2 wt%) for 10 sec and then 15 sec, wicking away excess staining solution each time.

#### 2.3.7. *Drug release kinetics*

Polymeric prodrug micelles at a concentration of  $1 \text{ mg mL}^{-1}$  were made in phosphate buffered saline (PBS) (1 M, pH 7.4) at  $25^\circ\text{C}$ . Two mL of solution was placed in a dialysis tube (Float-A-Lyzer, Spectra/Por) with a MWCO of 3.5 – 5 kD. The dialysis bag was then immersed in 50 mL PBS at room temperature. At specified time intervals, 5  $\mu\text{L}$  of sample was removed and replaced with fresh PBS. The amount of ACV released was analyzed by a plate reader (BioTek) at 254 nm. All experiments were carried out in triplicate.

#### 2.3.8. *Cytotoxicity test*

24-well plates were seeded with human colorectal HT29 cells (HTB-38; ATCC, Manassas, VA) suspended in 0.5 mL Dulbecco's modified Eagles' medium (DMEM, Corning Cellgro, Manassas, VA) supplemented with 10% fetal bovine serum (FBS, Atlanta biologicals, Flowery Branch, GA) and 1% penicillin-streptomycin (Sigma) and incubated at  $37^\circ\text{C}$  in 5%  $\text{CO}_2$  balanced with humidified air for 24 h. In each well, 500  $\mu\text{L}$  of  $1 \text{ mg mL}^{-1}$  ACV-PCL-MPEG or ACV-PCL-chitosan polymeric micelles (filtered by a 0.22  $\mu\text{m}$  filter) was added. After incubation for 48 h, cell viability was assessed using MTT assay. 200  $\mu\text{L}$  of sterile MTT solution ( $4 \text{ mg mL}^{-1}$ ) was added into the culture wells and incubated for 4 h. The medium containing unreacted MTT was removed and 300  $\mu\text{L}$  DMSO was added to dissolve the insoluble purple formazan crystals formed in cellular mitochondria. The absorbance at 590 nm was measured with a plate reader (BioTek) and results were recorded as viability percentage calculated against the control group without micellar challenge. All experiments were carried out in triplicate.

## 2.4. RESULTS AND DISCUSSION

### 2.4.1. Synthesis and characterization of amphiphilic prodrug polymers

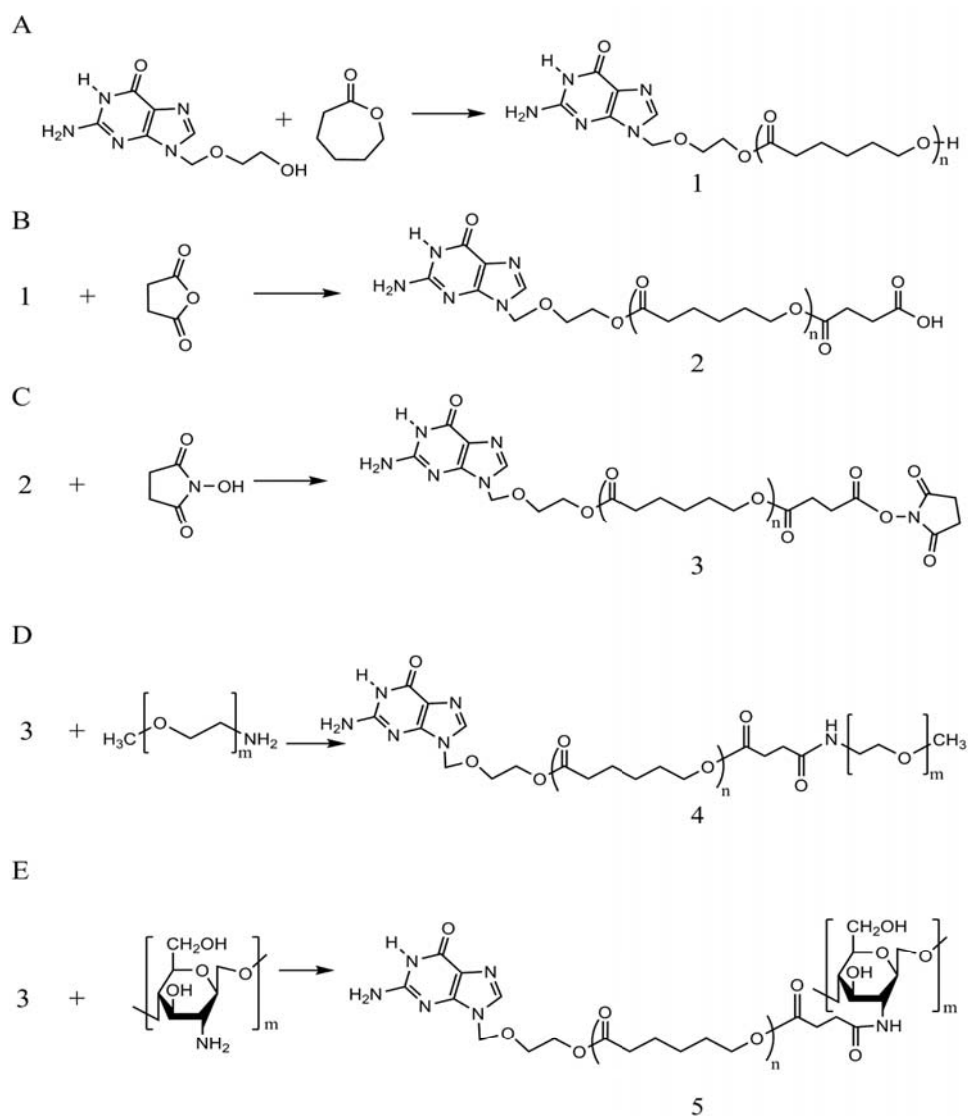


**Figure 2.1.** Synthetic scheme of (A) ACV-PCL, (B) ACV-PCL-COOH, (C) ACV-PCL-NHS, (D) ACV-PCL-MPEG, and (E) ACV-PCL-chitosan.

ACV-PCL was synthesized through ring-opening polymerization of  $\epsilon$ -CL, which was initiated exclusively by ACV (Figure 2.1 A). The  $^1\text{H}$  NMR spectra of guanosine-based prodrug ACV and ACV-PCL 24 h post-synthesis are shown in Figure 2.2 (i) and (ii), respectively. Judging from the ACV-PCL spectrum, chemical shifts at 3.75 (e, f- $\text{CH}_2$ ), 5.44 (d- $\text{CH}_2$ ), 7.68 (b-CH) were assigned to protons in ACV, while the peaks at  $\delta=1.36$  (3- $\text{CH}_2$ ), 1.64 (2- $\text{CH}_2$ ), 2.29 (1- $\text{CH}_2$ )

and 4.04 (4-CH<sub>2</sub>) correspond with the backbone chain of PCL polymer. The characteristic resonances of PCL and ACV were both observed in the synthesized polymer. Although the characteristic peaks of ACV in Figure 2.2 (ii) are much lower than those representing PCL, the evidence of coupling of ACV's protons in synthesized ACV-PCL is clear.



**Figure 2.2.** <sup>1</sup>H NMR spectra of (i) ACV and (ii) ACV-PCL.

By <sup>1</sup>H NMR spectra, the number average degree of polymerization was determined by taking the ratio of the integral values of the resonance peaks corresponding to the terminal methylene proton signal of PCL to the internal methylene proton signal of PCL according to the following equation:

$$\text{Degree of Polymerization (Xn, NMR)} = \frac{I_4 + I_{4'}}{I_{4'}} \quad (1)$$

Where  $I_4$  and  $I_{4'}$ , are the peak areas for the internal methylene protons of PCL (4.04 ppm) and the terminal methylene protons of PCL (3.63 ppm), respectively.

**Table 2.1.** Number-averaged molecular weight ( $M_n$ ) and degree of polymerization ( $X_n$ ) of ACV-PCL prepared by the ring-opening polymerization of  $\epsilon$ -CL using ACV as the initiator and  $\text{Sn}(\text{Oct})_2$  as the catalyst

Time (min)	$M_n^a$ (Da)	$X_{n, \text{GPC}}^a$	$X_{n, \text{NMR}}^b$
1440	8812	75.2	55.3
120	8356	71.2	50.3
60	8020	68.3	44.0
40	5819	49.0	42.7
30	5834	49.1	24.6
20	1388	10.2	19.8

<sup>a</sup>Calculated by GPC, <sup>b</sup>Calculated by  $^1\text{H}$  NMR

Table 2.1 summarizes the results concerning the ring-opening polymerization of ACV-PCL. It clearly indicates that polymers with high molecular weight were obtained given sufficient reaction time. The number-average molecular weight ( $M_n$ ) obtained via GPC increases as the polymerization reaches completion. By 60 min, the polymerization was unimodal and there was little change in molecular weight ( $M_w$ ) and  $M_n$  shows that the reaction is nearing completion. Degree of polymerization ( $X_{n, \text{GPC}}$ ) was obtained by GPC according to the following equation:

$$X_{n, \text{GPC}} = \frac{(M_n - M_{\text{ACV}})}{M_{\epsilon\text{-CL}}} \quad (2)$$

There is some discrepancy between the  $X_n$  obtained from GPC and NMR data. This is because GPC data was calibrated relative to polystyrene standards. It is surmised that the deviation could be decreased if attempts are made to correct the GPC data by using the Mark-Houwink equation [30, 38].

ACV-PCL was further conjugated with either MPEG or chitosan as shown in Figure 2.1 B-E. Successful conjugation of MPEG or chitosan was confirmed by

GPC,  $^1\text{H}$  NMR and FTIR analyses. The increase in  $M_n$  of ACV-PCL to 22 kDa from 17.5 kDa corresponds with the addition of MPEG (Table 2.2). Figure 2.3 shows the  $^1\text{H}$  NMR of MPEG-NH<sub>2</sub> and ACV-PCL-MPEG. The peak at 3.63 (A-OCH<sub>2</sub>) attributed to MPEG can be clearly seen in Figure 2.3 (iv). Due to the conjugation of MPEG to ACV-PCL through amide linkage (Scheme 2.1 D), the change of the peak at 1.79 (B-NH<sub>2</sub>) from a singlet in Figure 2.3 (iii) to a multiplet in Figure 2.3 (iv) further confirms conjugation of MPEG to ACV-PCL. Further characterization of successful grafting of MPEG to hydrophobic ACV-PCL was examined through FTIR analysis. FTIR spectra of ACV-PCL (A), MPEG-NH<sub>2</sub> (B) and ACV-PCL-MPEG (C) are shown in Figure 2.4. C-H stretching vibrations can be seen from 2945-2852  $\text{cm}^{-1}$  for all samples. The typical bending vibration of 1634  $\text{cm}^{-1}$  for the NH<sub>2</sub> bending amide I band can be seen in ACV-PCL and ACV-PCL-MPEG spectra, and is attributed to ACV. PCL and MPEG blocks were characterized by prominent absorptions at 1726  $\text{cm}^{-1}$  (C=O) and 1112  $\text{cm}^{-1}$  (C-O-C), respectively. These peaks are found in ACV-PCL-MPEG copolymer ascertaining successful bonding of MPEG to ACV-PCL.

**Table 2.2.** Characterization of ACV-PCL grafted with hydrophilic polymers<sup>a</sup>

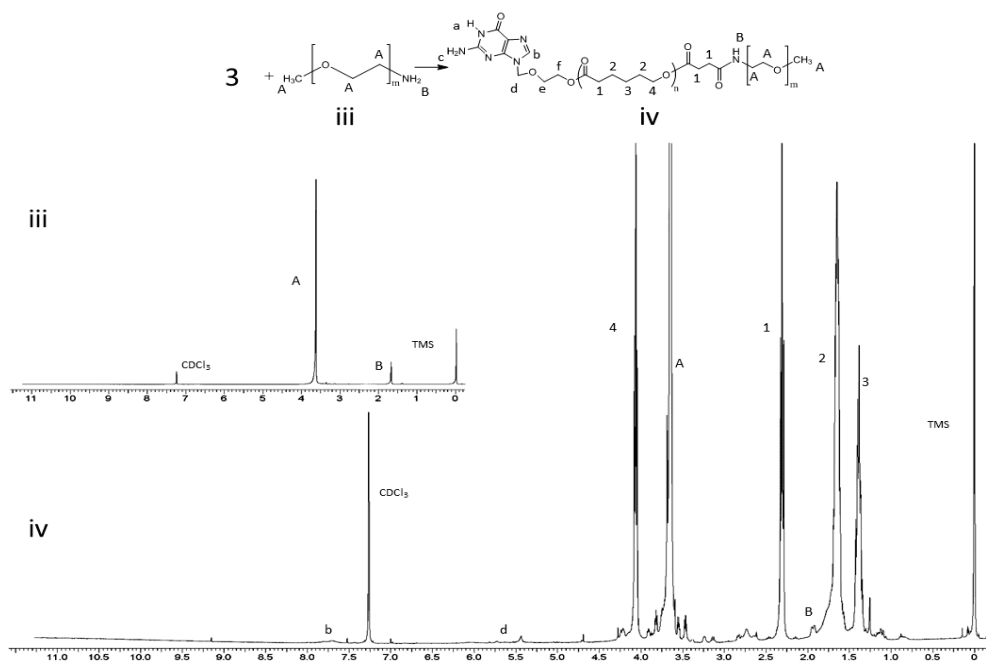
Sample	$M_w$ (Da)	$M_n$ (Da)	Polydispersity ( $M_w/M_n$ )
ACV-PCL (24 h)	28640	17491	1.64
ACV-PCL-MPEG	31746	22399	1.41
ACV-PCL-chitosan	30916	21745	1.42

<sup>a</sup>Measured by GPC

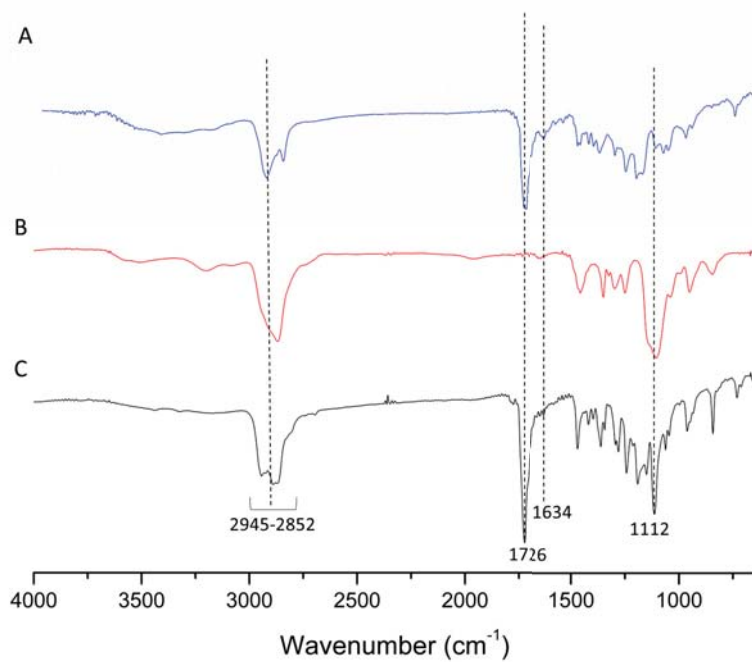
GPC analysis revealed that the  $M_n$  of ACV-PCL increased from 17.5 kDa to 21.7 kDa after grafting with chitosan and had a PDI of 1.42 (Table 2.2). Successful conjugation of chitosan to ACV-PCL was characterized similar to ACV-PCL-MPEG. Figure 2.5 reveals the  $^1\text{H}$  NMR of chitosan (v) and ACV-PCL-chitosan (vi). As shown in Scheme 2.1 E, conjugation of chitosan to ACV-PCL is made via amide linkage. The peak at 1.79 (A-NH<sub>2</sub>) from a singlet to a multiplet in



Figure 2.5 (vi) confirms conjugation of chitosan to ACV-PCL. Moreover, the peaks from the aromatic protons on C<sub>3</sub> – C<sub>6</sub> can be seen from  $\delta = 3.28 - 3.85$ , slightly shifted downward from the peaks shown in the original chitosan sample.



**Figure 2.3.** <sup>1</sup>H NMR spectra of (iii) MPEG and (iv) ACV-PCL-MPEG.



**Figure 2.4.** FTIR spectra of (A) ACV-PCL, (B) MPEG-NH<sub>2</sub>, and (C) ACV-PCL-MPEG.

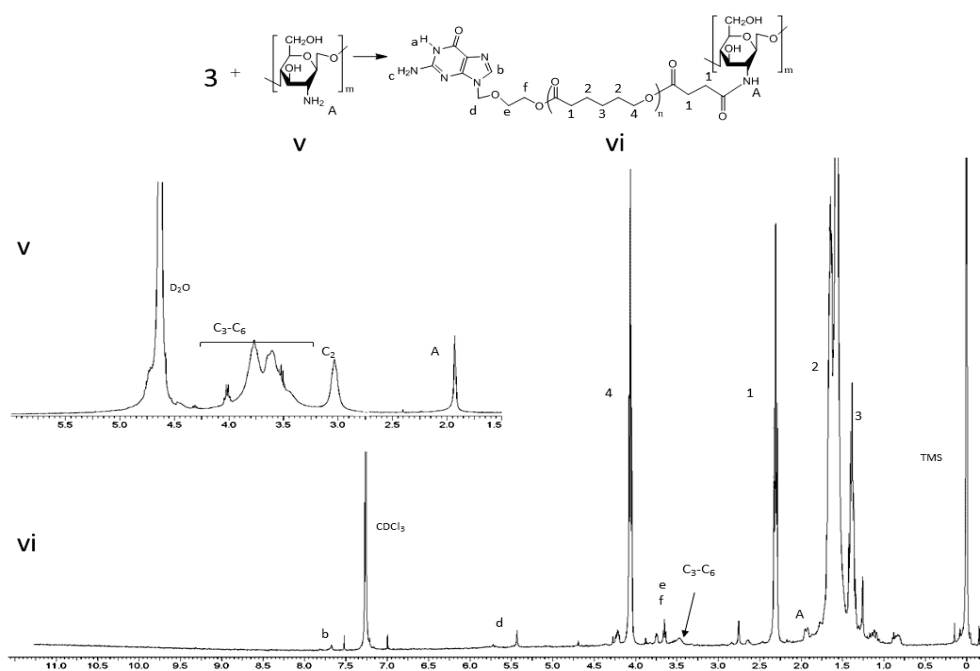


**Figure 2.5.** <sup>1</sup>H NMR spectra of (v) chitosan and (vi) ACV-PCL-chitosan.

Figure 2.6 depicts the FTIR spectra of ACV-PCL (A), chitosan (B), and ACV-PCL-chitosan (C). OH stretching from 3429 – 3167  $\text{cm}^{-1}$  as well as peaks at 1634  $\text{cm}^{-1}$  and 1521  $\text{cm}^{-1}$  corresponding to the N-H bending vibrations of the amide I and II bands are attributed to ACV and chitosan, respectively. The aforementioned peaks as well as the carbonyl absorption at 1726  $\text{cm}^{-1}$  associated with PCL and a peak at 1065  $\text{cm}^{-1}$  (C-O-C) seen in each spectra are found in ACV-PCL-chitosan. The FTIR results are in line with the results from  $^1\text{H}$  NMR and demonstrate successful synthesis of ACV-PCL-chitosan.

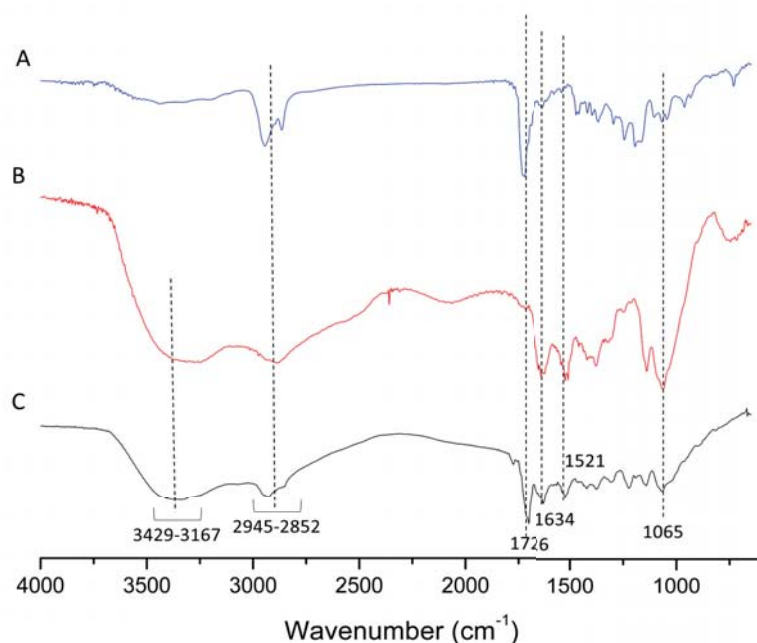


**Figure 2.6.** FTIR spectra of (A) ACV-PCL, (B) chitosan, and (C) ACV-PCL-chitosan.

#### 2.4.2. Formation and characterization of ACV-tagged polymeric micelles

Due to the amphiphilic nature of the synthesized ACV-PCL copolymers (i.e., ACV-PCL-MPEG and ACV-PCL-chitosan), they can self-assemble into polymeric prodrug micelles in aqueous medium. Here, ACV-PCL acts as the hydrophobic segment and MPEG or chitosan serve as the hydrophilic segments. Polymeric micelles of ACV-PCL copolymer were prepared via the evaporation method [39]. The CMC using pyrene as a hydrophobic fluorescent probe was carried out to

prove the formation of the micellar structures. Pyrene can preferentially partition into the interior hydrophobic microdomains and change the intensities of the first and third bands in the pyrene fluorescence spectrum [37]. For ACV-PCL-MPEG the shift found in the first and third bands was at  $I_{335}/I_{330}$  while for ACV-PCL-chitosan it was at  $I_{337}/I_{332}$ . It is believed that this change is due to different polymer compositions. Figure 2.7 A shows the CMC values of ACV-tagged polymeric micelles in aqueous medium. It was determined that the CMCs for ACV-PCL-MPEG and ACV-PCL-chitosan were 2.0 and 6.6 mg L<sup>-1</sup>, respectively (Figure 2.7 A (i) and (ii)). Kim *et al.* reported that the CMC values of block copolymers depends upon the block copolymer architecture [40]. In this study, the hydrophobic block was kept constant, as ACV-PCL, while the hydrophilic block was changed to either MPEG or chitosan. The low CMC value obtained for ACV-tagged polymeric micelles could provide evidence for their stability in dilute solutions.

In order to characterize the morphology of ACV-tagged polymeric micelles, DLS and TEM analyses were carried out. Figure 2.7 B shows the size and morphology of ACV-tagged polymeric micelles. As can be seen from DLS results, sizes of the two types of polymeric prodrug micelles were under 200 nm. ACV-PCL-MPEG (Figure 2.7 B (i)) and ACV-PCL-chitosan (Figure 2.7 B (ii)) micelles showed size distributions with mean diameters of 142.8 and 172.7 nm, respectively. The morphology of the micelles was further examined by TEM as shown in the insets of Figure 2.7 B. The size of the micelles in the TEM images was slightly lower than the results from DLS with an average particle size of ~100-150 nm. This size fluctuation is due to the fact that DLS records the hydrodynamic radius of particles which is often times slightly larger than the actual particle size. Zeta potential analysis of ACV-tagged polymeric micelles was also performed. An average zeta potential for ACV-PCL-MPEG micelles was 1.4 mV. Due to the fact that MPEG has a neutral charge, the results obtained for ACV-PCL-MPEG micelles are reasonable. In contrast, the detected zeta potential of ACV-PCL-

chitosan micelles was 32.3 mV. This is attributed to the positive charge of the hydrophilic chitosan segment deployed on micellar nanoparticles.

To determine the drug loading percentage of ACV per mg of micelle formulation, the absorbance of ACV-tagged polymeric micelles at  $t = 0$  and  $t = 48$  h was examined and compared to a standard calibration curve of ACV ranging from 0.002 to 1.0 mg/mL. It was found that ACV comprised 8.7% and 3.2% of ACV-PCL-MPEG and ACV-PCL-chitosan micelles, respectively. The difference in ACV loading percentage is due to different conditions employed for the synthesis of ACV-PCL-MPEG and ACV-PCL-chitosan amphiphilic copolymers. While MPEG-NH<sub>2</sub> can dissolve in organic solvent, chitosan requires an aqueous solvent for it to dissolve. Therefore, for ACV-PCL-chitosan synthesis, the ester bond between ACV and PCL is already weakened, thereby resulting in less ACV

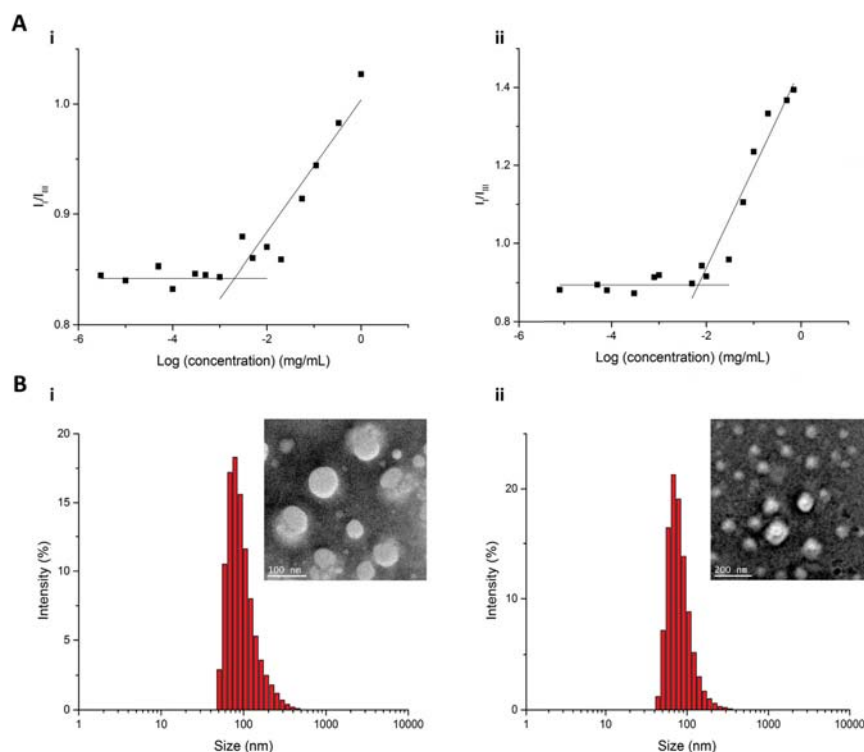


**Figure 2.7.** (A) Plot of the intensity ratio ( $I/I_{III}$ ) versus concentration of ACV-tagged polymeric micelles, and (B) particle size distribution of (i) ACV-PCL-MPEG and (ii) ACV-PCL-chitosan. Insets represent TEM images.

coupled with PCL than ACV-PCL-MPEG which is synthesized under organic solvent environment.

#### 2.4.3. *In vitro* release of ACV from polymeric micelles

The *in vitro* release behaviors of ACV from both types of polymeric prodrug micelles in PBS at 25°C were studied and the results are shown in Figure 2.8 and 2.9. A similar biphasic drug release profile of ACV-PCL-MPEG and ACV-PCL-chitosan micelles was observed, with initial burst release within the first 2 h (~50% accumulative release) followed by a sustained release pattern up to 48 h. The release of ACV from both polymeric prodrug micelles was caused by the hydrolysis of ester linkage between ACV and PCL. In the first phase, the rate of drug release from ACV-PCL-MPEG micelles was relatively rapid than that from ACV-PCL-chitosan ones. The reason for this phenomenon is speculated to be twofold. First, MPEG chains probably are more hydrophilic and flexible than chitosan chains on micellar nanoparticles, leading to a faster hydrolysis and

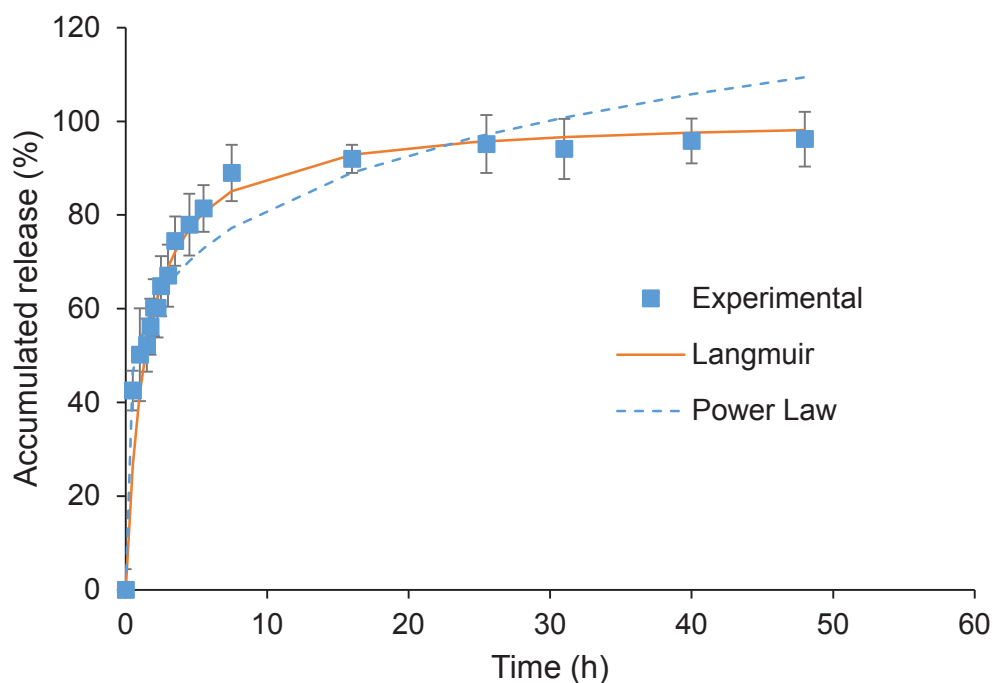


**Figure 2.8.** *In vitro* drug release profile of ACV-PCL-MPEG in PBS (mean  $\pm$  SD, n = 3).

concomitant ACV diffusion from hydrophobic PCL cores. Second, the diffusion of ACV molecules might be slowed down by the positively charged chitosan on ACV-PCL-chitosan micelles. Such different initial release trend continued and resulted in higher ACV accumulative release from ACV-PCL-MPEG micelles (96%) than from ACV-PCL-chitosan micelles (82%).

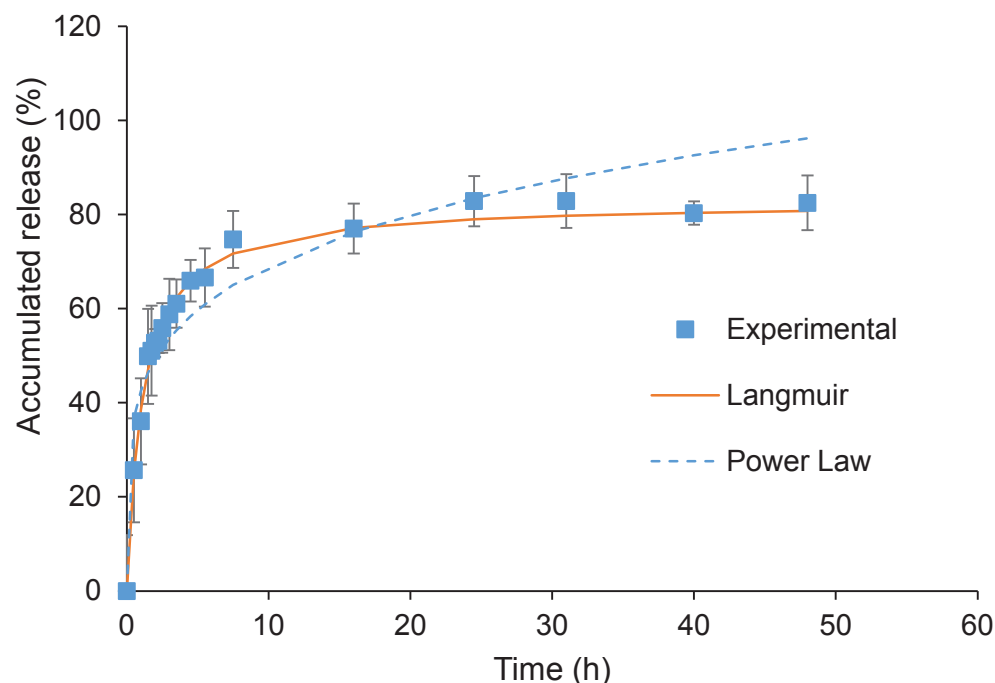


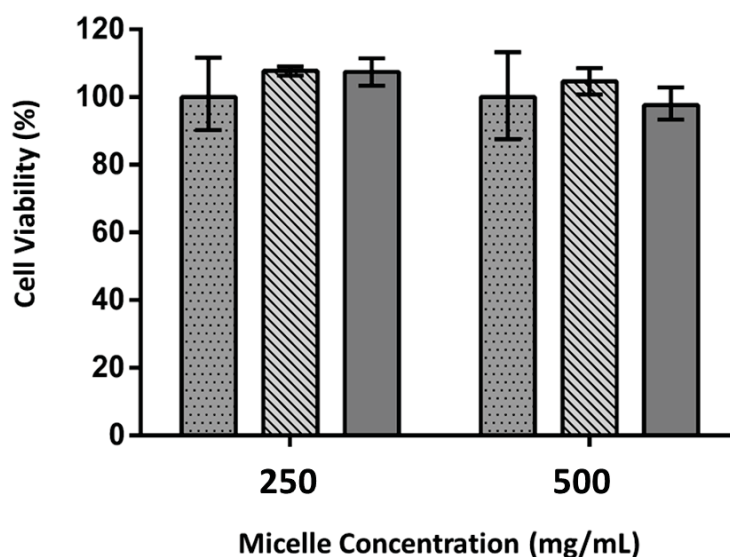
**Figure 2.9.** In vitro drug release profile of ACV-PCL-chitosan in PBS (mean  $\pm$  SD,  $n = 3$ ).




The release of ACV from the prodrug tagged micelles was modeled using both Langmuir and Power Law models. It can be seen from Figure 2.8 and 2.9, that the Power Law was not a good fit for release of ACV from polymeric micelles. Here,  $n$  was equal to 0.19 and 0.21 in ACV-PCL-MPEG and ACV-PCL-chitosan, respectively. The exponent,  $n$ , of a sphere with Fickian diffusion as the drug release mechanism is 0.43 [41], because our exponents are lower than this value, the drug release mechanism of ACV from polymeric micelles is not solely through diffusion. This makes sense seeing as we believe that the ester bond between prodrug ACV and PCL is broken via hydrolysis. Therefore, first the bond must be broken and then ACV can diffuse out of the micelle carrier. In contrast to the

Power Law, the Langmuir model fit the release of ACV from polymeric micelles well. The Langmuir model, is an enzyme kinetics model, and because ACV is released via reaction diffusion, the dissolution is taken into account with this model. Here, we found that the dissociation constant ( $K_d$ ) was equal to 1.40 and 1.14 in ACV-PCL-MPEG and ACV-PCL-chitosan, respectively.

#### 2.4.4. Cytotoxicity study

Biocompatibility is a vital necessity of polymer materials being used for drug delivery applications. To evaluate if ACV-tagged polymeric micelles showed any cytotoxicity towards HT29 colorectal cells, MTT assay was performed. As shown in Figure 2.10, the viability of HT29 cells after treatment for 48 h with either ACV-PCL-MPEG or ACV-PCL-chitosan has little change compared with the untreated control cells (i.e., cells without any micelle challenge). These results demonstrate that ACV-tagged polymeric micelles do not exhibit apparent toxicity, and are biocompatible.



**Figure 2.10.** Viability of HT29 colorectal cancer cells challenged with ACV-tagged polymeric micelles at different dosages.  Control (without micelle challenge),  ACV-PCL-MPEG micelles, and  ACV-PCL-chitosan micelles (mean  $\pm$  SD,  $n = 3$ ).



## 2.5. CONCLUSION

In this study, ACV-PCL-MPEG and ACV-PCL-chitosan polymeric micelles were synthesized and characterized. ACV was used to directly initiate polymerization of  $\epsilon$ -CL to form hydrophobic ACV-PCL. Compared to conventional methods of incorporating ACV into polymeric carriers by chemical conjugation or physical encapsulation, our approach is advantageous in terms of eliminating drug-loading steps, enhancing drug-carrying capacity, and decreasing production cost. By grafting ACV-PCL with either MPEG or chitosan, ACV-tagged amphiphilic polymers can self-assemble as micellar nanoparticles in aqueous medium. Structural analyses such as  $^1\text{H}$  NMR and FTIR were performed to confirm their conjugation. ACV-tagged polymeric micelles were found to have a mean size under 200 nm by both DLS and TEM and have a low CMC. Moreover, both ACV-PCL-MPEG and ACV-PCL-chitosan micelles were non-toxic to HT29 colorectal cells. ACV-tagged polymeric micelles are potential carriers for therapeutic and anticancer drug delivery.

## 2.6. REFERENCES

1. Corden TJ, Jones IA, Rudd CD *et al.* Physical and biocompatibility properties of poly- $\epsilon$ -caprolactone produced using in situ polymerisation: A novel manufacturing technique for long-fibre composite materials. *Biomaterials* 21(7), 713-724 (2000).
2. Duncan R, Vicent MJ. Polymer therapeutics-prospects for 21st century: The end of the beginning. *Advanced Drug Delivery Reviews* 65(1), 60-70 (2013).
3. Guan X, Quan D, Shuai X *et al.* Chitosan-graft-poly( $\epsilon$ -caprolactone)s: An optimized chemical approach leading to a controllable structure and enhanced properties. *Journal of Polymer Science Part A: Polymer Chemistry* 45(12), 2556-2568 (2007).
4. Soppimath KS, Aminabhavi TM, Kulkarni AR *et al.* Biodegradable polymeric nanoparticles as drug delivery devices. *Journal of Controlled Release* 70(1-2), 1-20 (2001).
5. Kalachandra S, Takamata T, Lin D *et al.* Stability and release of antiviral drugs from ethylene vinyl acetate (EVA) copolymer. *Journal of Materials Science: Materials in Medicine* 17(12), 1227-1236 (2006).
6. Zhang C, Ding Y, Ping Q *et al.* Novel chitosan-derived nanomaterials and their micelle-forming properties. *Journal of Agricultural and Food Chemistry* 54(22), 8409-8416 (2006).
7. Torchilin V. Micellar nanocarriers: Pharmaceutical perspectives. *Pharmaceutical Research* 24(1), 1-16 (2007).
8. Kataoka K, Harada A, Nagasaki Y. Block copolymer micelles for drug delivery: design, characterization and biological significance. *Advanced Drug Delivery Reviews* 47(1), 113-131 (2001).
9. Ashok B, Arleth L, Hjelm RP *et al.* In vitro characterization of PEGylated phospholipid micelles for improved drug solubilization: Effects of PEG chain length and PC incorporation. *Journal of Pharmaceutical Sciences* 93(10), 2476-2487 (2004).
10. Tabatabaei Rezaei SJ, Nabid MR, Niknejad H *et al.* Multifunctional and thermoresponsive unimolecular micelles for tumor-targeted delivery and site-specifically release of anticancer drugs. *Polymer* 53(16), 3485-3497 (2012).
11. Del Amo EM, Urtti A. Current and future ophthalmic drug delivery systems: A shift to the posterior segment. *Drug Discovery Today* 13(3-4), 135-143 (2008).
12. Nakanishi T, Fukushima S, Okamoto K *et al.* Development of the polymer micelle carrier system for doxorubicin. *Journal of Controlled Release* 74(1-3), 295-302 (2001).
13. Yokoyama M, Miyauchi M, Yamada N *et al.* Polymer micelles as novel drug carrier-adriamycin-conjugated poly(ethylene glycol) poly(aspartic acid) block copolymer. *Journal of Controlled Release* 11(1-3), 269-278 (1990).
14. Koizumi F, Kitagawa M, Negishi T *et al.* Novel SN-38-incorporating polymeric micelles, NK012, eradicate vascular endothelial growth factor-secreting bulky tumors. *Cancer Research* 66(20), 10048-10056 (2006).
15. Richards DM, Carmine AA, Brogden RN *et al.* Acyclovir a review of its pharmacodynamic properties and therapeutic efficacy. *Drugs* 26(5), 378-438 (1983).

16. Moolten FL, Wells JM. Curability of tumors bearing herpes thymidine kinase genes transferred by retroviral vectors. *Journal of the National Cancer Institute* 82(4), 297-300 (1990).
17. Cheon J, Kim HK, Moon DG *et al.* Adenovirus-mediated suicide-gene therapy using the herpes simplex virus thymidine kinase gene in cell and animal models of human prostate cancer: changes in tumour cell proliferative activity. *BJU International* 85(6), 759-766 (2000).
18. Chen SH, Shine HD, Goodman JC *et al.* Gene therapy for brain tumors: regression of experimental gliomas by adenovirus-mediated gene transfer in vivo. *Proceedings of the National Academy of Sciences* 91(8), 3054-3057 (1994).
19. Fillat C. Suicide gene therapy mediated by the herpes simplex virus thymidine kinase gene/ganciclovir system: Fifteen years of application. *Current Gene Therapy* 3(13-26) (2003).
20. Li X, Lu M, Wu Q *et al.* Novel designed polymer–acyclovir conjugates with linker-controlled drug release and hepatoma cell targeting. *Journal of Polymer Science Part A: Polymer Chemistry* 46(1), 117-126 (2008).
21. Tu J, Zhong S, Li P. Studies on acyclovir–dextran conjugate: Synthesis and pharmacokinetics. *Drug Development and Industrial Pharmacy* 30(9), 959-965 (2004).
22. Zacchigna M, Di Luca G, Maurich V *et al.* Syntheses, chemical and enzymatic stability of new poly(ethylene glycol)–acyclovir prodrugs. *Il Farmaco* 57(3), 207-214 (2002).
23. Genta I, Conti B, Perugini P *et al.* Bioadhesive microspheres for ophthalmic administration of acyclovir. *Journal of Pharmacy and Pharmacology* 49(8), 737-742 (1997).
24. Tao Y, Lu Y, Sun Y *et al.* Development of mucoadhesive microspheres of acyclovir with enhanced bioavailability. *International Journal of Pharmaceutics* 378(1-2), 30-36 (2009).
25. Jain SK, Gupta Y, Jain A *et al.* Enhanced transdermal delivery of acyclovir sodium via elastic liposomes. *Drug Delivery* 15(3), 141-147 (2008).
26. Li YY, Zhang XZ, Cheng H *et al.* Self-assembled, thermosensitive PCL-g-P(NIPAAm-co-HEMA) micelles for drug delivery. *Macromolecular Rapid Communications* 27(22), 1913-1919 (2006).
27. Sinha VR, Singla AK, Wadhawan S *et al.* Chitosan microspheres as a potential carrier for drugs. *International Journal of Pharmaceutics* 274(1-2), 1-33 (2004).
28. Dash TK, Konkimalla VB. Poly- $\epsilon$ -caprolactone based formulations for drug delivery and tissue engineering: A review. *Journal of Controlled Release* 158(1), 15-33 (2012).
29. Peng CL, Shieh MJ, Tsai MH *et al.* Self-assembled star-shaped chlorin-core poly( $\epsilon$ -caprolactone)–poly(ethylene glycol) diblock copolymer micelles for dual chemo-photodynamic therapies. *Biomaterials* 29(26), 3599-3608 (2008).
30. Schindler A, Hibionada YM, Pitt CG. Aliphatic polyesters. III. Molecular weight and molecular weight distribution in alcohol-initiated polymerizations of  $\epsilon$ -caprolactone. *Journal of Polymer Science: Polymer Chemistry Edition* 20(2), 319-326 (1982).
31. Aliabadi HM, Mahmud A, Sharifabadi AD *et al.* Micelles of methoxy poly(ethylene oxide)-b-poly( $\epsilon$ -caprolactone) as vehicles for the solubilization and controlled delivery of cyclosporine A. *Journal of Controlled Release* 104(2), 301-311 (2005).

32. Dubois P, Krishnan M, Narayan R. Aliphatic polyester-grafted starch-like polysaccharides by ring-opening polymerization. *Polymer* 40(11), 3091-3100 (1999).
33. Sonia T, Sharma C. Chitosan and its derivatives for drug delivery perspective. *Chitosan for Biomaterials I* 23-53 (2011).
34. Kang JS, Deluca PP, Lee KC. Emerging PEGylated drugs. *Expert Opinion on Emerging Drugs* 14(2), 363-380 (2009).
35. Calvo P, Gouritin B, Brigger I *et al.* PEGylated polycyanoacrylate nanoparticles as vector for drug delivery in prion diseases. *Journal of Neuroscience Methods* 111(2), 151-155 (2001).
36. Wilhelm M, Zhao CL, Wang Y *et al.* Poly(styrene-ethylene oxide) block copolymer micelle formation in water: a fluorescence probe study. *Macromolecules* 24(5), 1033-1040 (1991).
37. Kalyanasundaram K, Thomas JK. Environmental effects on vibronic band intensities in pyrene monomer fluorescence and their application in studies of micellar systems. *Journal of the American Chemical Society* 99(7), 2039-2044 (1977).
38. Hamaide T, Pantiru M, Fessi H *et al.* Ring-opening polymerisation of  $\epsilon$ -caprolactone with monosaccharides as transfer agents. A novel route to functionalised nanoparticles. *Macromolecular Rapid Communications* 22(9), 659-663 (2001).
39. Lu XY, Wu DC, Li ZJ *et al.* Polymer nanoparticles. *Progress in Molecular Biology and Translational Science* 104(299-323 (2011).
40. Kim KH, Cui GH, Lim HJ *et al.* Synthesis and micellization of star-shaped poly(ethylene glycol)-block-poly( $\epsilon$ -caprolactone). *Macromolecular Chemistry and Physics* 205(12), 1684-1692 (2004).
41. Siepmann J, Siepmann F. Mathematical modeling of drug delivery. *International Journal of Pharmaceutics* 364(2), 328-343 (2008).

## CHAPTER 3: GANCICLOVIR INTEGRATED POLYMERIC NANOCARRIERS FOR GENE-DIRECTED ENZYME PRODRUG THERAPY<sup>3</sup>

### 3.1. ABSTRACT

The most prominent suicide gene therapy is the use of herpes simplex virus thymidine kinase (HSV-TK) in conjunction with guanosine-based prodrug ganciclovir (GCV). This is a two-step process whereby first the gene (HSV-TK) is delivered to targeted cells and then the prodrug (GCV) is administered where it is then activated to its cytotoxic form, GCV-TP by the gene-expressed exogenous enzyme. Here, we propose a one-step delivery of gene and prodrug through polymeric micellar nanocarriers. In this study, Guanosine-based GCV was used as the initiator in ring-opening polymerization of  $\epsilon$ -caprolactone to form hydrophobic GCV-PCL which was then grafted to hydrophilic chitosan to form amphiphilic copolymers for the preparation of stable micellar nanoparticles. Successful synthesis of amphiphilic copolymers was followed by <sup>1</sup>H NMR and FTIR. Self-assembly behavior of micellar nanoparticles was determined by TEM, particle size and charge and critical micelle concentration (CMC). Polymeric nanocarriers with optimal characteristics encoded with HSV-TK plasmids were cultured with parental HT-29 colorectal cancer cells and toxicity measured. <sup>1</sup>H NMR analysis shows successful synthesis of GCV-PCL. FTIR spectra reveal characteristic absorption peaks associated with chitosan and PCL are simultaneously present in amphiphilic copolymer GCV-PCL-chitosan. CMC of GCV-PCL-chitosan copolymer was measured to be 11.2 mg L<sup>-1</sup> while size measured by dynamic light scattering was detected to be 93.4 nm, with a zeta potential of +38.5 mV. Toxicity results demonstrate that GCV-PCL-chitosan/TK nanovectors are a feasible approach to kill HT29 colon cancer cells.

### 3.2. INTRODUCTION

<sup>3</sup>The material contained in this chapter is planned for publication in *Molecules* and *Macromolecular Bioscience*.

Gene-directed enzyme prodrug therapy (GDEPT) is one of the most important and successful prodrug delivery approaches for cancer therapy. In GDEPT, a prodrug, a pharmacologically inactive molecule that requires enzymatic and/or chemical transformation to release a cytotoxic drug, is given to the patient. The prodrug contains the drug which will be used to destroy the targeted cancer cells. The gene for a foreign enzyme and the prodrug are administered in a two-step process. That is, first the foreign gene is introduced into the targeted cancer cells, expressed and released into the cytoplasm and then the prodrug is administered. The prodrug is activated by the gene-expressed exogenous enzyme and converted to its cytotoxic form [1, 2].

The most prominent GDEPT pair is the use of herpes simplex virus thymidine kinase (HSV-TK) in conjunction with a variety of guanosine-based prodrugs [3-5]. Ganciclovir (GCV) is the most widely used prodrug for HSV-TK, and is a well-known antiviral agent [3, 6-8]. The HSV-TK/GCV system has been used in the treatment of brain tumors [9, 10], colorectal tumors [11-13], and oral cancer [14]. Research has shown that HSV-TK/GCV exhibits not only direct cytotoxicity but also a bystander effect, which builds up the efficiency of the HSV-TK/GCV system in destroying malignant cells [13, 15, 16]. However, significant therapeutic benefit has yet to be demonstrated; most likely limited by inefficient gene and drug delivery to tumor cells. Most GDEPT studies, and those which have reached clinical trials, have been focused on using viral vectors to deliver the prodrug and activating gene [17, 18]. However, viruses harnessed in the gene therapy field are notorious for causing immunogenicity and tumorigenicity [19]. Safety concerns associated with viral vectors have prompted researchers to develop non-viral vectors for gene delivery.

In particular, polymeric nanoparticles have attracted attention because of their potential applications in medicine and pharmacy as drug delivery carriers. In recent years, polymeric micelles have been the focus of much interest as alternative vehicles for the solubilization of poorly water-soluble molecules

rendering clear advantages over current solubilizing agents in drug delivery [20]. Polymeric micelles are expected to withstand the diluting effect of blood, stay in a micellar form and even act as a circulating depot drug delivery system after intravenous administration. Moreover, there is no inclusion of potentially harmful surfactants and excipients in the process of encapsulating hydrophobic drug molecules. Due to the fact that micelles can be specifically synthesized to increase a drug's solubility and bioavailability, they are a model system for GDEPT [21-24].

Poly( $\epsilon$ -caprolactone) (PCL) having been widely used as the core-forming hydrophobic segment of nanoparticles was selected as the model polymer for this study. PCL is a semi-crystalline linear resorbable aliphatic polyester. It has been commonly used in drug delivery systems because it is biodegradable and biocompatible [25-27]. PCL is commonly synthesized by ring-opening polymerization of  $\epsilon$ -caprolactone using an alcohol (R-OH) as an initiator and stannous (II) octoate ( $\text{Sn}(\text{Oct})_2$ ) as a catalyst [28, 29]. In addition to using R-OH as the initiator, methoxy-poly(ethylene oxide) and starch have been employed as macroinitiators to form amphiphilic polymers [30, 31]. In this study, prodrug GCV possessing hydroxyl groups was used as the initiator to obtain GCV-PCL. Then, hydrophilic chitosan was grafted on the hydrophobic GCV-PCL to form the amphiphilic block copolymer which already has the drug attached started from the ring-opening polymerization. Chitosan is a natural polysaccharide derived from deacetylation of chitin. Chitosan's biocompatible and biodegradable features attract much attention in biomedical and pharmaceutical research [25, 31].

The synthesized GCV-tagged amphiphilic copolymer can be self-assembled in aqueous medium to form polymeric prodrug micelles and were used to evaluate anticancer effectiveness to HT29/TK cells (cells which overexpressed HSV-TK gene plasmid). Moreover, the positive charge endowed on the micelles by chitosan was used to bind HSV-TK gene plasmid onto the

micelles for a one-step GDEPT cancer therapy to parental HT29 colorectal cells. Our results indicate that GCV-PCL-chitosan/TK micelles are effective carriers for GDEPT.

### 3.3. MATERIALS AND METHODS

#### 3.3.1. *Materials*

GCV was purchased from TCI (Tokyo, Japan). N,N'-dicyclohexyl carbodiimide (DCC),  $\epsilon$ -CL, pyrene, and succinic anhydride were purchased from Acros Organics (Geel, Belgium). Sn(Oct)<sub>2</sub>, CDCl<sub>3</sub> with 1% tetramethylsilane (TMS), deuterated dimethyl sulfoxide (DMSO-d<sub>6</sub>), dimethyl sulfoxide (DMSO), tetrahydrofuran (THF), dichloromethane (DCM), methanol, 2-propanol, hexane, toluene, and chitosan oligosaccharide lactate (MW = 5,000) were all purchased from Sigma-Aldrich (St. Louis, MO). Ethyl ether was purchased from J.T. Baker (Austin, TX). N-Hydroxysuccinimide (NHS) was purchased from Alfa Aesar (Ward Hill, MA). Acetone was purchased from Pharmco-AAPER (Shelbyville, KY). Pyridine and hydrochloric acid (HCl) were purchased from EMD (Philadelphia, PA). Sodium chloride (NaCl) and magnesium sulfate were purchased from Showa (Tokyo, Japan). All reagents were used as received without further purification.

#### 3.3.2. *Characterization methods*

Gel permeation chromatography (GPC) analyses were performed on a Waters 1525 binary HPLC pump equipped with a Waters 2414 refractive index detector (Milford, MA). Waters styragel HR 3 (MW = 500 – 30,000) and HR 4E (MW = 50 – 100,000) columns were equipped. Molecular weight calibration was performed with polystyrene standards that covered a MW range of 400 –  $4.3 \times 10^4$ . GPC analyses were performed in THF at a flow rate of 1 mL min<sup>-1</sup> with an injected volume of 50  $\mu$ l. <sup>1</sup>H NMR spectra were obtained from a Varian Unity/Inova 400 MHz instrument (Sparta, NJ). To obtain FTIR spectra by a Jasco FTIR-4200 spectrometer (Tokyo, Japan), a small amount of polymeric sample was loaded



onto a silicon wafer and THF was added dropwise to dissolve the sample and evaporated afterwards. This was repeated until the entire sample was dissolved and a film had formed.

### 3.3.3. *Synthesis of GCV-tagged amphiphilic polymers*

GCV (50 mg) was weighed and mixed with  $\epsilon$ -CL (2.25 mL) under a sonication bath for 5 min at room temperature.  $\text{Sn}(\text{Oct})_2$  (0.5 wt% of  $\epsilon$ -CL) was then added into the mixture. The entire solution was placed into a 3-necked round-bottom flask. The system was purged with nitrogen and immersed in an oil bath at 140°C for 24 h. The crude product was cooled to room temperature, dissolved in DCM, and precipitated by cold methanol. The product was then vacuum dried by a rotary evaporator at 40°C.

GCV-PCL (0.5 mmol) and succinic anhydride (1 mmol) were weighed and dissolved in toluene in a 3-necked round-bottom flask. One mmol pyridine was added and the solution was reacted under nitrogen at 70°C for 48 h. The product was then precipitated by cold hexane, and spun down. The pellet was re-dissolved in DCM and washed twice each with 10% (v/v) HCl and saturated NaCl solution. The organic phase was isolated and dried with magnesium sulfate then filtered. The carboxylated GCV-PCL was recovered by precipitation in cold hexane and then vacuum dried by rotary evaporation at 40°C.

GCV-PCL-COOH (0.54 mmol) and NHS (2.7 mmol) were weighed and mixed in 15 mL DCM, and then DCC (2.7 mmol) was added. The reaction was run under a nitrogen environment at room temperature for 24 h. The precipitated byproduct 1,3-dicyclohexylurea was removed by vacuum filtration. The filtrate was added into 35 mL diethyl ether and cooled to 4°C for 4 h to precipitate GCV-PCL-NHS. The precipitate was collected by centrifugation at 3,500 rpm for 5 min, washed with 2-propanol and solvent removed by rotary evaporation at 40°C.

GCV-PCL-NHS (10 mg) was dissolved in 5 mL acetone and slowly added to chitosan solution (20 mg chitosan oligosaccharide lactate dissolved in 25 mL deionized water). The mixture, purged with nitrogen, was stirred in a round-bottom flask for 24 h. The reacted solution was vacuum dried to remove acetone and then lyophilized. The amphiphilic polymer was then dissolved in DCM and dialyzed (MWCO = 6-8 kD, Spectra/Por) against pure DCM to remove unreacted chitosan. ACV-PCL-chitosan was recovered by rotary evaporation at 40°C.

#### 3.3.4. *Preparation of polymeric prodrug micelles*

GCV-PCL-chitosan micelles and control MPEG-PCL-chitosan micelles were formed similarly. Briefly, 10 mg of GCV-tagged amphiphilic polymer was dissolved in 2 mL acetone. The solution was then added dropwise to 10 mL deionized water under sonication. Acetone was removed by rotary evaporation and the final solution was collected by filtering through a 0.45 µm filter.

#### 3.3.5. *Determination of critical micelle concentration*

The CMC was estimated by using pyrene as a fluorescent probe [32]. Briefly, 1 mg mL<sup>-1</sup> of polymeric prodrug micelle was formed. Various amounts of deionized water and micellar solution were added respectively to glass vials to obtain micellar concentrations ranging from 5 × 10<sup>-7</sup> to 1 mg mL<sup>-1</sup>. Pyrene in acetone was then added separately to the prepared vials to get a final concentration of pyrene in water of 6.0 × 10<sup>-7</sup> mg mL<sup>-1</sup>, slightly lower than the saturation solubility of pyrene in water [33]. The solutions were then allowed to equilibrate for 8 h. Fluorescent spectra were determined by a plate reader (Synergy MX, BioTek, Winooski, VT) with an excitation wavelength of 334 nm.

#### 3.3.6. *Size and morphology of polymeric prodrug micelles*

The average particle size of polymeric prodrug micelles was determined by a dynamic light scattering (DLS) instrument (Zetasizer Nano ZS, Malvern

Instruments, United Kingdom) equipped with a red laser at a wavelength of 633 nm and scattering angle of 90° at 25°C. The zeta potential of the micelles dispersed in deionized water was determined with a zeta potential analyzer (Zetasizer Nano ZS). Transmission electron microscopy (TEM) image of micelles was performed on a JEM-4000FX (JEOL, Tokyo, Japan) at 80 kV. The TEM samples were prepared by adding 10 µL of micellar solution (1 mg mL<sup>-1</sup>) onto a Formvar grid for 5 min and wicking away solution in excess. The samples were negatively stained with 10 µL phosphotungstic acid solution (2 wt%) for 10 sec and then 15 sec, wicking away excess staining solution each time.

### 3.3.7. *Drug release kinetics*

Polymeric prodrug micelles at a concentration of 1 mg mL<sup>-1</sup> were made in phosphate buffered saline (PBS) (1 M, pH 7.4) at 25°C. Two mL of solution was placed in a dialysis tube (Float-A-Lyzer, Spectra/Por) with a MWCO of 3.5 – 5 kD. The dialysis bag was then immersed in 50 mL PBS at 37°C with and without esterase (3 units/2 mL). At specified time intervals, 5 µL of sample was removed and replaced with fresh PBS. The amount of GCV released was analyzed by a plate reader (BioTek) at 254 nm. All experiments were carried out in triplicate.

### 3.3.8. *Establishing TK-overexpressed HT29 cells*

Human colorectal HT29 cells (HTB-38; ATCC, Manassas, VA) were plated at a cell density of 6 x 10<sup>5</sup>, and incubated with 2.5 µL TK plasmid DNA and 5 µL TransIT-2020 transfection reagent (Mirus, Madison, WI). After 48 h, cells were trypsinized and suspended in fresh medium containing 400 µg mL<sup>-1</sup> G418 antibiotic (Invitrogen, Grand Island, NY). Cells were selected for several weeks in order to obtain a stable TK overexpressing HT29 cell line (termed HT29/TK).

### 3.3.9. *Development of GCV-PCL-chitosan/TK nanovectors*

In preparation for one-step delivery of both prodrug and gene to cells, GCV-PCL-chitosan/TK nanovectors were prepared. Here, GCV-PCL-chitosan micelles were prepared as previously described. To 1 mL aliquots of micelle solution various amounts of TK DNA solution (1.5 – 10.5  $\mu\text{g}$  DNA) was added. The solution was vortexed briefly and then allowed to incubate at room temperature for 30 min before DLS and zeta measurements were taken.

### 3.3.10. *Cytotoxicity studies*

24-well plates were seeded with HT29 colorectal cells suspended in 0.5 mL Dulbecco's modified Eagles' medium (DMEM, Corning Cellgro, Manassas, VA) supplemented with 10% fetal bovine serum (FBS, Atlanta biologicals, Flowery Branch, GA) and 1% penicillin-streptomycin (Sigma) and incubated at 37°C in 5% CO<sub>2</sub> balanced with humidified air for 24 h. For two-step delivery cytotoxicity studies, parental HT29 and TK gene transfected HT29 cells (HT29/TK) were challenged with various concentrations of GCV-PCL-chitosan micelle solution. Similarly, for one-step cytotoxicity studies, HT29 parental cells were treated with GCV-PCL-chitosan/TK nanovectors (GCV-PCL-chitosan micelles complexed with TK gene plasmid). After incubation for 72 h, cell viability was assessed using MTT assay. 200  $\mu\text{L}$  of sterile MTT solution (4 mg mL<sup>-1</sup>) was added into the culture wells and incubated for 4 h. The medium containing unreacted MTT was removed and 300  $\mu\text{L}$  DMSO was added to dissolve the insoluble purple formazan crystals formed in cellular mitochondria. The absorbance at 590 nm was measured with a plate reader (BioTek) and results were recorded as viability percentage calculated against the control group without micellar challenge. All experiments were carried out in triplicate.

## 3.4. RESULTS AND DISCUSSION

### 3.4.1. *Synthesis and characterization of amphiphilic prodrug polymers*

GCV-PCL was synthesized through ring-opening polymerization of  $\epsilon\text{-CL}$  exclusively by GCV (Figure 3.1 A). The <sup>1</sup>H NMR spectra of prodrug GCV and

GCV-PCL are shown in Figure 3.2 (i) and (ii), respectively. Chemical shifts at  $\delta=$  1.37 (3-CH<sub>2</sub>), 1.62 (2-CH<sub>2</sub>), 2.27 (1-CH<sub>2</sub>) and 4.04 (4-CH<sub>2</sub>) ppm correspond with the backbone chain of PCL polymer. Peaks at  $\delta=$  3.63 (e, f-CH<sub>2</sub>), 5.47 (d-CH<sub>2</sub>) and 7.76 (b-CH) are assigned to protons in GCV. Evidence of GCV grafting to PCL is clearly seen by the characteristics resonances observed in the synthesized polymer, confirming the synthesis of GCV-PCL.

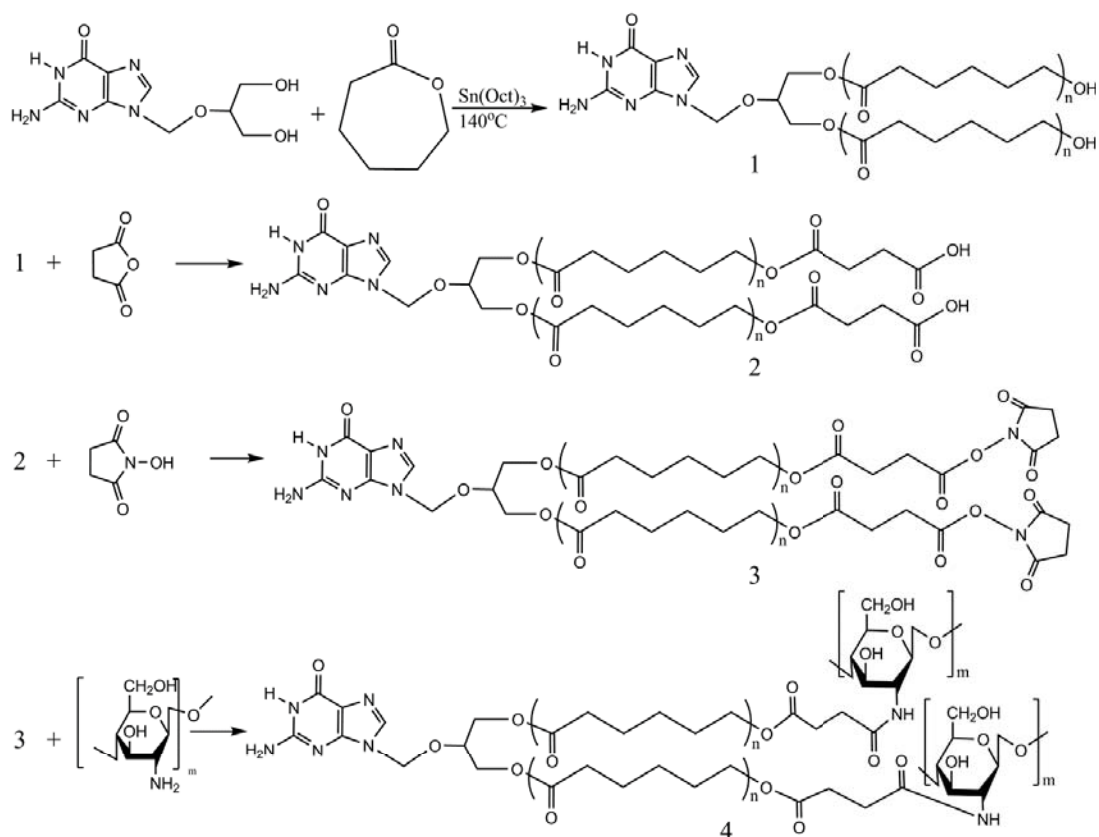


**Figure 3.1.** Synthetic scheme of (A) GCV-PCL, (B) GCV-PCL-COOH, (C) GCV-PCL-NHS, and (D) GCV-PCL-chitosan.

GCV-PCL was further conjugated with chitosan as shown in Figure 3.1 B-D. Successful conjugation of chitosan was confirmed by analytical means. Table 3.1, shows the GPC data concerning the formation of amphiphilic copolymer GCV-PCL-chitosan. The increase in number-average molecular weight ( $M_n$ ) from 11 kDa to 17 kDa corresponds with the addition of chitosan (MW = 5000).

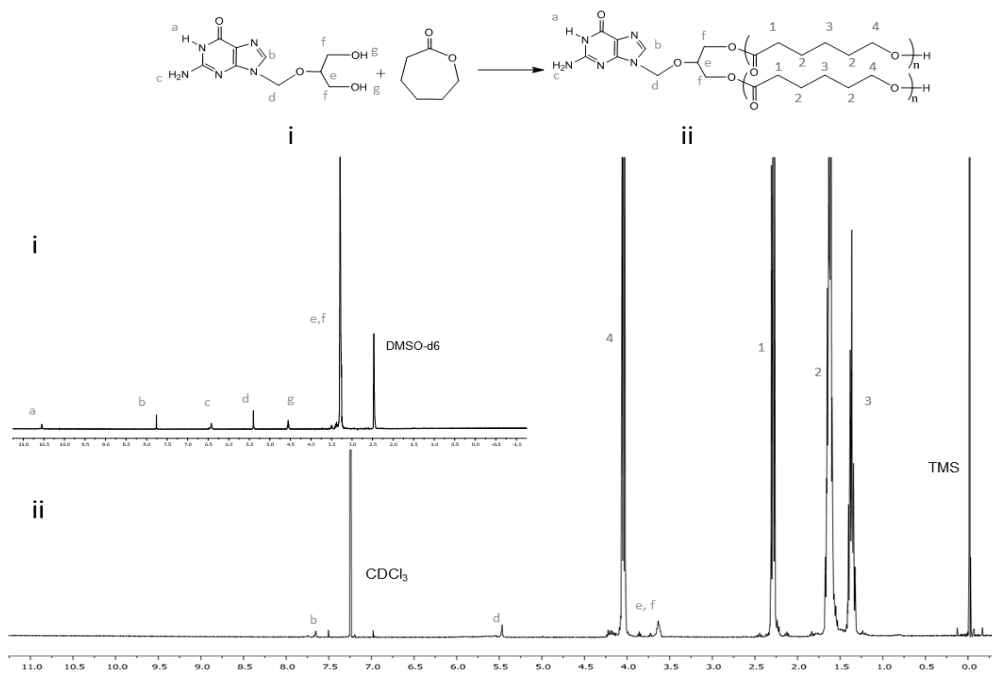


**Figure 3.2.** <sup>1</sup>H NMR spectra of (i) GCV and (ii) GCV-PCL.

**Table 3.1.** Characterization of GCV-PCL-chitosan<sup>a</sup>

Sample	M <sub>w</sub> (Da)	M <sub>n</sub> (Da)	Polydispersity (M <sub>w</sub> /M <sub>n</sub> )
GCV-PCL	12996	11454	1.13
GCV-PCL-chitosan	20354	17231	1.18

<sup>a</sup>Measured by GPC

Furthermore, as shown in Figure 3.3,  $^1\text{H}$  NMR analysis showed successful conjugation of chitosan to GCV-PCL hydrophobic polymer. As shown in Figure 3.1 D, conjugation of chitosan to GCV-PCL is made via amide linkage. The peak at 1.79 (A-NH<sub>2</sub>) from a singlet to a multiplet in Figure 3.3 (iv) confirms conjugation of chitosan to GCV-PCL. Moreover, the peaks from the aromatic protons on C<sub>3</sub> – C<sub>6</sub> of chitosan can be seen from  $\delta = 3.28 - 3.85$ , slightly shifted downward from the peaks shown in the original chitosan sample (Figure 3.3 (iii)).

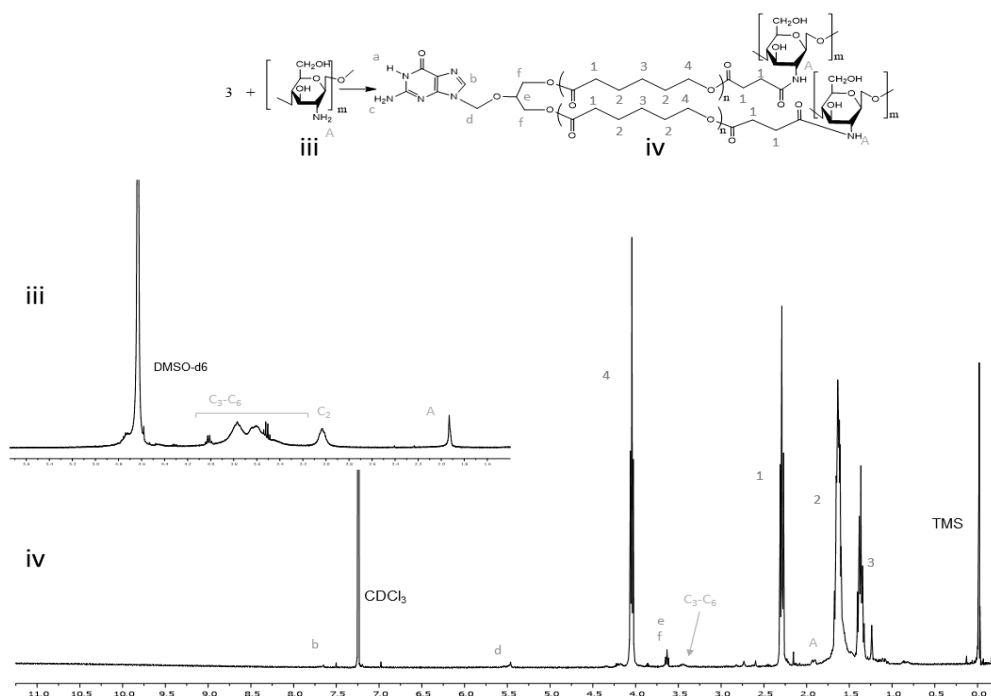


**Figure 3.3.**  $^1\text{H}$  NMR spectra of (iii) chitosan and (iv) GCV-PCL-chitosan.

Figure 3.4, depicts the FTIR spectra of GCV-PCL (A), chitosan (B), and GCV-PCL-chitosan. OH stretching from 3604 – 3167  $\text{cm}^{-1}$  as well as peaks at 1634  $\text{cm}^{-1}$  and 1295  $\text{cm}^{-1}$  corresponding to the N-H bending vibrations of the primary and secondary amine attributed to chitosan and GCV, respectively. The aforementioned peaks as well as the carbonyl absorption at 1721  $\text{cm}^{-1}$  associated with PCL and a peak at 1044  $\text{cm}^{-1}$  (C-O-C) seen in each spectra are found in GCV-PCL-chitosan. The FTIR results are in line with the results from  $^1\text{H}$  NMR and demonstrate successful synthesis of GCV-PCL-chitosan.

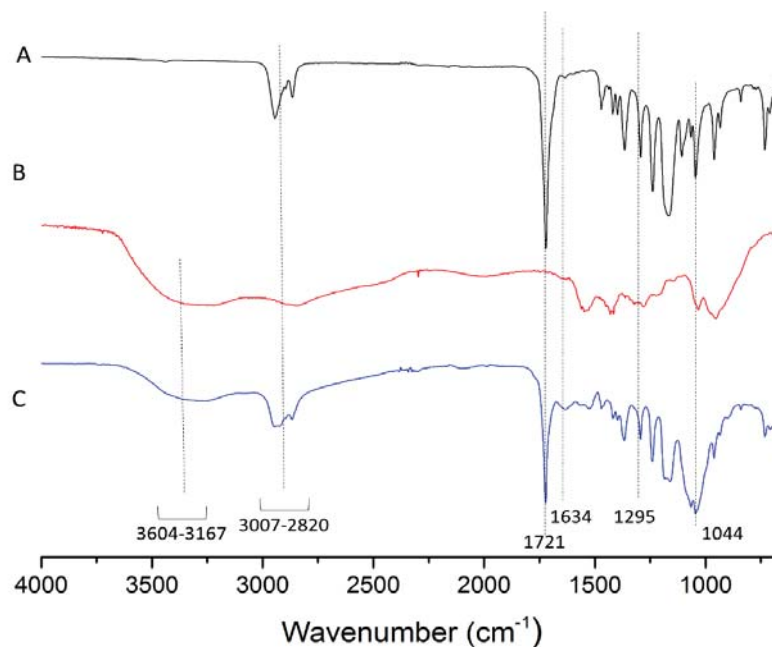


**Figure 3.4.** FTIR spectra of (A) GCV-PCL, (B) chitosan, and (C) GCV-PCL-chitosan.

### 3.4.2. *Formation and characterization of GCV-tagged polymeric micelles*

Through the solvent evaporation method, polymeric micelles of GCV-PCL-chitosan were formed. Here, the hydrophobic core segment was GCV-PCL and chitosan was the cationic and hydrophilic corona segment. Utilizing pyrene as a hydrophobic fluorescent probe, the critical micelle concentration (CMC) of GCV-PCL-chitosan micelles was examined. Pyrene can preferentially partition into the interior hydrophobic microdomains and change the intensities of the first and third bands in the pyrene fluorescence spectrum [33]. A low critical micelle concentration is indicative that the micellar solution are stable at high dilutions. For GCV-PCL-chitosan, the shift of the first and third bands was found at  $I_{338}/I_{329}$ . The CMC was determined to be  $11.2 \text{ mg L}^{-1}$  (Figure 3.5 A).



The morphology of GCV-PCL-chitosan micelles was examined through DLS and TEM analysis. Figure 3.5 (B) shows the size and morphology of GCV-tagged polymeric micelles. The average size as reported by DLS was 93.4 nm with a zeta potential of 38.5 mV. The positive charge is attributed to chitosan used as the hydrophilic segment on the micelle carriers. TEM analysis are shown in the insets of Figure 3.5 (B). The size of the micelles in the TEM images was around 100 nm. The results from DLS and TEM show good agreement.

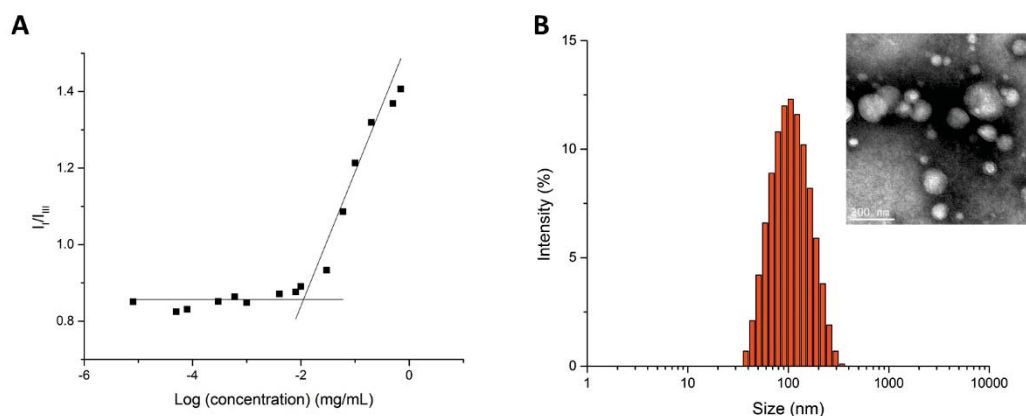


**Figure 3.5.** (A) Plot of the intensity ratio ( $I/I_{III}$ ) versus concentration of GCV-PCL-chitosan micelles and (B) particle size distribution of GCV-PCL-chitosan. Insets represent TEM images.

After formation of GCV-PCL-chitosan, various concentrations of TK DNA plasmid was incubated with 1 mL of micelle solution. Due to ionic interactions, the negatively charged TK DNA was able to form a complex with the positively charged chitosan used as the hydrophilic segment in micelle nanocarriers. Size and charge was measured by DLS and the results are shown in Table 3.2. As can be seen from DLS results, when the DNA was given 30 min to complex with the micelles, the size of GCV-PCL-chitosan micelles was relatively stable increasing only to 146 nm with the addition of 10.5  $\mu$ g TK DNA. Charge began to decrease from 38.5 mV to 28.2 mV with the addition 0 and 3  $\mu$ g TK DNA, respectively. However, after the addition of 4.5, 7.5 and 10.5  $\mu$ g TK DNA the charge did not continue to decrease as expected.

**Table 3.2.** Size and charge of GCV-PCL-chitosan after addition of TK DNA as measured by zetasizer

Amount of DNA ( $\mu\text{g}$ )	Size (nm)	Zeta Potential (mV)
0	93.4	38.5
1.5	92.4	37.9
2	92.4	30.1
3	92.8	28.2
4.5	128.4	37.5
7.5	177.5	35.0
10.5	146	33.9

To determine the drug loading percentage of GCV per mg of prepared micelle solution, the absorbance of GCV-PCL-chitosan was examined at  $t = 0$  and  $t = 72$  h and compared to a standard calibration curve of GCV ranging from 0.002 to 1.0 mg mL<sup>-1</sup>. It was found that GCV comprised 4.8% of the micelles.

#### 3.4.3. *In vitro* release of GCV from polymeric micelles

The *in vitro* release behavior of GCV at 37°C with and without esterase was studied. To mimic cellular conditions, esterase at a concentration of 3 units/2 mL was used [34]. As can be seen from Figure 3.6, the release of GCV with esterase was much quicker than without reaching a maximum release of 81% within 30 h. In contrast it took 48 h without esterase for GCV to reach a maximum release of 77% (Figure 3.7). Moreover, it took up to 2 h before a substantial difference in the release rate was seen. This is due to the time needed for esterase to diffuse into the micelle core and for activation.

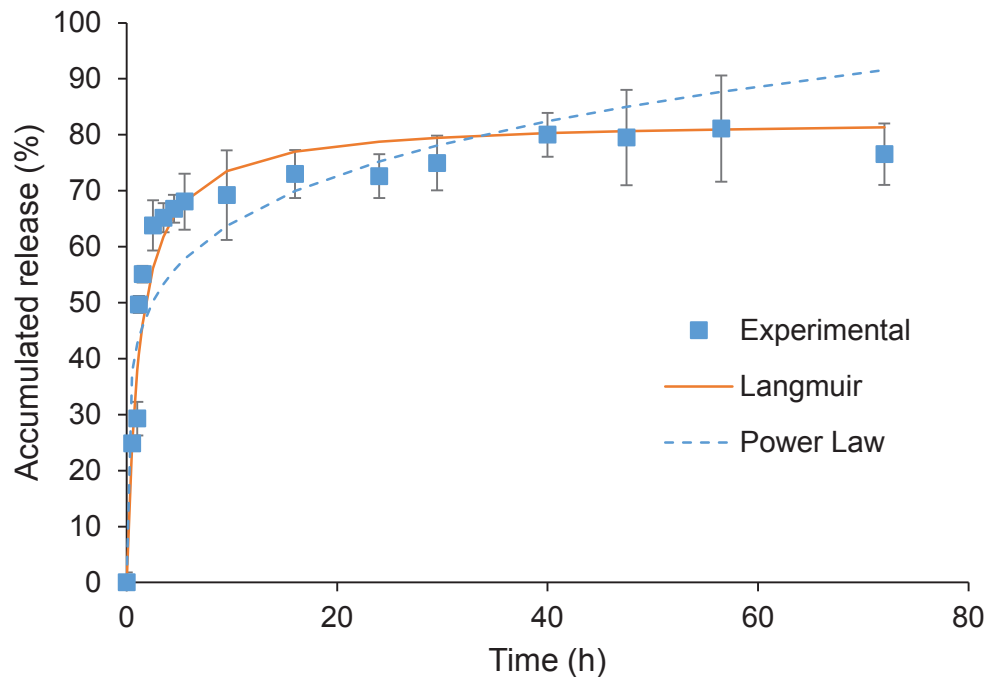


**Figure 3.6.** In vitro drug release profile of GCV from GCV-PCL-chitosan in PBS at 37°C with esterase (3 units/ 2 mL) (mean  $\pm$  SD, n = 3).

The release of GCV from GCV-PCL-chitosan was modeled using both Power Law and Langmuir models. As can be seen from Figure 3.6 and 3.7, Power Law was not a good fit for the release of GCV from polymeric micelles. Here, the exponent,  $n$ , was equal to 0.18 and 0.29 in GCV-PCL-chitosan micelles with and without esterase, respectively. Similar to the release of ACV in Chapter 2, the drug release mechanism does not occur solely through diffusion [35]. Here, without esterase, GCV release will occur by hydrolysis of the ester bond. The release rate is increased by the addition of esterase to GCV-PCL-chitosan which in addition to hydrolysis will break the ester bond. Due to the fact that GCV release occurs through reactive diffusion, the Langmuir model was also chosen for fitting the data. As can be seen in Figure 3.6 and 3.7, the release of GCV from GCV-PCL-chitosan with and without esterase using the Langmuir model fits the experimental data well. In addition, the dissociation constant ( $K_d$ ) for release of GCV from GCV-PCL-chitosan, was found to be 1.18 and 2.79 with and without esterase, respectively. Relating this data to the release of ACV in Chapter 2 leads

to several conclusions. First, GCV has a stronger association to PCL than ACV ( $K = 2.79$  and  $1.14$ , respectively). Secondly, the addition of esterase will increase the release rate to a similar release to ACV. We hypothesized that the increase in the dissociation constant was due to GCV having two reactive points to initiate ring-opening polymerization of  $\epsilon$ -CL compared to ACV which only has one. In our results with 5'DFUR (Chapter 3), a similar trend to GCV release was seen, confirming our hypothesis.

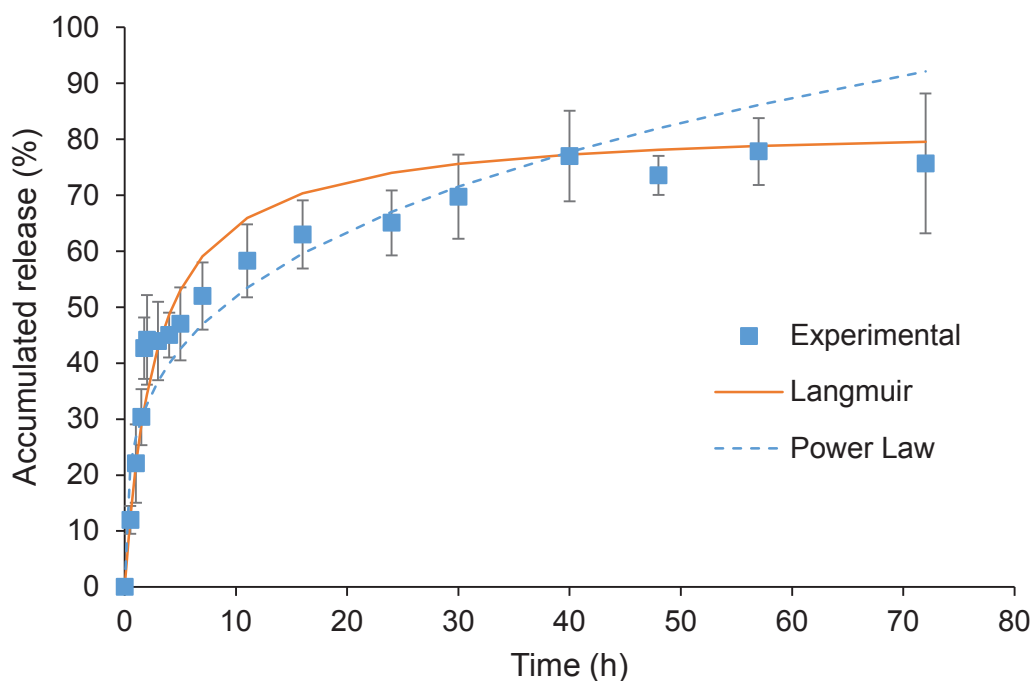


**Figure 3.7.** In vitro drug release profile of GCV-PCL-chitosan in PBS at 37°C (mean  $\pm$  SD,  $n = 3$ ).

#### 3.4.4. Cytotoxicity studies

To examine the potential of GCV for suicide gene therapy, HT29 colorectal cells were transfected with HSV-TK gene plasmid. The growth of both parental HT29 and HT29/TK cells are shown in Figure 3.8. It can be seen that the growth kinetics revealed that both HT29 and HT29/TK cells followed a similar growth rate after transfection and selection of a stable transfected cell line was not altered.

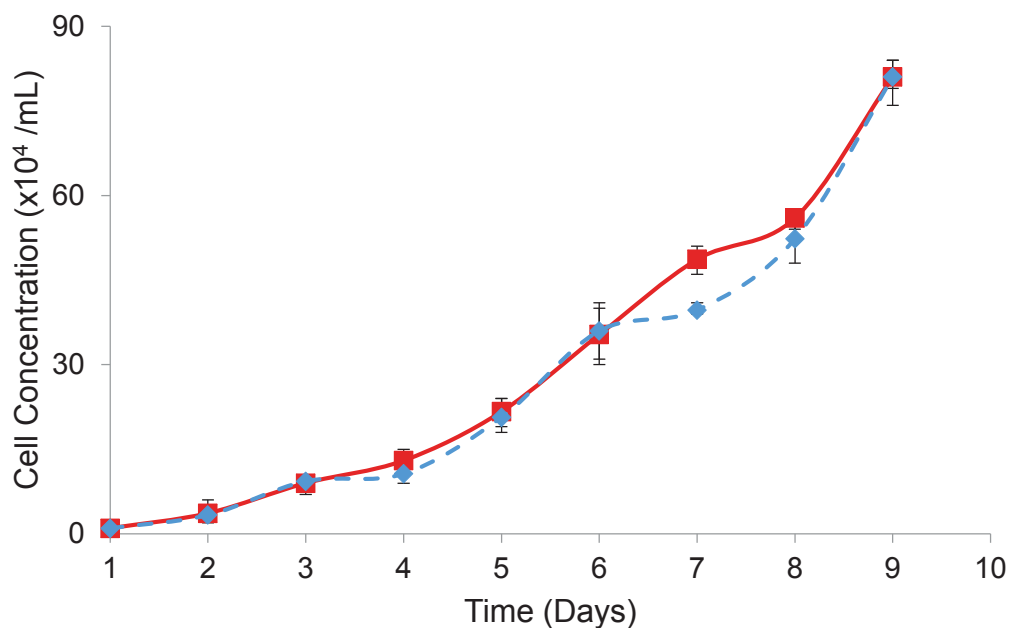


**Figure 3.8.** Cell growth kinetics profiles of HT29 (—■—) and HT29/TK (—◆—).

After obtaining a stable transfected cell line, HT29 and HT29/TK cells were challenged with GCV-tagged polymeric prodrug micelles. Through MTT assay, cytotoxicity of GCV-PCL-chitosan polymeric micelles ranging in concentration of 25 to 250  $\mu\text{g mL}^{-1}$  for 24, 48 and 72 h were investigated. Due to the fact that parental HT29 cells do not have any endogenous TK gene plasmid to convert GCV to its toxic form, cell viability was not affected (Figure 3.9 A). In contrast, HT29/TK cells which had upregulated TK gene expression showed cell death up to 35% at a dosage of 250  $\mu\text{g mL}^{-1}$  for 72 h treatment (Figure 3.9 B). These results confirmed that GCV can be converted to its active and toxic form via overexpressed TK gene in colon cancer cells for the classical two-step treatment.

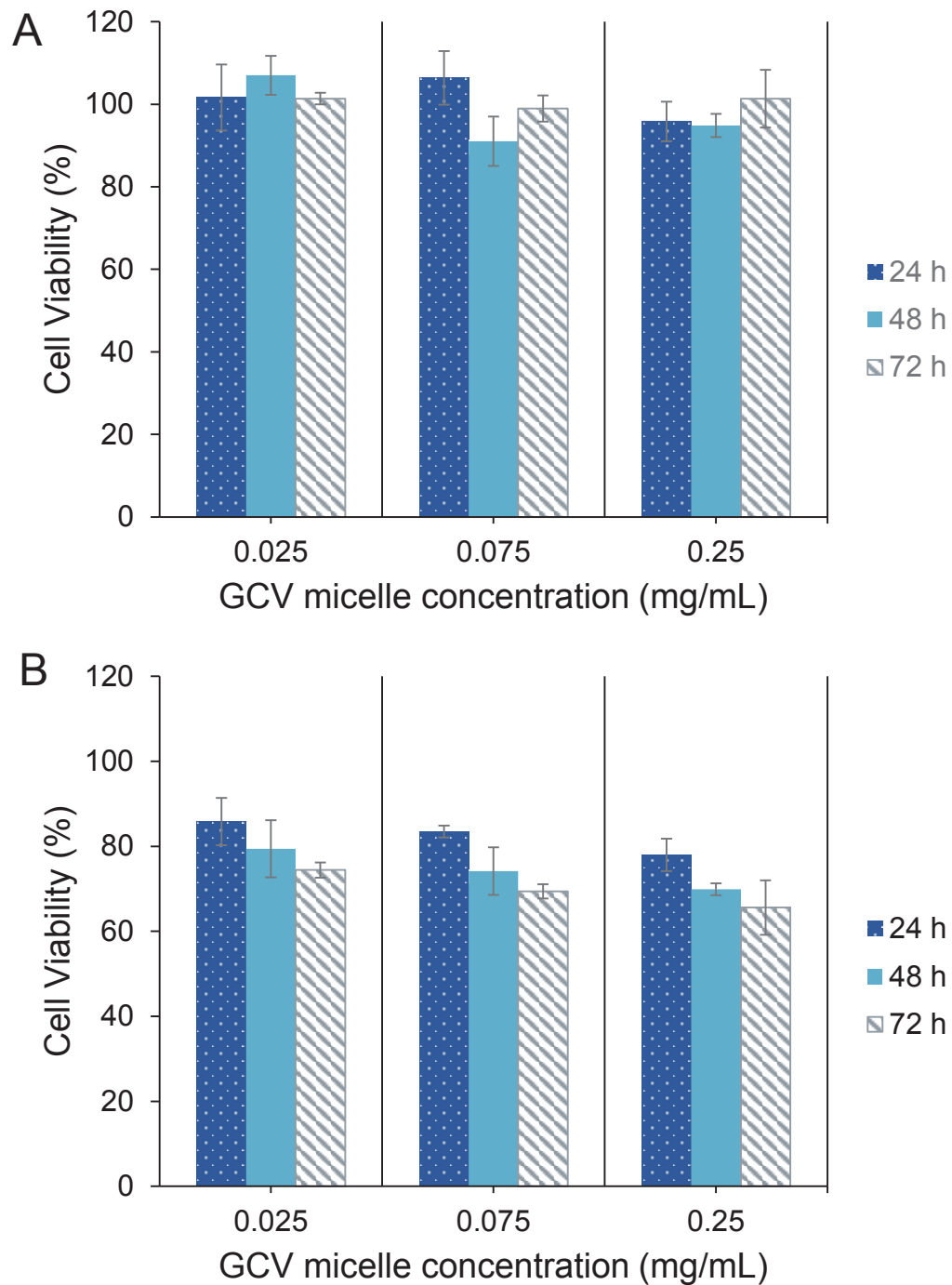


**Figure 3.9.** Cell viability after treatment with GCV-PCL-chitosan micelles (A) parental HT29, and (B) HT29/TK cells.

In an effort to examine the feasibility of a one-step anticancer therapy, TK DNA (1.5 and 6  $\mu\text{g}$ ) was complexed onto GCV-PCL-chitosan micelles via ionic interactions. Here, expression of the gene plasmid and subsequent toxicity was followed for three days and five days. As can be seen in Figure 3.10, expression of the plasmid in the cells after three days was sufficient to cause cell death. An additional two days did not cause a significant increase in cell toxicity. Moreover, it was seen that when TK gene plasmid was complexed onto control micelles (MPEG-PCL-chitosan), no cell toxicity was observed. These observations are expected because the micelle alone is not toxic to the cells, it is the prodrug GCV converted to its cytotoxic form by HSV-TK which causes cell death. From these results, subsequent one-step studies were carried out with 3 days for gene expression and subsequent toxicity.

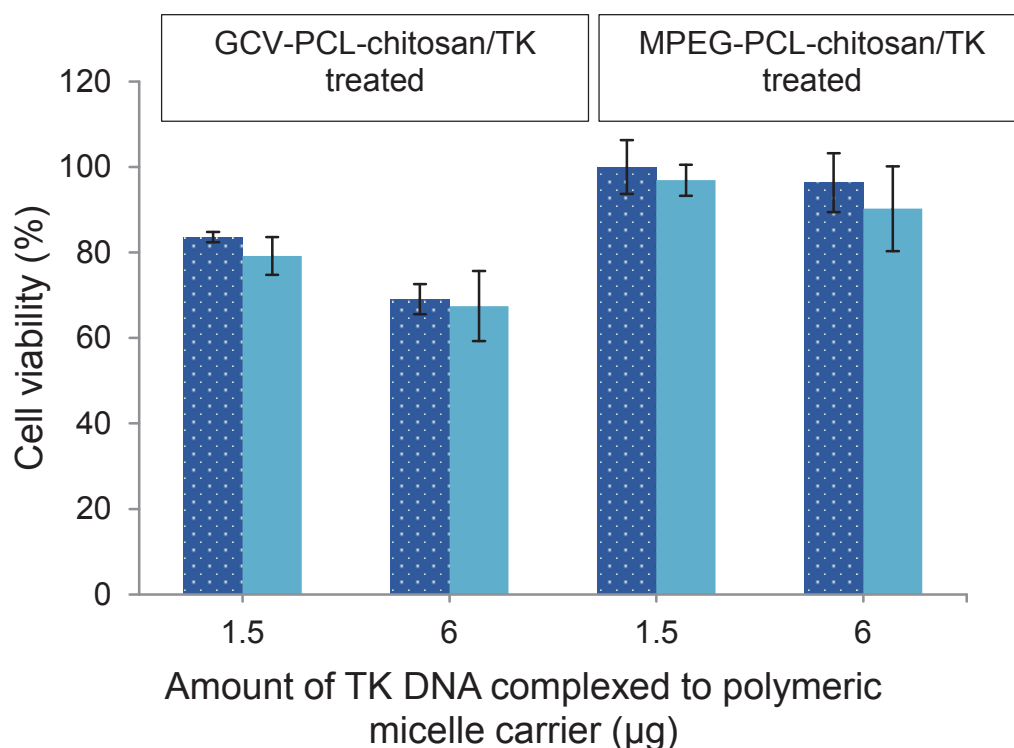


**Figure 3.10.** Expression of HSV-TK gene plasmid. 1.5 and 6  $\mu\text{g}$  HSV-TK DNA was complexed onto GCV-PCL-chitosan and MPEG-PCL-chitosan micelles and the gene expression followed for 3 (dark blue) and 5 (light blue) days.

After expression studies, parental HT29 cells were then treated with various concentrations of GCV-PCL-chitosan/TK nanovectors complexed with 1.5 - 10.5  $\mu\text{g}$  TK DNA and cytotoxicity observed as shown in Figure 3.11. Toxicity followed a similar trend to what was expected. By increasing the amount of DNA, there is more conversion of GCV to its cytotoxic form and therefore, more cell death. In this study, cell viability was decreased to around 52% with a micelle concentration of 250  $\mu\text{g mL}^{-1}$  and 4.5  $\mu\text{g}$  DNA. It appears that 4.5  $\mu\text{g}$  TK DNA is the upper limit for DNA complexation with GCV-PCL-chitosan micelles. Increasing the TK DNA amounts to 7.5 and 10.5  $\mu\text{g}$  did not show an increase in cell death.

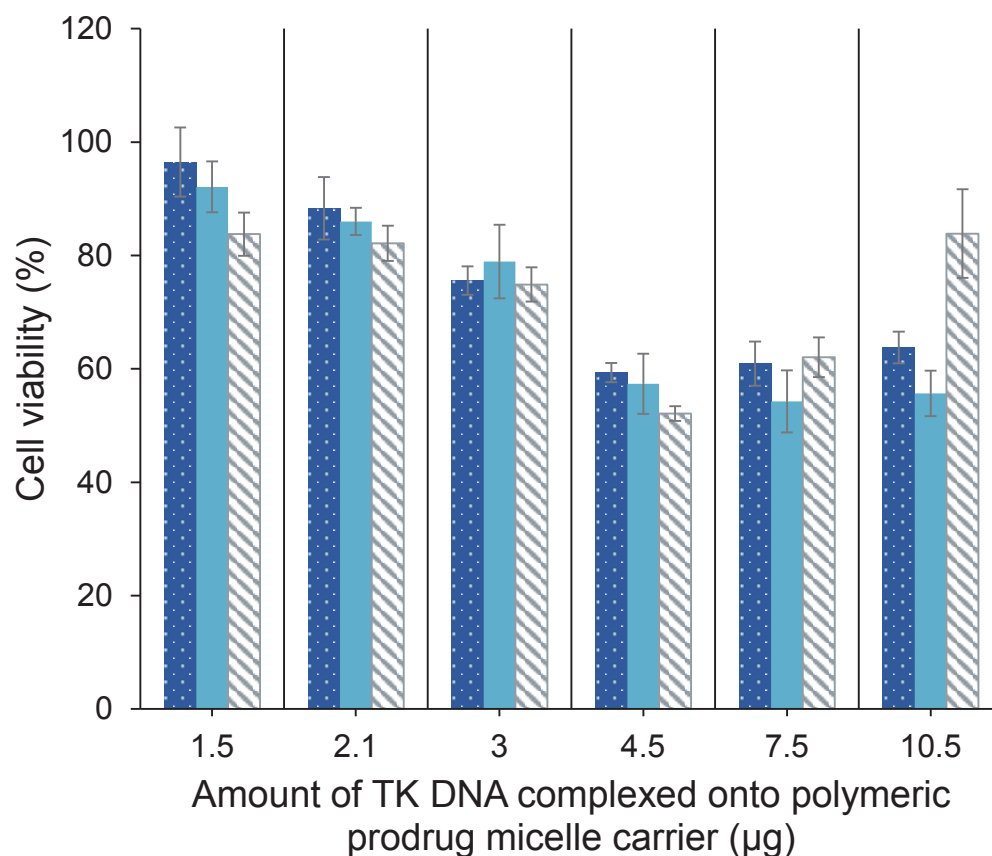


**Figure 3.11.** One-step delivery of gene and prodrug. Parental HT29 cells were challenged with 250 (hatched), 75 (solid blue), and 25 (dotted blue)  $\mu\text{g mL}^{-1}$  GCV-PCL-chitosan/TK nanovectors for 3 days.



### 3.5. CONCLUSION

GDEPT is a promising gene therapy method to combat cancer. However, developing an efficient carrier for both the gene and prodrug required for enhanced cancer therapy. In this study, we have developed a micelle carrier which achieved both of these goals, sufficient gene and prodrug delivery. Moreover, our polymer micelle carriers deliver both the gene and prodrug simultaneously, which is ideal for patients. Our results indicate that GCV-PCL-chitosan nanocarriers can reduce viability of HT29 colorectal cells by 52% in a one-step approach. Developing similar drug nanocarriers could have broad impact and enhance the effectiveness of GDEPT.

### 3.6. REFERENCES

1. Greco O, Dachs GU. Gene directed enzyme/prodrug therapy of cancer: Historical appraisal and future prospectives. *Journal of Cellular Physiology* 187(1), 22-36 (2001).
2. Zhang J, Kale V, Chen M. Gene-directed enzyme prodrug therapy. *The AAPS Journal* 1-9 (2014).
3. Denny WA. Prodrugs for gene-directed enzyme-prodrug therapy (suicide gene therapy). *Journal of Biomedicine and Biotechnology* 2003(1), 48-70 (2003).
4. Cheon J, Kim HK, Moon DG *et al.* Adenovirus-mediated suicide-gene therapy using the herpes simplex virus thymidine kinase gene in cell and animal models of human prostate cancer: Changes in tumour cell proliferative activity. *BJU International* 85(6), 759-766 (2000).
5. Chen SH, Shine HD, Goodman JC *et al.* Gene therapy for brain tumors: regression of experimental gliomas by adenovirus-mediated gene transfer in vivo. *Proceedings of the National Academy of Sciences* 91(8), 3054-3057 (1994).
6. Matthews T, Boehme R. Antiviral activity and mechanism of action of ganciclovir. *Review of Infectious Diseases* 10, S490-S494 (1988).
7. Ding Z, Mathur V, Ho PP *et al.* Antiviral drug ganciclovir is a potent inhibitor of microglial proliferation and neuroinflammation. *The Journal of Experimental Medicine* 211(2), 189-198 (2014).
8. Schnepf N, Corvo J, Pors MJSL *et al.* Antiviral activity of ganciclovir and artesunate towards human cytomegalovirus in astrocytoma cells. *Antiviral Research* 89(2), 186-188 (2011).
9. Ribot EJ, Miraux S, Konsman JP *et al.* In vivo MR tracking of therapeutic microglia to a human glioma model. *NMR in Biomedicine* 24(10), 1361-1368 (2011).
10. Staquicini FI, Ozawa MG, Moya CA *et al.* Systemic combinatorial peptide selection yields a non-canonical iron-mimicry mechanism for targeting tumors in a mouse model of human glioblastoma. *Journal of Clinical Investigation* 121(1), 161-173 (2011).
11. Chen LS, Wang M, Ou WC *et al.* Efficient gene transfer using the human JC virus-like particle that inhibits human colon adenocarcinoma growth in a nude mouse model. *Gene Therapy* 17(8), 1033-1041 (2010).
12. Ambade AV, Joshi GV, Mulherkar R. Effect of suicide gene therapy in combination with immunotherapy on antitumour immune response & tumour regression in a xenograft mouse model for head & neck squamous cell carcinoma. *The Indian Journal of Medical Research* 132, 415-422 (2010).
13. Fillat C. Suicide gene therapy mediated by the herpes simplex virus thymidine kinase gene/ganciclovir system: Fifteen years of application. *Current Gene Therapy* 3(13-26) (2003).
14. Greish K, Frandsen J, Scharff S *et al.* Silk-elastinlike protein polymers improve the efficacy of adenovirus thymidine kinase enzyme prodrug therapy of head and neck tumors. *Journal of Gene Medicine* 12(7), 572-579 (2010).
15. Mesnil M, Yamasaki H. Bystander effect in herpes simplex virus-thymidine kinase/ganciclovir cancer gene therapy: Role of gap-junctional intercellular communication. *Cancer Research* 60(15), 3989-3999 (2000).
16. Elshami A, Saavedra A, Zhang H *et al.* Gap junctions play a role in the 'bystander effect' of the herpes simplex virus thymidine kinase/ganciclovir system in vitro. *Gene therapy* 3(1), 85-92 (1996).

17. Wirth T, Hedman M, Makinen K *et al.* Safety profile of plasmid/liposomes and virus vectors in clinical gene therapy. *Current Drug Safety* 1(3), 253-257 (2006).
18. Muhammad AKMG, Puntel M, Candolfi M *et al.* Study of the efficacy, biodistribution, and safety profile of therapeutic gutless adenovirus vectors as a prelude to a phase I clinical trial for glioblastoma. *Clinical Pharmacology and Therapeutics* 88(2), 204-213 (2010).
19. Kay MA, Glorioso JC, Naldini L. Viral vectors for gene therapy: The art of turning infectious agents into vehicles of therapeutics. *Nature Medicine* 7(1), 33-40 (2001).
20. Kwon GS. Polymeric micelles for delivery of poorly water-soluble compounds. *Critical Reviews in Therapeutic Drug Carrier Systems* 20(5), 357-403 (2003).
21. Del Amo EM, Urtti A. Current and future ophthalmic drug delivery systems: A shift to the posterior segment. *Drug Discovery Today* 13(3-4), 135-143 (2008).
22. Nakanishi T, Fukushima S, Okamoto K *et al.* Development of the polymer micelle carrier system for doxorubicin. *Journal of Controlled Release* 74(1-3), 295-302 (2001).
23. Hamaguchi T, Matsumura Y, Suzuki M *et al.* NK105, a paclitaxel-incorporating micellar nanoparticle formulation, can extend in vivo antitumour activity and reduce the neurotoxicity of paclitaxel. *British Journal of Cancer* 92(7), 1240-1246 (2005).
24. Koizumi F, Kitagawa M, Negishi T *et al.* Novel SN-38-incorporating polymeric micelles, NK012, eradicate vascular endothelial growth factor-secreting bulky tumors. *Cancer Research* 66(20), 10048-10056 (2006).
25. Sinha VR, Singla AK, Wadhawan S *et al.* Chitosan microspheres as a potential carrier for drugs. *International Journal of Pharmaceutics* 274(1-2), 1-33 (2004).
26. Dash TK, Konkimalla VB. Poly- $\epsilon$ -caprolactone based formulations for drug delivery and tissue engineering: A review. *Journal of Controlled Release* 158(1), 15-33 (2012).
27. Peng CL, Shieh MJ, Tsai MH *et al.* Self-assembled star-shaped chlorin-core poly( $\epsilon$ -caprolactone)-poly(ethylene glycol) diblock copolymer micelles for dual chemo-photodynamic therapies. *Biomaterials* 29(26), 3599-3608 (2008).
28. Schindler A, Hibionada YM, Pitt CG. Aliphatic polyesters. III. Molecular weight and molecular weight distribution in alcohol-initiated polymerizations of  $\epsilon$ -caprolactone. *Journal of Polymer Science: Polymer Chemistry Edition* 20(2), 319-326 (1982).
29. Aliabadi HM, Mahmud A, Sharifabadi AD *et al.* Micelles of methoxy poly(ethylene oxide)-b-poly( $\epsilon$ -caprolactone) as vehicles for the solubilization and controlled delivery of cyclosporine A. *Journal of Controlled Release* 104(2), 301-311 (2005).
30. Dubois P, Krishnan M, Narayan R. Aliphatic polyester-grafted starch-like polysaccharides by ring-opening polymerization. *Polymer* 40(11), 3091-3100 (1999).
31. Sonia T, Sharma C. Chitosan and its derivatives for drug delivery perspective. *Chitosan for Biomaterials I* 23-53 (2011).
32. Wilhelm M, Zhao CL, Wang Y *et al.* Poly(styrene-ethylene oxide) block copolymer micelle formation in water: A fluorescence probe study. *Macromolecules* 24(5), 1033-1040 (1991).
33. Kalyanasundaram K, Thomas JK. Environmental effects on vibronic band intensities in pyrene monomer fluorescence and their application in studies of micellar systems. *Journal of the American Chemical Society* 99(7), 2039-2044 (1977).

34. Liewald F, Demmel N, Wirsching R *et al.* Intracellular pH, esterase activity, and DNA measurements of human lung carcinomas by flow cytometry. *Cytometry* 11(3), 341-348 (1990).
35. Siepmann J, Siepmann F. Mathematical modeling of drug delivery. *International Journal of Pharmaceutics* 364(2), 328-343 (2008).

## **CHAPTER 4: ENHANCED ANTICANCER ACTIVITY OF 5'-DFUR-PCL-MPEG POLYMERIC PRODRUG MICELLES ENCAPSULATING CHEMOTHERAPEUTIC DRUGS<sup>4</sup>**

### **4.1. ABSTRACT**

In this study, chemotherapy prodrug 5-doxifluridine (5'-DFUR) associated with amphiphilic copolymer poly( $\epsilon$ -caprolactone)-methoxy poly(ethylene glycol) (5'-DFUR-PCL-MPEG) was synthesized, characterized, and self-assembled into functional polymeric micelles. To demonstrate that prodrug 5'-DFUR could convert into cytotoxic 5-fluorouracil (5-FU) by endogenous thymidine phosphorylase (TP), HT29 colon cancer cells were treated with 5'-DFUR-PCL-MPEG polymeric micelles for various time periods and showed up to 40% cell death rate after 72 h treatment. In contrast, HT29 cells challenged with 5'-DFUR-tagged polymeric micelles which encapsulated DOX or SN-38, chemotherapeutic drugs, remained only 36% and 31% in cell viability. Our results demonstrated that the developed 5'-DFUR-PCL-MPEG polymeric micellar nanoparticles have the potential for gene-directed enzyme prodrug therapy.

### **4.2. INTRODUCTION**

5-Fluorouracil (5-FU) is one of the main anti-tumor agents used to treat colon, breast and gastric cancers. Due to the short plasma half-life of 5-FU, it is often administered to patients through continuous infusion [1]. 5-FU however, is poorly tumor selective and its therapy causes several severe adverse side effects in patients including intestinal discomfort. To circumvent toxicity, 5-doxifluridine (5'-DFUR), a prodrug of 5-FU, is commonly administered to patients [2]. 5'-DFUR is converted to its active and toxic form 5-FU through metabolic conversion by thymidine phosphorylase (TP), a gene overexpressed in many cancer types [3]. Several groups have exploited the enzyme-prodrug activation model of TP and

<sup>4</sup>The material contained in this chapter is planned for publication in *The Journal of Controlled Release*.

5'-DFUR and shown that by transfection of cancer cell lines with TP, sensitivity of tumor cells to this prodrug is enhanced by the increased TP expression [4, 5].

Clinically, 5'-DFUR has been established for treatment of various cancer types [6-8]. Moreover, several studies have evaluated combination therapies of 5'-DFUR with other chemotherapy drugs such as tamoxifen, medroxyprogesterone acetate, and docetaxel with successful results [9-11]. While 5'-DFUR itself is slightly hydrophilic, intrinsic issues that are associated with other "free drugs," such as poor solubility, unwanted toxicity, and short circulation times have propelled research into alternative drug delivery systems. There are several factors which contribute to success of a synthesized therapeutic carrier. One must first address the physiochemical limitations of the drugs; second, one needs to address the biological hurdles in reaching the targeted tumorous tissue. Polymeric nanocarriers for drug delivery are being developed for a wide variety of cancers and chemotherapeutic drugs [12-14]. Specifically, several polymeric micelle carriers which house hydrophobic chemotherapy drugs doxorubicin (DOX), paclitaxel or 7-ethyl-10-hydroxycamptothecin (SN-38) in their core are advancing into clinical trials with great success [15-17].

SN-38 is a biologically active metabolite of irinotecan hydrochloride (CPT-11). While CPT-11 is a prodrug which can be converted to SN-38 by carboxylesterases, SN-38 has shown to have 1,000-fold more potent toxicity towards various cancer cells in vitro [18]. Moreover, metabolic conversion of CPT-11 to SN-38 in the liver and tumor has shown to be less than 10% of its original volume [19, 20]. Therefore, direct use of SN-38 is advantageous for cancer treatment. Similarly, DOX is another widely used antitumor drug effective in the treatment of carcinomas of the breast, lung, thyroid and colon. However, due to the ensuing toxicity and low water solubility of free SN-38 and DOX, use of a drug carrier is warranted.

It has been shown previously that the hydroxyl groups on 5'-DFUR can be used for initiation in the ring-opening polymerization of  $\epsilon$ -caprolactone to form hydrophobic 5'-DFUR-polycaprolactone (5'-DFUR-PCL) [21]. Poly( $\epsilon$ -caprolactone) (PCL) is commonly used for biomedical applications because of its excellent biodegradability and biocompatibility [22]. In this study, we further grafted hydrophobic 5'-DFUR-PCL with hydrophilic biodegradable methoxy poly(ethylene glycol) MPEG, widely used for drug delivery to form amphiphilic copolymers for micelle preparation [23-25]. Moreover, because camptothecin-based drugs are often used in conjunction with 5-FU as a first therapy [26], and the anticancer effectiveness of DOX, we encapsulated SN-38 or DOX into our prodrug-tagged polymeric micelles for an additive anticancer therapy.

To evaluate anticancer effectiveness of our synthesized polymeric micelle carriers, HT29 colon cancer cells, which express endogenous TP levels, were treated with our micelle carrier. Moreover, SN-38 and DOX, chemotherapeutic drugs, used to treat a wide variety of cancer types, were encapsulated into our micelle carriers and the additive effect of both 5'-DFUR and chemotherapeutic drugs on HT29 cell death was examined. Our results indicate that 5'-DFUR-PCL-MPEG micelle carriers are an effective and efficient means to deliver 5'-DFUR and chemotherapeutic drugs to tumor cells.

### 4.3. MATERIALS AND METHODS

#### 4.3.1. *Materials*

5'-DFUR was purchased from Tokyo Chemical Industry Co. Ltd. (TCI, Japan). N,N'-dicyclohexyl carbodiimide (DCC),  $\epsilon$ -CL, pyrene, and succinic anhydride were purchased from Acros Organics (Geel, Belgium). Sn(Oct)<sub>2</sub>, CDCl<sub>3</sub> with 1% tetramethylsilane (TMS), deuterated dimethyl sulfoxide (DMSO-d<sub>6</sub>), dimethyl sulfoxide (DMSO), tetrahydrofuran (THF), dichloromethane (DCM), methanol, 2-propanol, hexane, toluene, SN-38, DOX, methoxypolyethylene glycol amine (MPEG-NH<sub>2</sub>; MW = 5,000), and MPEG (MW = 350) were all purchased from Sigma-Aldrich (St. Louis, MO). Ethyl ether was purchased from J.T. Baker

(Austin, TX). N-Hydroxysuccinimide (NHS) was purchased from Alfa Aesar (Ward Hill, MA). Acetone was purchased from Pharmco-AAPER (Shelbyville, KY). Pyridine and hydrochloric acid (HCl) were purchased from EMD (Philadelphia, PA). Sodium chloride (NaCl) and magnesium sulfate were purchased from Showa (Tokyo, Japan). All reagents were used as received without further purification.

#### 4.3.2. *Characterization methods*

Gel permeation chromatography (GPC) analyses were performed on a Waters 1525 binary HPLC pump equipped with a Waters 2414 refractive index detector (Milford, MA). Waters styragel HR 3 (MW = 500 – 30,000) and HR 4E (MW = 50 – 100,000) columns were equipped. Molecular weight calibration was performed with polystyrene standards that covered a MW range of 400 –  $4.3 \times 10^4$ . GPC analyses were performed in THF at a flow rate of  $1 \text{ mL min}^{-1}$  with an injected volume of 50  $\mu\text{L}$ .  $^1\text{H}$  NMR spectra were obtained from a Varian Unity/Inova 400 MHz instrument (Sparta, NJ). To obtain FTIR spectra by a Jasco FTIR-4200 spectrometer (Tokyo, Japan), a small amount of polymeric sample was loaded onto a silicon wafer and THF was added dropwise to dissolve the sample and evaporated afterwards. This was repeated until the entire sample was dissolved and a film had formed.

#### 4.3.3. *Synthesis of 5'DFUR-tagged amphiphilic polymers*

5'DFUR (50 mg) was weighed and mixed with  $\epsilon$ -CL (2.25 mL) under a sonication bath for 5 min at room temperature.  $\text{Sn}(\text{Oct})_2$  (0.5 wt% of  $\epsilon$ -CL) was then added into the mixture. The entire solution was placed into a 3-necked round-bottom flask. The system was purged with nitrogen and immersed in an oil bath at  $140^\circ\text{C}$  for 24 h. The crude product was cooled to room temperature, dissolved in DCM, and precipitated by cold methanol. The product was then vacuum dried by a rotary evaporator at  $40^\circ\text{C}$ .



5'DFUR-PCL (0.5 mmol) and succinic anhydride (1 mmol) were weighed and dissolved in toluene in a 3-necked round-bottom flask. One mmol pyridine was added and the solution was reacted under nitrogen at 70°C for 48 h. The product was then precipitated by cold hexane, and spun down. The pellet was re-dissolved in DCM and washed twice each with 10% (v/v) HCl and saturated NaCl solution. The organic phase was isolated and dried with magnesium sulfate then filtered. The carboxylated 5'DFUR-PCL was recovered by precipitation in cold hexane and then vacuum dried by rotary evaporation at 40°C.

5'DFUR-PCL-COOH (0.54 mmol) and NHS (2.7 mmol) were weighed and mixed in 15 mL DCM, and then DCC (2.7 mmol) was added. The reaction was run under a nitrogen environment at room temperature for 24 h. The precipitated byproduct 1,3-dicyclohexylurea was removed by vacuum filtration. The filtrate was added into 35 mL diethyl ether and cooled to 4°C for 4 h to precipitate 5'DFUR-PCL-NHS. The precipitate was collected by centrifugation at 3,500 rpm for 5 min, washed with 2-propanol and solvent removed by rotary evaporation at 40°C.

5'DFUR-PCL-NHS (10 mg) and MPEG-NH<sub>2</sub> (10 mg) were weighed and dissolved by 20 mL DCM in a round-bottom flask. The flask was purged with nitrogen and the solution was stirred for 24 h. The solution was then dialyzed (MWCO = 6-8 kD, Spectra/Por, Rancho Dominguez, CA) against pure DCM to remove remaining MPEG-NH<sub>2</sub>. 5'DFUR-PCL-MPEG was recovered by rotary evaporation at 40°C.

#### 4.3.4. *Preparation of polymeric prodrug micelles*

5'DFUR-PCL-MPEG and chemotherapy drug loaded 5'DFUR-PCL-MPEG micelles were formed similarly. Briefly, 10 mg of 5'DFUR-tagged amphiphilic polymer, with or without 0.2 mg DOX or 0.1 mg SN-38, were dissolved in 2 mL acetone under bath sonication. The solution was then added dropwise to 10 mL deionized water under bath sonication. Acetone was removed by rotary

evaporation and the final solution was collected by filtering through a 0.45  $\mu\text{m}$  filter.

#### 4.3.5. *Determination of critical micelle concentration*

The critical micelle concentration (CMC) was estimated by using pyrene as a fluorescent probe [27]. Briefly, 1 mg mL<sup>-1</sup> of polymeric prodrug micelle was formed. Various amounts of deionized water and micellar solution were added respectively to glass vials to obtain micellar concentrations ranging from 5  $\times 10^{-7}$  to 1 mg mL<sup>-1</sup>. Pyrene in acetone was then added separately to the prepared vials to get a final concentration of pyrene in water of 6.0  $\times 10^{-7}$  mg mL<sup>-1</sup>, slightly lower than the saturation solubility of pyrene in water [28]. The solutions were then allowed to equilibrate for 8 h. Fluorescent spectra were determined by a plate reader (Synergy MX, BioTek, Winooski, VT) with an excitation wavelength of 334 nm.

#### 4.3.6. *Size and morphology of polymeric prodrug micelles*

The average particle size of polymeric prodrug micelles was determined by a dynamic light scattering (DLS) instrument (Zetasizer Nano ZS, Malvern Instruments, United Kingdom) equipped with a red laser at a wavelength of 633 nm and scattering angle of 90° at 25°C. The zeta potential of the micelles dispersed in deionized water was determined with a zeta potential analyzer (Zetasizer Nano ZS). Transmission electron microscopy (TEM) image of micelles was performed on a JEM-4000FX (JEOL, Tokyo, Japan) at 80 kV. The TEM samples were prepared by adding 10  $\mu\text{L}$  of micellar solution (1 mg mL<sup>-1</sup>) onto a Formvar grid for 5 min and wicking away solution in excess. The samples were negatively stained with 10  $\mu\text{L}$  phosphotungstic acid solution (2 wt%) for 10 sec and then 15 sec, wicking away excess staining solution each time.

#### 4.3.7. *Drug loading content and entrapment efficiency*

To determine the drug loading percentage of 5'DFUR per mg of micelle formulation, the absorbance of 5'DFUR-PCL-MPEG micelles at t=0 and t=72 h was examined ( $\lambda=269$ , BioTek) and compared to a standard calibration curve of 5'DFUR ranging from 0.002 to 1.0 mg mL<sup>-1</sup>. To obtain drug loading content and entrapment efficiency of DOX or SN-38 encapsulated in micelles, the obtained micellar solutions were frozen and lyophilized by a freezer dryer system to obtain dried nanoparticle product. The weighed nanoparticles were dissolved in chloroform/DMSO (1:1, v/v) and the absorbance of the solutions read at 485 nm (DOX) or 366 nm (SN-38) using a plate reader. The weight of the entrapped drug was calculated by a calibration curve from 0.01 mg mL<sup>-1</sup> to 1 mg mL<sup>-1</sup>. Drug loading content and entrapment efficiency were determined by equations (1) and (2), respectively:

$$\text{Drug loading content (\%)} = \frac{\text{weight of drug in nanoparticles}}{\text{weight of nanoparticles}} \times 100 \quad (1)$$

$$\text{Entrapment efficiency (\%)} = \frac{\text{weight of drug in nanoparticles}}{\text{weight of drug fed initially}} \times 100 \quad (2)$$

#### 4.3.8. *Drug release kinetics*

Polymeric prodrug micelles at a concentration of 1 mg mL<sup>-1</sup> were made in phosphate buffered saline (PBS) (1 M, pH 7.4) at 37°C. 2 mL of solution was placed in a dialysis tube (Float-A-Lyzer, Spectra/Por) with a MWCO of 3.5 – 5 kD. The dialysis bag was then immersed in 50 mL PBS at room temperature and 37°C with and without esterase (3 units/2 mL) to mimic cellular conditions. At specified time intervals, 5  $\mu$ L of sample was removed and replaced with fresh PBS. The amount of 5'DFUR released was analyzed by a plate reader (BioTek) at 269 nm. All experiments were carried out in triplicate.

#### 4.3.9. *Cytotoxicity studies*

24-well plates were seeded with human colorectal HT29 cells (HTB-38; ATCC, Manassas, VA) suspended in 0.5 mL Dulbecco's modified Eagles' medium

(DMEM, Corning Cellgro, Manassas, VA) supplemented with 10% fetal bovine serum (FBS, Atlanta biologicals, Flowery Branch, GA) and 1% penicillin-streptomycin (Sigma) and incubated at 37°C in 5% CO<sub>2</sub> balanced with humidified air for 24 h. In one well, 1 mL of 2 mg mL<sup>-1</sup> of polymeric micelle solution (filtered by a 0.45 µm filter) was added. Serial dilutions were performed to a final concentration of 0.25 mg mL<sup>-1</sup>. After incubation for 72 h, cell viability was assessed using MTT assay. 200 µL of sterile MTT solution (4 mg mL<sup>-1</sup>) was added into the culture wells and incubated for 4 h. The medium containing unreacted MTT was removed and 300 µL DMSO was added to dissolve the insoluble purple formazan crystals formed in cellular mitochondria. The absorbance at 590 nm was measured with a plate reader (BioTek) and results were recorded as viability percentage calculated against the control group without micellar challenge. All experiments were carried out in triplicate.

#### 4.4. RESULTS AND DISCUSSION

##### 4.4.1. *Synthesis and characterization of amphiphilic prodrug polymers*

Figure 1 A-D describes the preparation of 5'DFUR-PCL-MPEG copolymer. First, 5'DFUR-PCL was directly synthesized via the ring-opening polymerization of ε-CL initiated by 5'DFUR as previously reported [21]. <sup>1</sup>H NMR spectra of prodrug 5'DFUR and 5'DFUR-PCL post synthesis are shown in Figure 4.2 (i) and (ii), respectively. Characteristic resonance peaks associated with 5'-DFUR including δ = 1.43 (g-CH<sub>3</sub>), 4.20 (f-CH), 5.02 (e-CH), 5.25 (d-CH), 5.95 (c-CH), and 7.97 (b-CH) ppm were seen in synthesized 5'-DFUR-PCL. Chemical shifts associated with PCL were seen at 1.40 (3-CH<sub>2</sub>), 1.65 (2-CH<sub>2</sub>), 2.34 (1-CH<sub>2</sub>), 3.62 (4'-CH<sub>2</sub>), and 4.05 (4-CH<sub>2</sub>) ppm. These spectra demonstrated evidence of ring-opening polymerization of ε-CL by prodrug 5'-DFUR. GPC data concerning the polymerization of PCL by 5'DFUR is given in Table 4.1, accordingly, the number average molecular weight (M<sub>n</sub>) of 5'DFUR-PCL polymer was approximately 15 kDa with a polydispersity index (PDI) of 1.24.

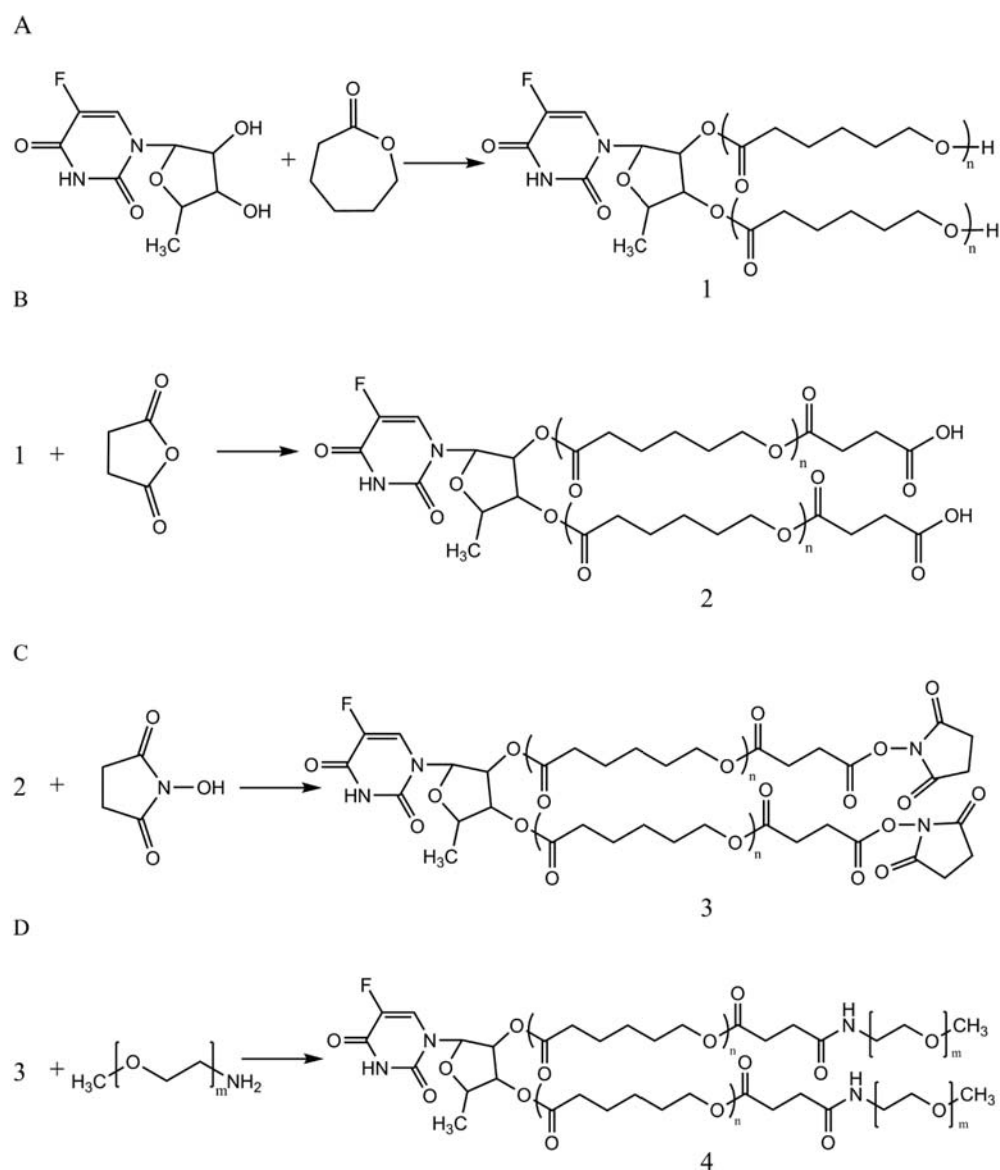


**Figure 4.1.** Synthetic scheme of (A) 5'DFUR-PCL, (B) 5'DFUR -PCL-COOH, (C) 5'DFUR -PCL-NHS, and (D) 5'DFUR -PCL-MPEG.

Hydrophobic 5'DFUR-PCL was further grafted with MPEG (MW=5,000) as shown in Figure 4.1 B-D. GPC analysis revealed that 5'DFUR-PCL-MPEG amphiphilic copolymer had a  $M_n$  of 28 kDa and PDI of 1.19 (Table 4.1). Figure 4.3 (iii) and (iv), shows the  $^1\text{H}$  NMR of MPEG-NH<sub>2</sub> and 5'DFUR-PCL-MPEG. The peaks at 3.63 (A-OCH<sub>2</sub>) attributed to MPEG can be clearly seen in Figure 4.3 (iv). Due to the conjugation of MPEG to 5'DFUR-PCL through amide linkage (Scheme

4.1 D), the change of the peak at 1.79 (B-NH<sub>2</sub>) from a singlet in Figure 4.3 (iii) to a multiplet in Figure 4.3 (iv) further confirms conjugation of MPEG to hydrophobic 5'DFUR-PCL. Further characterization of successful grafting of MPEG to hydrophobic 5'DFUR-PCL was examined through FTIR analysis.

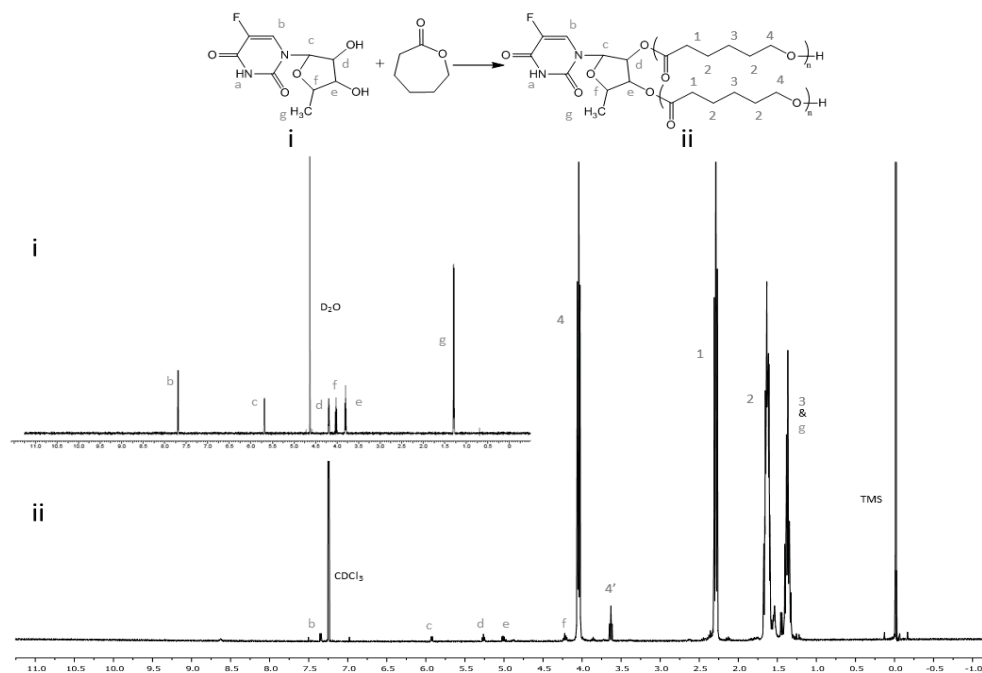


**Figure 4.2.** <sup>1</sup>H NMR spectra of (i) 5'DFUR and (ii) 5'DFUR-PCL.

FTIR was employed to show the successful grafting of MPEG to 5'-DFUR-PCL-NHS (Scheme 4.1 D). FTIR spectra of 5'DFUR-PCL (A), MPEG-NH<sub>2</sub> (B) and 5'DFUR-PCL-MPEG (C) are shown in Figure 4.4. C-H stretching vibrations can be seen from 2957-2839 cm<sup>-1</sup> for all samples. Typical FTIR absorption peaks of PCL and MPEG at 1721 cm<sup>-1</sup> attributed to the C=O stretching and at 1103 cm<sup>-1</sup> of the C-O-C, respectively, were seen in the FTIR spectra. These peaks, as well as characteristic peaks contributed from 5'-DFUR such as C-F stretching at 1049 cm<sup>-1</sup>, C-N stretching of the primary and secondary aromatic amine at 1627 and 1237 cm<sup>-1</sup> were all found in Figure 4.4 (A) and (C). Showing successful initiation of polymerization of  $\epsilon$ -CL by 5'DFUR.

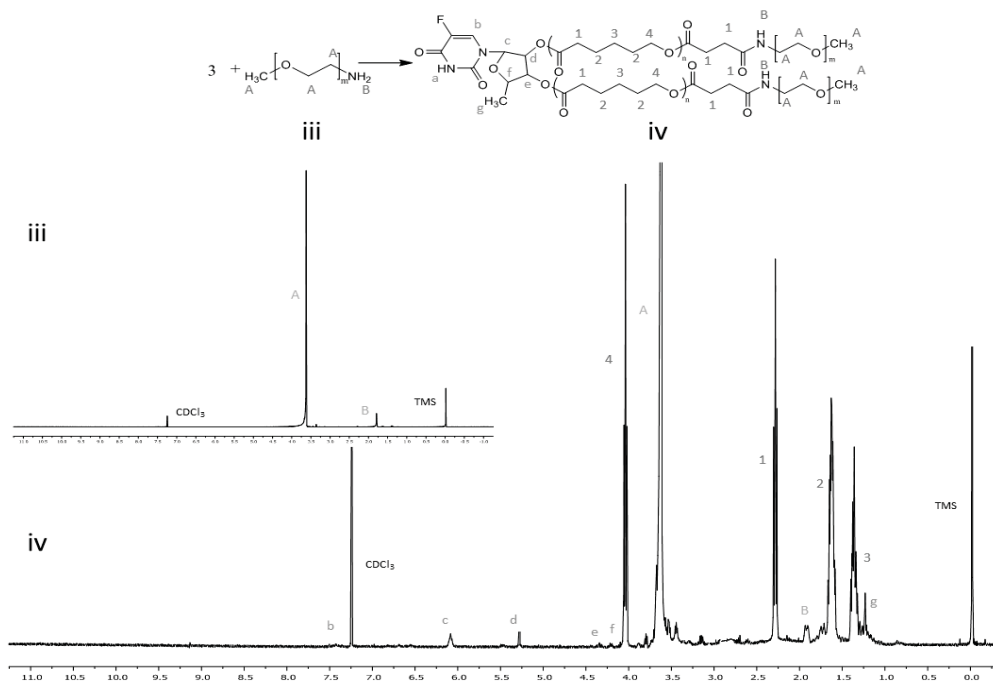


**Figure 4.3.** <sup>1</sup>H NMR spectra of (iii) MPEG and (iv) 5'DFUR-PCL-MPEG.

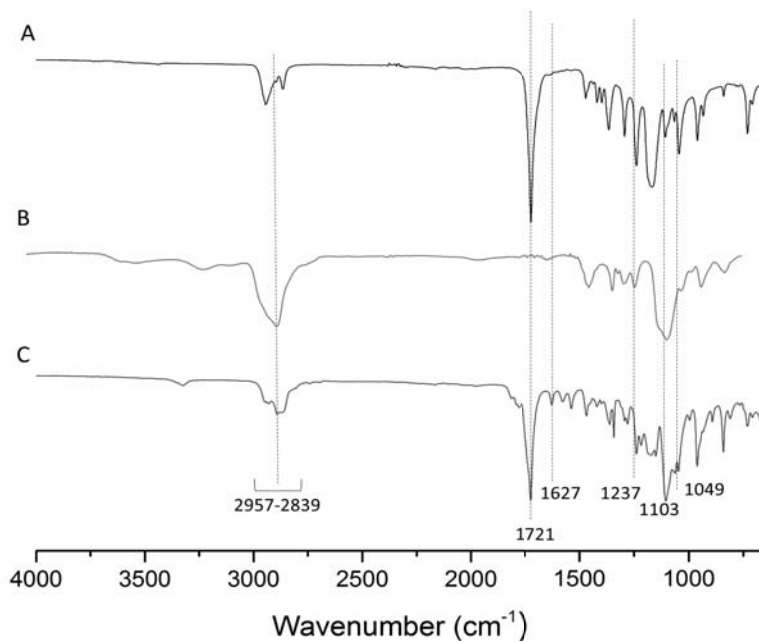


**Figure 4.4.** FTIR spectra of (A) 5'DFUR-PCL, (B) MPEG-NH<sub>2</sub>, and (C) 5'DFUR-PCL-MPEG.

**Table 4.1.** Characterization of 5'DFUR-PCL-MPEG amphiphilic copolymer<sup>a</sup>

Sample	M <sub>w</sub> (Da)	M <sub>n</sub> (Da)	Polydispersity (M <sub>w</sub> /M <sub>n</sub> )
5'DFUR-PCL	18796	15158	1.24
5'DFUR-PCL-MPEG	33927	28510	1.19
MPEG <sub>350</sub> -PCL	24600	17053	1.44
MPEG <sub>350</sub> -PCL-MPEG	19415	21624	1.36

<sup>a</sup>Measured by GPC

#### 4.4.2. Formation and characterization of 5'DFUR-tagged polymeric micelles

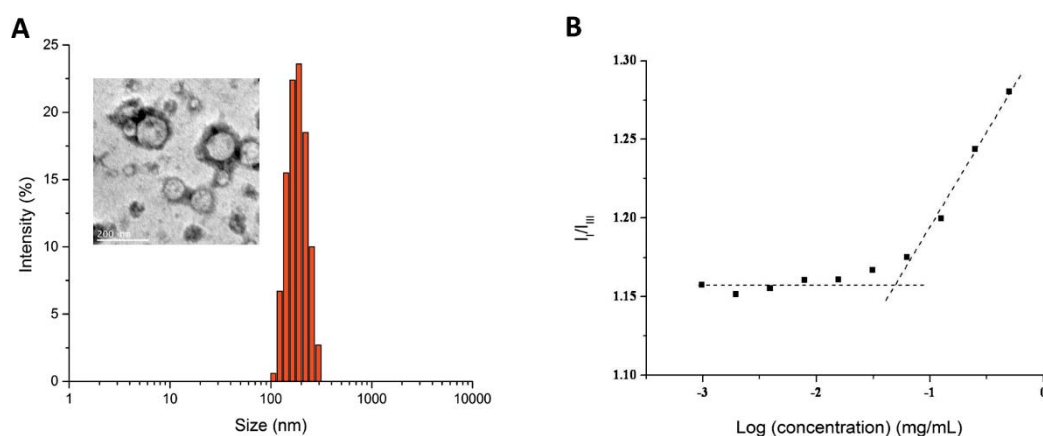
It is known that amphiphilic polymers can self-assemble into micelles in selected solvent. The amphiphilic 5'DFUR-PCL-MPEG copolymer used in this study, could self-assemble into micelles in aqueous solution by the solvent-evaporation method. Here, despite 5'DFUR being slightly water soluble, 5'DFUR-PCL was the hydrophobic core segment and MPEG was the hydrophilic outside shell. In control micelles, MPEG<sub>350</sub>-PCL was the hydrophobic core segment and MPEG was the hydrophilic segment. The average size of 5'DFUR-tagged micelles and control micelles with and without encapsulating DOX or SN-38 and zeta potential as determined by dynamic light scattering (DLS) and zetasizer are shown in Table 4.2. The size of 5'DFUR-PCL-MPEG micelles was around 220.5 nm with a zeta potential of 1.2 mV due to the neutral change of MPEG (Figure 4.5 (A)). Micelles were also characterized by TEM analysis as shown in the Figure 4.5 inset. The size of the micelles in the TEM images was slightly lower than the results from DLS with an average particle size of ~150 nm. This size fluctuation is due to the fact that DLS records the hydrodynamic radius of particles which is often times slightly larger than the actual particle size. As shown in Table 4.2, encapsulation of DOX or SN-38 did not affect the particle size substantially with an average size of 167.5 and 267.5 nm, respectively.



**Table 4.2.** Characteristics and drug loading of 5'DFUR-tagged polymeric micelles

Sample	Size (nm)	Zeta (mV)	Drug loading content (%)	Entrapment efficiency (%)
5'DFUR-PCL-MPEG	220.5	1.23	--	--
5'DFUR-PCL-MPEG (DOX)	167.5	-0.11	10.8	68.8
5'DFUR-PCL-MPEG (SN-38)	267.5	1.01	3.4	86.3
MPEG <sub>350</sub> -PCL-MPEG	202.5	0.74	--	--
MPEG <sub>350</sub> -PCL-MPEG (DOX)	222	2.15	10.4	65.6
MPEG <sub>350</sub> -PCL-MPEG (SN-38)	148	1.21	3.9	97.6

The CMC of 5'DFUR-PCL-MPEG was determined using pyrene as a hydrophobic fluorescent probe to confirm formation of micellar structures [28]. Figure 4.5 B shows the CMC value of 5'DFUR-tagged polymeric micelles in

**Figure 4.5.** (A) Particle size distribution, and (B) plot of the intensity ratio ( $I_I/I_{III}$ ) versus concentration of 5'DFUR-PCL-MPEG micelles. Inset represents TEM image.

aqueous medium. The intensity ratio of the first and third vibrational bands ( $I_{338}/I_{335}$ ) against polymer concentration ( $\text{Log}(\text{concentration})$ ) in pyrene excitation spectra was plotted. A flat region in the low concentration extreme and sigmoidal region in the crossover region was found, and the CMC of 5'DFUR-tagged micelles was  $56 \text{ mg L}^{-1}$ .

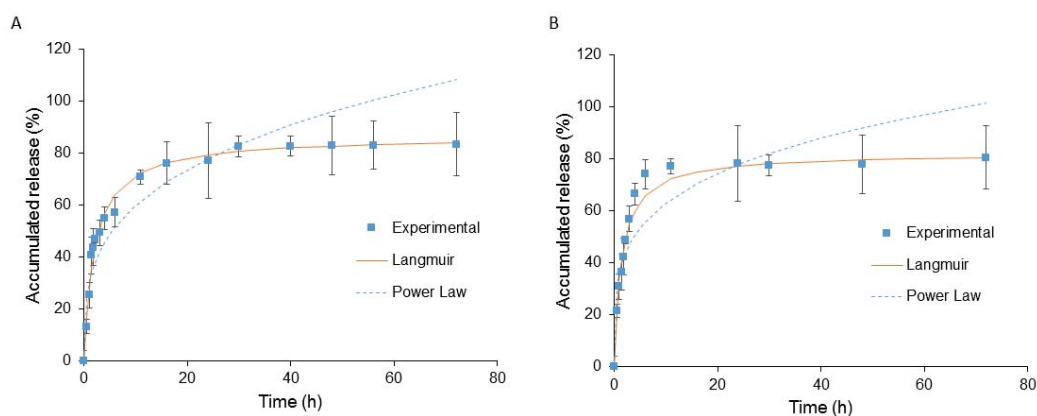
#### 4.4.3 Evaluation of drug loading content and entrapment efficiency

Table 4.2 summarizes the drug loading content and entrapment efficiency of 5'DFUR, DOX, and SN-38 in both 5'DFUR-tagged polymeric micelles and control micelles. To determine the drug loading percentage of 5'DFUR per mg of micelle formulation, the absorbance of 5'DFUR before and after drug release ( $t=0$ ,  $t=72$  h) was examined and compared to a standard calibration curve of 5'DFUR. It was found that 5'DFUR comprised 9.8% of 5'DFUR-PCL-MPEG micelles. Due to the hydrophobic nature of SN-38, it was surmised that the extent of drug loading and entrapment would be high. As can be seen in Table 4.2, our results showed that the drug loading content and entrapment efficiency of SN-38 in 5'DFUR-PCL-MPEG and control micelles was 3.4% and 86.3% and 3.9% and 97.6%, respectively. In contrast, DOX which is slightly hydrophilic had a lower encapsulation efficiency at 68.8% and 65.6% in prodrug-tagged polymeric micelles and control micelles, respectively. However, due to the fact that more DOX was used for encapsulation, the drug loading content was higher at 10.8% and 10.4%. It is known that drug encapsulation efficiency is a crucial design parameter in the development of therapeutic nanocarriers. An ideal nano-carrier should have a high drug encapsulation efficiency and small size to evade the MPS. The synthesized 5'DFUR-tagged micelles developed here exhibit both of these qualities.

#### 4.4.4 In vitro drug release

The *in vitro* release behavior of 5'DFUR both at  $37^\circ\text{C}$  with and without esterase was studied and the results are shown in Figure 4.6 A and B, respectively. To

mimic cellular conditions, esterase at a concentration of 3 units/2 mL was chosen [29]. A two-phase release profile was observed in all conditions with a burst release within the first 2 h followed by sustained release pattern up to 72 h. It was found that it required 2 h before esterase was able to increase the release of 5'DFUR. This observation is in line with other researchers due to the fact that esterase has to take time to diffuse into the micelle and to activate [30, 31]. The release of 5'DFUR in samples without esterase was caused by hydrolysis of ester linkage between 5'DFUR and PCL. It is surmised that the sustained release of 5'DFUR compared to previously reported prodrug release is due to that fact that polymerization can be initiated at two hydroxyl points [32]. Accumulative release of each sample reached a maximum between 78-86%.



**Figure 4.6.** In vitro drug release profile of 5'DFUR from 5'DFUR-PCL-MPEG micelles in PBS at 37°C (A) with esterase, (B) without esterase (mean  $\pm$  SD,  $n = 3$ ).

The release of 5'DFUR from 5'DFUR-PCL-MPEG was modeled using both Power Law and Langmuir models as shown in Figure 4.6 A and B. The Power Law model was not a good fit for the release of 5'DFUR from polymeric micelles. Here, we obtained an exponent,  $n$ , value equal to 0.24 and 0.30 with and without esterase, respectively. If  $n$  is 0.43, for a sphere, this would indicate Fickian diffusion [33]. Due to the fact that our release is not solely through diffusion (i.e. 5'DFUR is chemically bound to PCL through ester bond), our release is reaction

diffusion. Here, the prodrug 5'DFUR, is released through hydrolysis (Figure 4.6 B) or a combination of hydrolysis and esterase (Figure 4.6 A). Therefore, we chose to also model our data with the Langmuir model. The Langmuir model is an enzyme kinetics model, and as can be seen in Figure 4.6, a good fit for the release of 5'DFUR from polymeric micelles. The dissociation constant ( $K_d$ ) for the release of 5'DFUR from 5'DFUR-PCL-MPEG was found to be 1.48 and 3.07 with and without esterase, respectively. Similar to the release of GCV in Chapter 3, our  $K$  value was higher when esterase was not added showing that the association of 5'DFUR to PCL is stronger than ACV (Chapter 2). We speculate that this stronger association is due to the fact that 5'DFUR, like GCV, has two reactive points to initiate polymerization of  $\epsilon$ -CL.

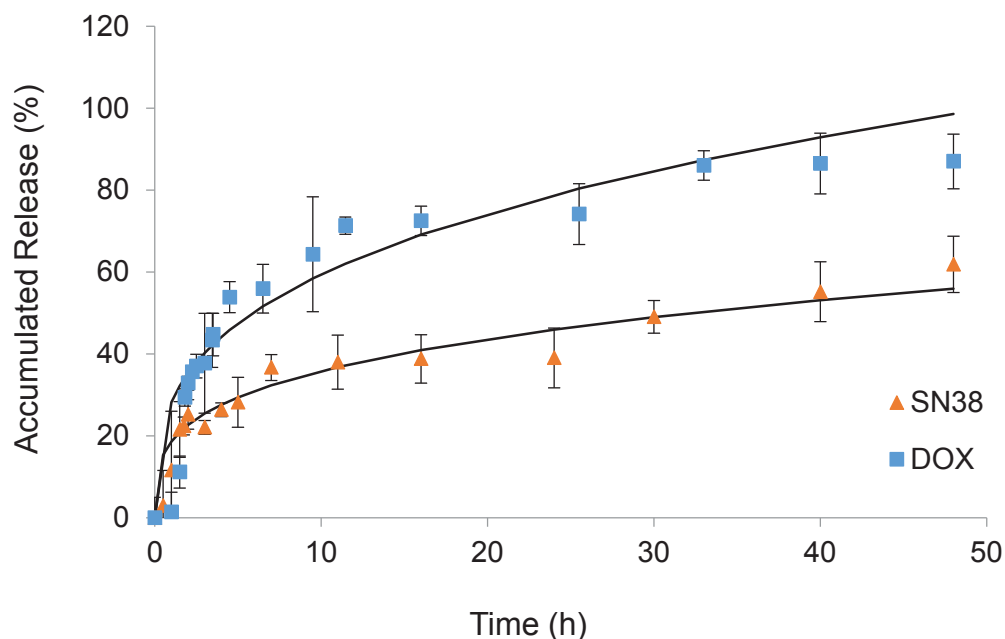


**Figure 4.7.** In vitro drug release profiles of DOX and SN-38 from 5'DFUR-PCL-MPEG micelles in PBS at 37°C (mean  $\pm$  SD, n = 3).

The release of DOX and SN-38 at 37°C in 5'DFUR-PCL-MPEG is shown in Figure 4.7. The release profiles showed that a cumulative release of DOX and SN-38 from 5'DFUR-tagged micelles in PBS at 37°C was 87% and 62%, respectively, after 48 h. Moreover, we modeled the data using the Power Law

and it was found to be a good fit for both of the encapsulated chemotherapeutic drugs. For the release of DOX and SN-38, we obtained  $n$  values of 0.41 and 0.43. These values are very close to the exponent value  $n$  (0.43) for the Fickian diffusion of a sphere. Indicating that Fickian diffusion is most likely the release mechanism for encapsulated chemotherapy drugs DOX and SN-38.

#### 4.4.5. *Cytotoxicity of 5'DFUR-tagged polymeric micelles loaded with chemotherapeutic agents*

*In vitro* toxicity of polymeric prodrug micelles to parental HT29 cells was evaluated. Due to the fact that HT29 cells express endogenous TP levels [34], 5'DFUR released from micelles would be converted to its active and toxic form 5-FU. Figure 4.8 compares the viability of control micelles and 5'DFUR-PCL-MPEG micelles. Here, it can be seen that micelles without prodrug are nontoxic up to a concentration of 2 mg mL<sup>-1</sup> (Figure 4.8 A). In contrast, the viability of HT29 cells is decreased to 60% when challenged with 2 mg mL<sup>-1</sup> 5'DFUR-PCL-MPEG micelles for 72 h (Figure 4.8 B). Moreover, it is shown that a concentration of 5'DFUR-tagged micelle greater than or equal to 0.5 mg mL<sup>-1</sup> is needed for cell death to occur. For this reason subsequent cytotoxicity studies with chemotherapeutic drugs DOX and SN-38 were not evaluated below 0.5 mg mL<sup>-1</sup>.

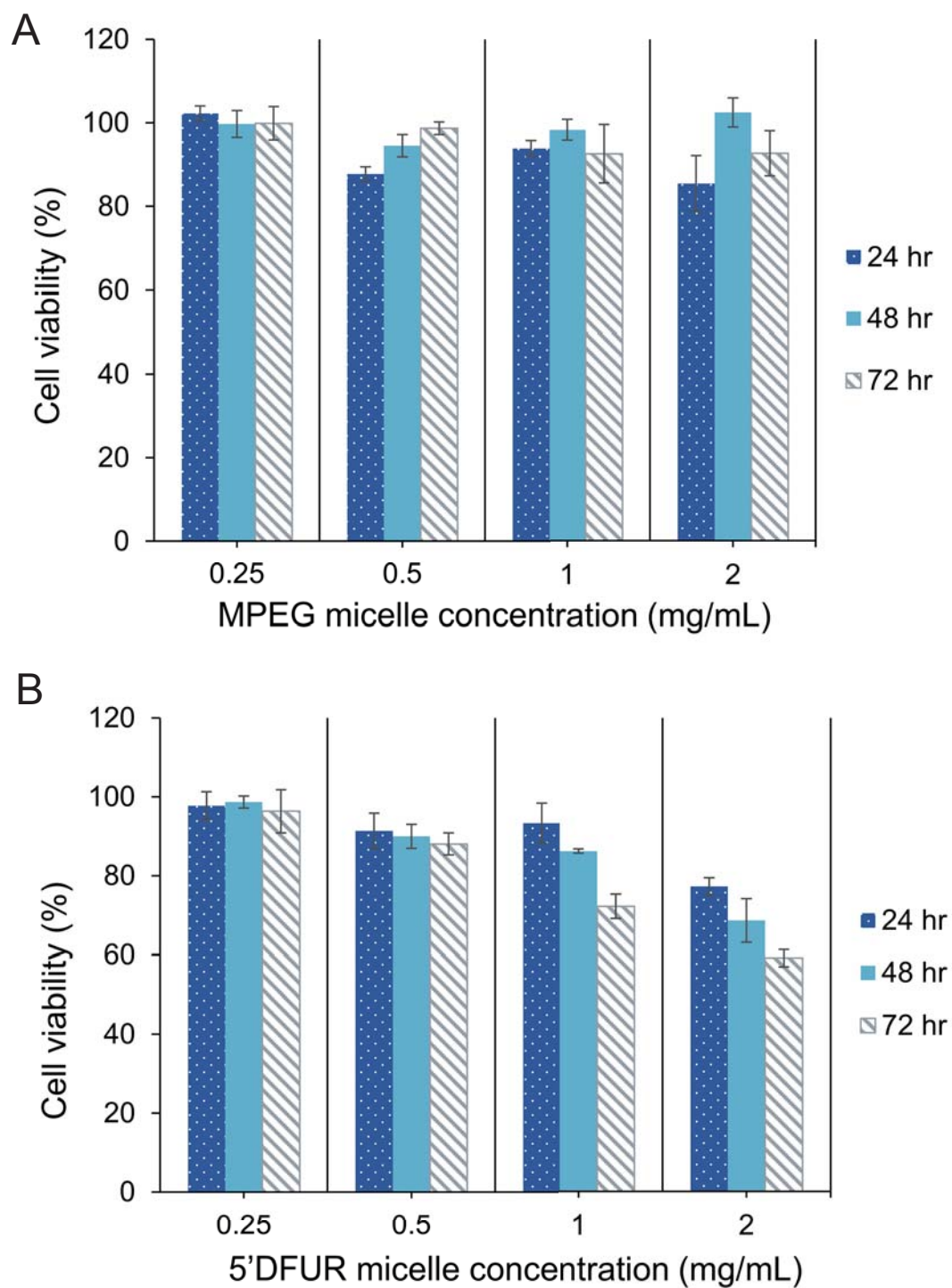


**Figure 4.8.** Cell viability of HT29 cells after treatment with polymeric micelles for 24, 48, and 72 h. (A) MPEG-PCL-MPEG polymeric micelles, (B) 5'DFUR-PCL-MPEG polymeric micelles.

As can be seen from Figure 4.9 and Figure 4.10, HT29 cell viability was decreased in both control (A) and prodrug-tagged micelles with encapsulated chemotherapy drug (B). Control micelles without chemotherapy drug, showed little to no toxicity (Figure 4.8 A), after the encapsulation of DOX or SN-38 into MPEG-PCL-MPEG micelles, viability was reduced to 53% and 43%, respectively, with the highest dose for 72 h (Figure 4.9 A and Figure 4.10 A). Toxicity of HT29 cells treated with 5'DFUR-PCL-MPEG micelle with encapsulated DOX showed an increased cell death from 60% viability without DOX to 36.6% viability (Figure 4.9 B). This corresponds to an additive effect from both 5'DFUR converted to 5-FU by endogenous TP gene plasmid and DOX chemotherapy drug. The toxicity of 5'DFUR-tagged micelles which encapsulated SN-38 was also increased from 60% cell viability to 31% again showing an additive effect between 5'DFUR and chemotherapy drug SN-38 in cancer cell treatment. The results of cell viability show that delivery of 5'DFUR-tagged polymeric micelles can decrease viability of HT29 cells and that encapsulation of chemotherapy drugs can substantially increase cell death.

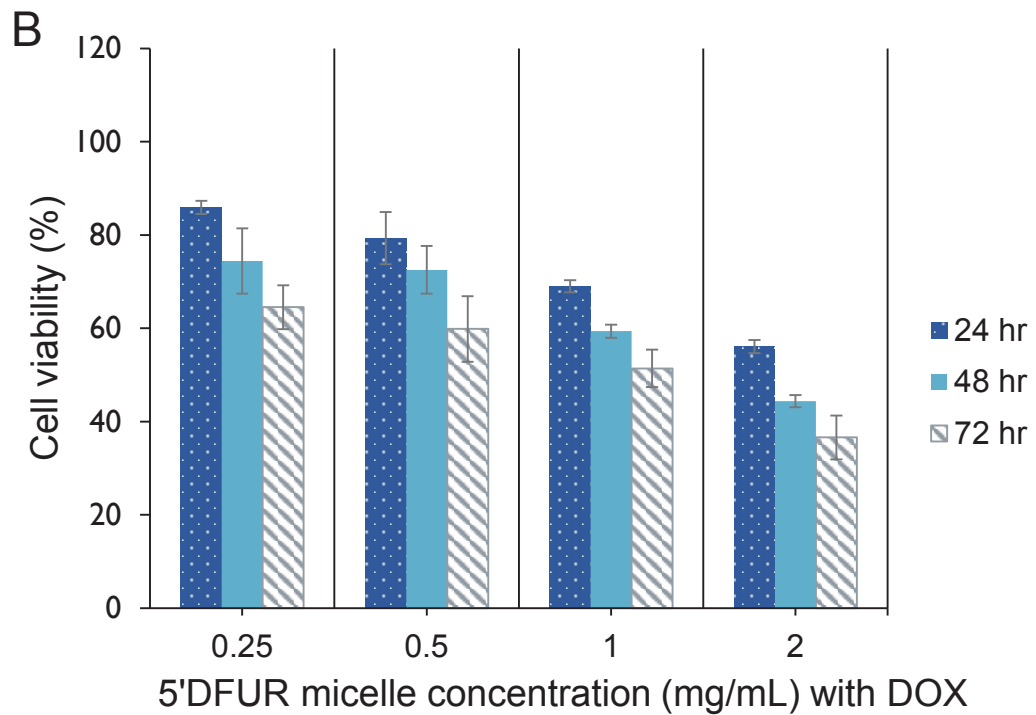
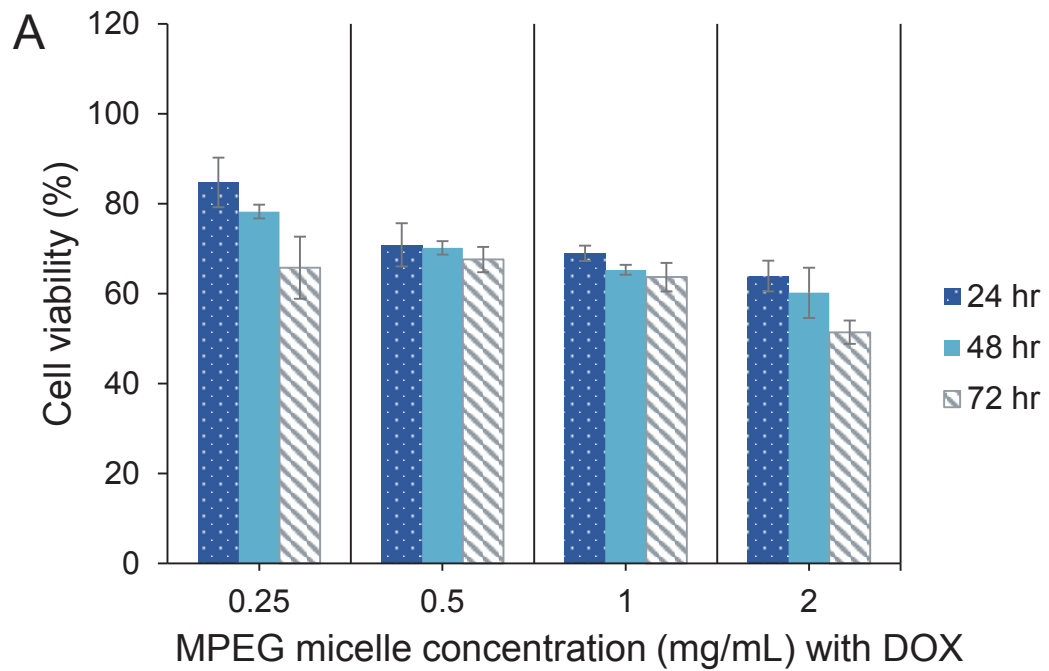


**Figure 4.9.** Cell viability of HT29 cells after treatment with polymeric micelles encapsulating DOX for 24, 48, and 72 h. (A) MPEG-PCL-MPEG polymeric micelles, (B) 5'DFUR-PCL-MPEG polymeric micelles.



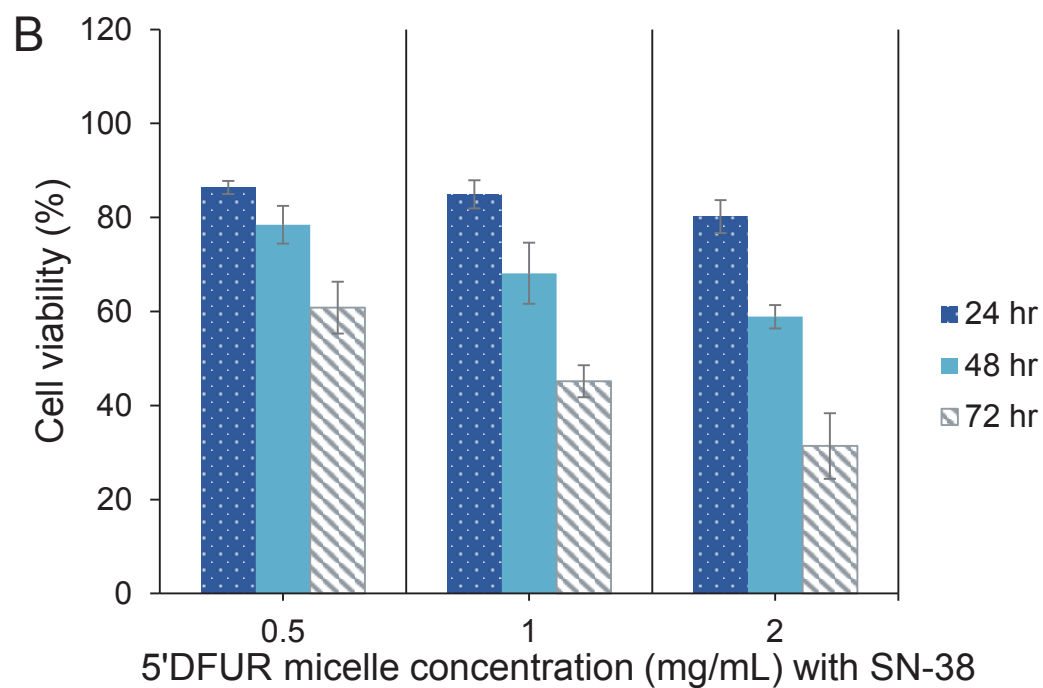
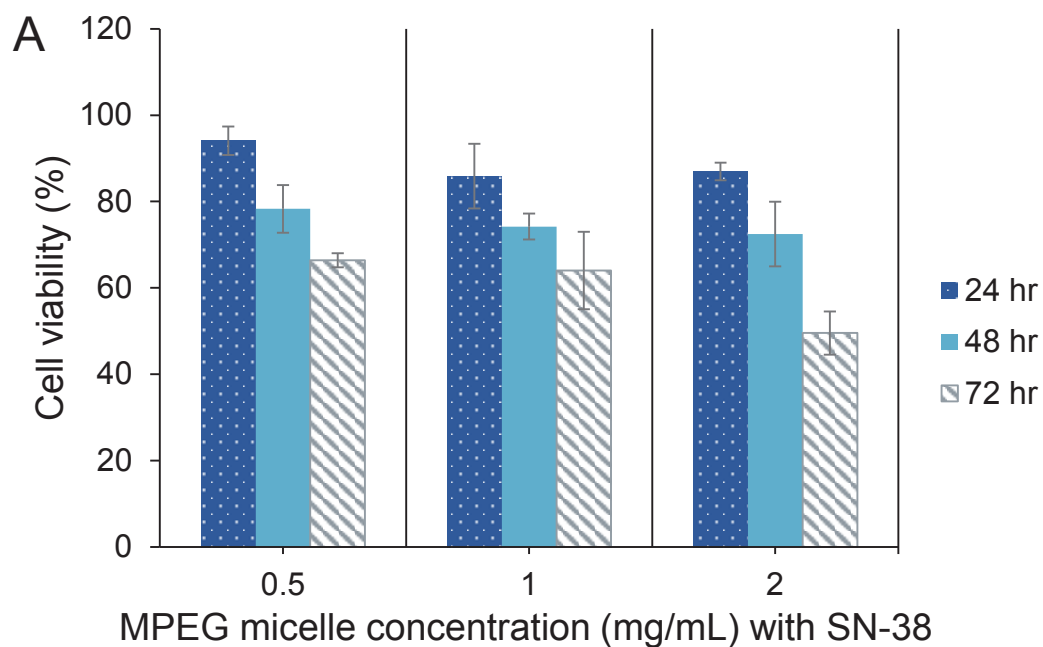


**Figure 4.10.** Cell viability of HT29 cells after treatment with polymeric micelles encapsulating SN-38 for 24, 48, and 72 h. (A) MPEG-PCL-MPEG polymeric micelles, (B) 5'DFUR-PCL-MPEG polymeric micelles.

#### 4.5. CONCLUSION

The results of this study show that 5'DFUR-PCL-MPEG micelles were synthesized and characterized. Moreover, results showed that polymeric micelles of 5'DFUR-PCL-MPEG successfully delivered prodrug into HT29 colon cancer cells and it was clearly revealed that endogenous TP in parental HT29 colon cancer cells could convert prodrug 5'DFUR into cytotoxic 5-FU thereby killing the cells. Moreover, co-delivery of 5'DFUR and DOX or SN-38 greatly enhanced the cell death. Development of similar prodrug nanocarrier show potential for enhancing the effectiveness of gene-directed enzyme prodrug therapy.

#### 4.6. REFERENCES

1. De Gramont A, Louvet C, André T *et al.* A review of GERCOD trials of bimonthly leucovorin plus 5-fluorouracil 48-h continuous infusion in advanced colorectal cancer: evolution of a Regimen. *European Journal of Cancer* 34(5), 619-626 (1998).
2. Shimma N, Umeda I, Arasaki M *et al.* The design and synthesis of a new tumor-selective fluoropyrimidine carbamate, Capecitabine. *Bioorganic and Medicinal Chemistry* 8(7), 1697-1706 (2000).
3. Bronckaers A, Gago F, Balzarini J *et al.* The dual role of thymidine phosphorylase in cancer development and chemotherapy. *Medicinal Research Reviews* 29(6), 903-953 (2009).
4. Patterson AV, Zhang H, Moghaddam A *et al.* Increased sensitivity to the prodrug 5'-deoxy-5-fluorouridine and modulation of 5-fluoro-2'-deoxyuridine sensitivity in MCF-7 cells transfected with thymidine phosphorylase. *British Journal of Cancer* 72(3), 669-675 (1995).
5. Haraguchi M, Furukawa T, Sumizawa T *et al.* Sensitivity of human KB cells expressing platelet-derived endothelial cell growth factor to pyrimidine antimetabolites. *Cancer Research* 53(23), 5680-5682 (1993).
6. Nakano Y, Ohota J, Fujita M *et al.* Clinical effect of 5'-deoxy-5-fluorouridine (5'-DFUR). *Gan No Rinsho* 31(6 Suppl), 746-750 (1985).
7. Sumimoto R, Takahashi M, Etoh T *et al.* Effectiveness of high-dose, intermittent 5'-DFUR therapy for advanced gastric cancer. *Gan To Kagaku Ryoho* 28(1), 83-86 (2001).
8. Hirano M, Kato A, Murakami N *et al.* A case of recurrent colon cancer treated markedly effective with 5'-DFUR. *Gan To Kagaku Ryoho* 20(8), 1063-1066 (1993).
9. Tagaya N, Kakihara Y, Hamada K *et al.* Docetaxel (TXT), epirubicin (EPI) and doxifluridine (5'-DFUR) combination neoadjuvant chemotherapy for outpatients with locally advanced breast cancer. *Gan To Kagaku Ryoho* 31(13), 2155-2158 (2004).
10. Iba T, Kidokoro A, Fukunaga M *et al.* The efficacy of combination chemotherapy of 5'-deoxy-5-fluorouridine (5'-DFUR), cyclophosphamide (CPA) and medroxyprogesterone acetate (MPA) for bone metastasis in breast cancer patients. *Gan To Kagaku Ryoho* 28(7), 973-977 (2001).
11. Takatsuka Y, Yayoi E, Miyauchi K *et al.* A comparative study with 5'-DFUR alone or in combination with tamoxifen (TAM) or medroxyprogesterone acetate (MPA) for advanced or recurrent breast cancer. *Gan To Kagaku Ryoho* 19(5), 631-636 (1992).
12. Pierri E, Avgoustakis K. Poly(lactide)-poly(ethylene glycol) micelles as a carrier for griseofulvin. *Journal of Biomedical Materials Research Part A* 75A(3), 639-647 (2005).
13. Yue J, Liu S, Wang R *et al.* Transferrin-conjugated micelles: Enhanced accumulation and antitumor effect for transferrin-receptor-overexpressing cancer models. *Molecular Pharmaceutics* 9(7), 1919-1931 (2012).
14. Tabatabaei Rezaei SJ, Nabid MR, Niknejad H *et al.* Multifunctional and thermoresponsive unimolecular micelles for tumor-targeted delivery and site-specifically release of anticancer drugs. *Polymer* 53(16), 3485-3497 (2012).
15. Matsumura Y, Kataoka K. Preclinical and clinical studies of anticancer agent-incorporating polymer micelles. *Cancer Science* 100(4), 572-579 (2009).

16. Hamaguchi T, Kato K, Yasui H *et al.* A phase I and pharmacokinetic study of NK105, a paclitaxel-incorporating micellar nanoparticle formulation. *British Journal of Cancer* 97(2), 170-176 (2007).
17. Matsumura Y, Hamaguchi T, Ura T *et al.* Phase I clinical trial and pharmacokinetic evaluation of NK911, a micelle-encapsulated doxorubicin. *British Journal of Cancer* 91(10), 1775-1781 (2004).
18. Chabner BA, Longo DL. Cancer chemotherapy and biotherapy: Principles and practice. Lippincott Williams & Wilkins, (2011).
19. Slatter JG, Schaaf LJ, Sams JP *et al.* Pharmacokinetics, metabolism, and excretion of irinotecan (CPT-11) following iv infusion of [<sup>14</sup>C] CPT-11 in cancer patients. *Drug Metabolism and Disposition* 28(4), 423-433 (2000).
20. Rothenberg ML, Kuhn JG, Burris H *et al.* Phase I and pharmacokinetic trial of weekly CPT-11. *Journal of Clinical Oncology* 11(11), 2194-2204 (1993).
21. Chang KY, Lee YD. Ring-opening polymerization of  $\epsilon$ -caprolactone initiated by the antitumor agent doxifluridine. *Acta Biomaterialia* 5(4), 1075-1081 (2009).
22. Albertsson A-C, Varma IK. Recent Developments in Ring Opening Polymerization of Lactones for Biomedical Applications. *Biomacromolecules* 4(6), 1466-1486 (2003).
23. Cerrai P, Tricoli M. Block copolymers from L-lactide and poly(ethylene glycol) through a non-catalyzed route. *Die Makromolekulare Chemie, Rapid Communications* 14(9), 529-538 (1993).
24. Zhang Y, Li X, Zhou Y *et al.* Preparation and Evaluation of Poly(Ethylene Glycol)-Poly(Lactide) Micelles as Nanocarriers for Oral Delivery of Cyclosporine A. *Nanoscale Research Letters* 5(6), 917 - 925 (2010).
25. Xue B, Wang Y, Tang X *et al.* Biodegradable self-assembled MPEG-PCL micelles for hydrophobic oridonin delivery in vitro. *Journal of Biomedicine and Nanotechnology* 8(1), 80-89 (2012).
26. Brannon-Peppas L, Blanchette JO. Nanoparticle and targeted systems for cancer therapy. *Advanced Drug Delivery Reviews* 56(11), 1649-1659 (2012).
27. Wilhelm M, Zhao CL, Wang Y *et al.* Poly(styrene-ethylene oxide) block copolymer micelle formation in water: a fluorescence probe study. *Macromolecules* 24(5), 1033-1040 (1991).
28. Kalyanasundaram K, Thomas JK. Environmental effects on vibronic band intensities in pyrene monomer fluorescence and their application in studies of micellar systems. *Journal of the American Chemical Society* 99(7), 2039-2044 (1977).
29. Liewald F, Demmel N, Wirsching R *et al.* Intracellular pH, esterase activity, and DNA measurements of human lung carcinomas by flow cytometry. *Cytometry* 11(3), 341-348 (1990).
30. Fukuda M, Kunugi S. Kinetic studies of wheat carboxypeptidase-catalyzed reaction: Differences in pressure and temperature dependence of peptidase and esterase activities. *Journal of Biochemistry* 101(1), 233-240 (1987).
31. Guichard S, Terret C, Hennebelle I *et al.* CPT-11 converting carboxylesterase and topoisomerase activities in tumour and normal colon and liver tissues. *British Journal of Cancer* 80(3-4), 364-370 (1999).
32. Sawdon AJ, Peng CA. Polymeric micelles for acyclovir drug delivery. *Colloids and Surfaces B: Biointerfaces* 122(1), 738-745 (2014).
33. Siepmann J, Siepmann F. Mathematical modeling of drug delivery. *International Journal of Pharmaceutics* 364(2), 328-343 (2008).

34. Schwartz EL, Baptiste N, Wadler S *et al.* Thymidine phosphorylase mediates the sensitivity of human colon carcinoma cells to 5-fluorouracil. *Journal of Biological Chemistry* 270(32), 19073-19077 (1995).

## CHAPTER 5: DEVELOPMENT OF ANTIPHAGOCYtic CD47-TAGGED POLYMERIC MICELLES TO TARGET $\alpha_v\beta_3$ INTEGRIN-BEARING TUMOR CELLS<sup>5</sup>

### 5.1. ABSTRACT

Methoxy(polyethylene glycol) (MPEG) was used as the initiator in ring-opening polymerization of  $\epsilon$ -caprolactone to form hydrophobic MPEG-polycaprolactone, which was then grafted to hydrophilic cationic polymeric polyethyleneimine to form amphiphilic copolymers for the preparation of stable micellar nanoparticles. The formed polymeric micelles were biotinylated via the interaction of biotin/EDC with the amines on cationic polymers. CD47-streptavidin (extracellular domain of self-marker CD47) fusion protein was expressed in BL21(DE3) bacteria and then the crude protein used directly. Through biotin-streptavidin affinity, CD47 was bound to biotinylated polymeric prodrug micelles and showed antiphagocytic efficacy when CD47-tagged polymeric micelles were exposed to J774A.1 macrophages. Since CD47 is not only an antiphagocytic ligand but also an integrin associated protein, it can be employed to target integrin  $\alpha_v\beta_3$ , which is overexpressed on tumor-activated neovascular endothelial cells. In this study, CD47-tagged polymeric prodrug micelles were employed to treat two cells lines -one expressing integrin  $\alpha_v\beta_3$  and one without integrin  $\alpha_v\beta_3$  expression. Results show that functionalized polymeric micelle drug carriers were successfully targeted to integrin  $\alpha_v\beta_3$  by using CD47 as a targeting moiety.

### 5.2. INTRODUCTION

Drug delivery carriers have the potential not only to treat but also diagnose many diseases. However, they still lack in complexity of natural particulates. Red blood cells, for example, exhibit all of the traits researchers want for their carriers: they possess a small size, flexibility and ability to evade the immune system for up to

<sup>5</sup>The material contained in this chapter is planned for publication in *ACS Biomaterials*.

4 months [1]. In 2000, Oldenborg et al., reported that CD47 functioned as a marker of self on red blood cells [2]. It was found that as a red blood cell ages, CD47 expression levels do indeed decrease [3]. Moreover, it has been shown that CD47-streptavidin (CD47-SA) fusion protein endowed antiphagocytic effect to perfluorocarbon-based oxygen carriers [4]. Furthermore, since CD47 is an integrin associated protein [5], it might be employed to target integrin  $\alpha_v\beta_3$ , which is overexpressed on tumor-activated neovascular endothelial cells and unexpressed on mature quiescent ones lined in blood vessels [6]. In this study, CD47-SA was bound on to biotinylated micelle carriers and the antiphagocytic properties as well as ability to target  $\alpha_v\beta_3$  integrin examined.

To this end, polymeric micelles were chosen as a model system for this study. Here, methoxy(poly ethylene glycol) (MPEG) possessing a hydroxyl group was used as the initiator of  $\epsilon$ -caprolactone to obtain MPEG-poly( $\epsilon$ -caprolactone) (MPEG-PCL). PCL, is widely used as a core-forming hydrophobic segment because of its biodegradability and biocompatibility [7-9]. To form amphiphilic block copolymers for micelle preparation, hydrophilic polyethylenimine (PEI) was grafted onto hydrophobic MPEG-PCL. PEI is widely used for nonviral gene delivery [10-12]. Our results show that CD47-tagged polymer micelles can evade phagocytosis for up to 6 h. Moreover, carriers targeted to cells bearing high levels of integrin  $\alpha_v\beta_3$  had much higher uptake of micelles after 4 h of treatment.

### 5.3. MATERIALS AND METHODS

#### 5.3.1. *Materials*

N,N'-dicyclohexyl carbodiimide (DCC),  $\epsilon$ -CL, pyrene, and succinic anhydride were purchased from Acros Organics (Geel, Belgium). Sn(Oct)<sub>2</sub>, CDCl<sub>3</sub> with 1% tetramethylsilane (TMS), deuterated dimethyl sulfoxide (DMSO-d<sub>6</sub>), dimethyl sulfoxide (DMSO), tetrahydrofuran (THF), dichloromethane (DCM), methanol, 2-propanol, hexane, toluene, MPEG (MW = 350), PEI (MW = 10K), Biotin, and 1-Ethyl-3-(3-dimethylaminopropyl)carbodiimide (EDC) were all purchased from

Sigma-Aldrich (St. Louis, MO). Ethyl ether was purchased from J.T. Baker (Austin, TX). N-Hydroxysuccinimide (NHS) was purchased from Alfa Aesar (Ward Hill, MA). Acetone was purchased from Pharmco-AAPER (Shelbyville, KY). Pyridine and hydrochloric acid (HCl) were purchased from EMD (Philadelphia, PA). Sodium chloride (NaCl) and magnesium sulfate were purchased from Showa (Tokyo, Japan). All reagents were used as received without further purification.

### 5.3.2. *Synthesis of MPEG-PCL-PEI*

MPEG (50 mg) was weighed and mixed with  $\epsilon$ -CL (2.25 mL) under a sonication bath for 5 min at room temperature. Sn(Oct)<sub>2</sub> (0.5 wt% of  $\epsilon$ -CL) was then added into the mixture. The entire solution was placed into a 3-necked round-bottom flask. The system was purged with nitrogen and immersed in an oil bath at 140°C for 24 h. The crude product was cooled to room temperature, dissolved in DCM, and precipitated by cold methanol. The product was then vacuum dried by a rotary evaporator at 40°C.

MPEG-PCL (0.5 mmol) and succinic anhydride (1 mmol) were weighed and dissolved in toluene in a 3-necked round-bottom flask. One mmol pyridine was added and the solution was reacted under nitrogen at 70°C for 48 h. The product was then precipitated by cold hexane, and spun down. The pellet was re-dissolved in DCM and washed twice each with 10% (v/v) HCl and saturated NaCl solution. The organic phase was isolated and dried with magnesium sulfate then filtered. The carboxylated MPEG-PCL was recovered by precipitation in cold hexane and then vacuum dried by rotary evaporation at 40°C.

MPEG-PCL-COOH (0.54 mmol) and NHS (2.7 mmol) were weighed and mixed in 15 mL DCM, and then DCC (2.7 mmol) was added. The reaction was run under a nitrogen environment at room temperature for 24 h. The precipitated byproduct 1,3-dicyclohexylurea was removed by vacuum filtration. The filtrate



was added into 35 mL diethyl ether and cooled to 4°C for 4 h to precipitate MPEG-PCL-NHS. The precipitate was collected by centrifugation at 3,500 rpm for 5 min, washed with 2-propanol and solvent removed by rotary evaporation at 40°C.

MPEG-PCL-NHS (10 mg) and PEI (MW = 10K) (10 mg) were weighed and dissolved by 20 mL DCM in a round-bottom flask. The flask was purged with nitrogen and the solution was stirred for 24 h. The solution was then dialyzed (MWCO = 6-8 kD, Spectra/Por, Rancho Dominguez, CA) against pure DCM to remove remaining PEI. MPEG-PCL-PEI was recovered by rotary evaporation at 40°C.

#### 5.3.3. *Preparation of polymeric micelles*

MPEG-PCL-PEI were formed by adding 10 mg of MPEG-PCL-PEI amphiphilic polymer, to 2 mL acetone and dissolving under bath sonication. The solution was then added dropwise to 10 mL deionized water under bath sonication. Acetone was removed by rotary evaporation and the final solution was collected by filtering through a 0.45 µm filter.

#### 5.3.4. *Size and zeta potential measurements*

The average particle size of polymeric prodrug micelles was determined by a dynamic light scattering (DLS) instrument (Zetasizer Nano ZS, Malvern Instruments, United Kingdom) equipped with a red laser at a wavelength of 633 nm and scattering angle of 90° at 25°C. The zeta potential of the micelles dispersed in deionized water was determined with a zeta potential analyzer (Zetasizer Nano ZS).

#### 5.3.5. *Biotinylation of polymeric micelles*

EDC was used to activate biotin for subsequent reaction with polymeric micelles. Here, 1 mg Biotin and 1 mg EDC were dissolved in PBS for 15 min. Biotin/EDC

mixture was then added to MPEG-PCL-PEI micelles ( $1 \text{ mg mL}^{-1}$ ) and mixed. After 30 min,  $10 \text{ }\mu\text{L}$  FITC ( $5 \text{ mg mL}^{-1}$  in DMSO) was added to the micelle/biotin/EDC mixture. After 3 h, the biotinylated micelles were purified by dialysis (MWCO = 6-8 kD, Spectra/Por, Rancho Dominguez, CA) to remove excess biotin/EDC and FITC.

### 5.3.6. *Amplification and expression of CD47-SA fusion protein*

Mouse CD47 cDNA clone pME18S-FL3 CD47 was obtained from Dr. Stanley Tahara at University of Southern California. The extracellular domain of CD47 was amplified from full-length mouse CD47 cDNA by polymerase chain reaction (PCR) with the sense primer 5'-GGCTCATGACAGCTCAACTACTGTTTAGT-3' and the antisense primer 5'-GCGGGATCCTTTTCATTTGGAG-3'. The core streptavidin coding region was amplified by PCR from pSTE2-215 (yol), which is single chain antibody fused to core streptavidin, using PCR primers 5'-CGGATCCTGGTGCTGCTGAAGCAGGTATCACCT-3' and 5'-GCTCGAGGGAGGCGGCGGACGG-3'. Core streptavidin was inserted between BamHI and XhoI site of pET20b (Novagen) to give pMA005. The extracellular domain of CD47 PCR product was inserted between the NcoI and BamHI site of pMA005 to yield pMA006.

DH5 $\alpha$  competent cells (Invitrogen) were used for plasmid amplification of pMA006. Briefly,  $2 \text{ }\mu\text{L}$  of plasmid solution was mixed with  $100 \text{ }\mu\text{L}$  competent cells. After incubating on ice for 30 min cells were heat-shocked for 45 sec in a  $42^\circ\text{C}$  water bath. Cells were added to  $0.9 \text{ mL}$  SOC medium and agitated in a shaker incubator at  $37^\circ\text{C}$  for 1 h. Cell suspension was added to agar plated containing  $50 \text{ }\mu\text{g mL}^{-1}$  ampicillin and grown overnight. For CD47-SA expression, BL21(DE3) cells (Invitrogen) were used. Here,  $5 \text{ }\mu\text{L}$  pMA006 was added to  $100 \text{ }\mu\text{L}$  BL21(DE3) cells, incubated on ice for 30 min and then heat-shocked for 30 sec in a  $42^\circ\text{C}$  water bath. The cells were added to  $0.250 \text{ mL}$  SOC medium and then agitated in a shaker incubator at  $37^\circ\text{C}$  for 1 h. Cells were then spread on agar plates

containing 100 µg mL<sup>-1</sup> ampicillin and incubated overnight at 37°C. One colony was chosen from the plate and grown until they reached mid-log (OD = 0.4). For induction, 1 mM isopropylthiogalactoside (IPTG) was added. Protein was purified from bacterial lysates by standard methods and then used directly for subsequent studies.

### 5.3.7. *Quantification of CD47-SA binding*

The amount of biotin conjugated onto the micelle surface was determined through the spectrophotometric method proposed by Green et al [13]. The basis of this assay is that the dye HABA binds to avidin, but is stoichiometrically displaced by biotin. Briefly, 10 mL DI water was added to HABA/avidin reagent (Sigma). In a 96-well plate, 90 µL HABA/avidin reagent and 10 µL sample was added. The absorbance at 500 nm was then read. Using the Beer Lambert law, the amount of biotin/micelle particle was determined:

$$\frac{\text{Biotin}}{\text{Micelle particles}} = \frac{\frac{\Delta A_{500} \text{ mmole}}{34000 * l \text{ ml}}}{\frac{\text{micelle particles}}{\text{ml}}} \quad (1)$$

Where A is the absorbance of the sample at 500 nm, ε is the absorptivity of extinction coefficient, l is the cell path length expressed in cm and C is the concentration of the sample expressed in molarity. The amount of biotin calculated was then assumed to directly relate to the amount of CD47-SA bound onto the particle surface.

### 5.3.8. *Macrophage studies*

Murine macrophage cell line J774A.1 (ATCC) was used for phagocytosis assays. Cells (10<sup>6</sup>) were plated in 6-well plates with 2 mL Dulbecco's modified Eagles' medium (DMEM, Corning Cellgro, Manassas, VA) supplemented with 10% fetal bovine serum (FBS, Atlanta biologicals, Flowery Branch, GA) and 1% penicillin-streptomycin (Sigma) and incubated at 37°C in 5% CO<sub>2</sub> balanced with humidified

air for 24 h.. Macrophage cells were then treated with CD47-tagged polymeric micelles and biotinylated polymeric micelles. The cells were imaged under Leica DMI3000 B microscope equipped with a Leica DFC360 FX camera (Leica Microsystems, Wetzlar, Germany) at 2 h, 4 h and 6 h. After each time point, cells were washed with PBS and then trypan blue solution ( $2 \text{ mg mL}^{-1}$ ) was added to quench outside fluorescence and imaged again. Cells were then used directly for flow cytometry analysis (BD Accuri C6).

#### 5.3.9. *Integrin targeting*

PC3 cells (ATCC), which overexpress integrin  $\alpha_v\beta_3$ , and BHK21 cells, which have low integrin  $\alpha_v\beta_3$  expression, were used for integrin targeting studies. Cells ( $10^6$ ) were plated in 6-well plates with 2 mL Dulbecco's modified Eagles' medium supplemented with 10% fetal bovine serum and 1% penicillin-streptomycin and incubated at  $37^\circ\text{C}$  in 5%  $\text{CO}_2$  balanced with humidified air for 24 h. Cells were then treated with CD47-tagged polymeric micelles and biotinylated polymeric micelles. After 2 h and 4 h, cells were washed and  $2 \text{ mg mL}^{-1}$  trypan blue solution was added to quench outside fluorescent. Cells were imaged by fluorescent microscopy (Leica).

### 5.4. RESULTS AND DISCUSSION

#### 5.4.1. *Characterization of polymeric micelles*

Figure 5.1 (A-D), shows the synthesis of MPEG-PCL-PEI copolymer. Size and zeta analysis of polymeric prodrug micelles can be seen in Figure 5.2. An average size of 153.2 nm and zeta potential of 43.4 mV was seen for MPEG-PCL-PEI micelles.

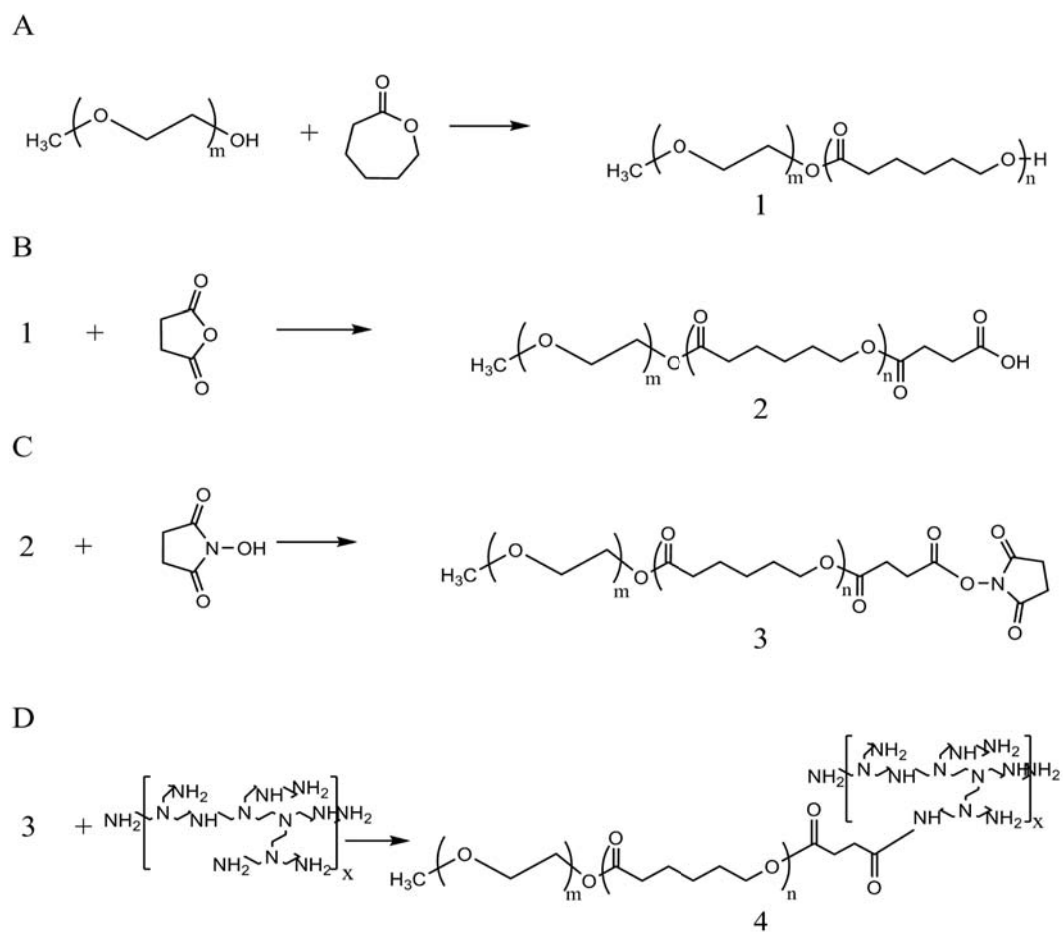


**Figure 5.1.** Synthetic scheme of (A) MPEG-PCL, (B) MPEG-PCL-COOH, (C) MPEG-PCL-NHS, and (D) MPEG-PCL-PEI

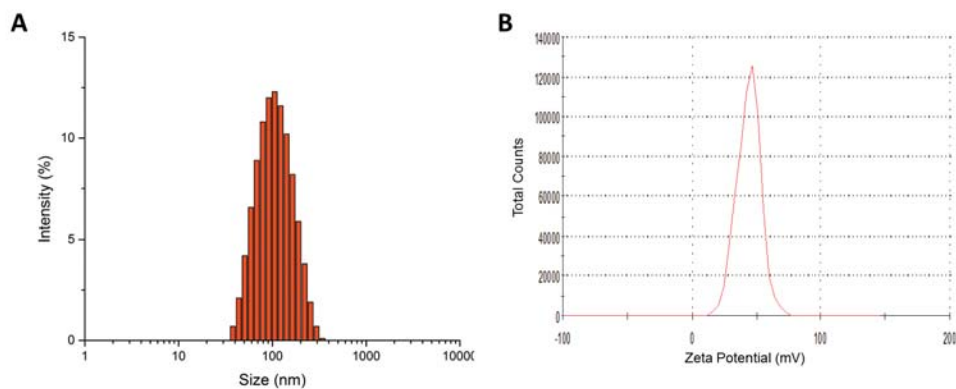


**Figure 5.2.** Size and zeta analysis of MPEG-PCL-MPEG.

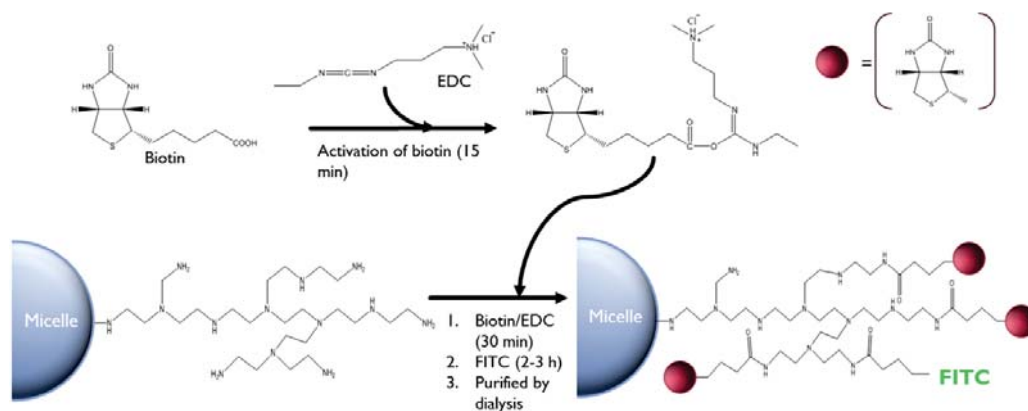


**Figure 5.3.** Synthetic scheme of biotinylation and fluorescence of micelles.

After synthesis of the copolymer, and self-assembly into micellar nanoparticles, biotin was added through EDC crosslinking (Figure 5.3). Here, biotin was activated by EDC and then allowed to bind onto the micelle surface for 30 min before the addition of FITC for fluorescence. Biotin on the surface of polymeric micelles was measured using the HABA/avidin assay. A solution of HABA/avidin shows absorbance at 500 nm as avidin is displaced by the biotin which is bound on the micelle surface, the absorbance at 500 nm will decrease. As seen in Figure 5.4 (A), as the amount of biotinylated micelle added to the assay was decreased (0.5 dilution), the absorbance at 500 nm decreased. In contrast, after binding CD47-SA to the biotinylated micelle, no absorbance change was observed (Figure 5.4 B). This tells us two things, first we have successful binding of CD47-SA to biotinylated micelles and second, that the CD47-SA amount is sufficient to bind to all of the biotin molecules on the micelle surface.

Using the Beer Lambert law, we were able to quantify the amount of biotin and therefore CD47-SA bound onto the micelle surface. Using equation 1, we found that the amount of biotin/micelle particle was equal to  $2.25 \times 10^{-17}$  mol Biotin/ micelle particle. After multiplying by Avogadro's number, we found that the concentration of biotin on the surface of the micelles was  $1.4 \times 10^7$  biotin molecules/micelle particle. Despite the fact that biotin and streptavidin have four

potential binding sites, CD47-SA at 26 kDa is much larger than one biotin molecule. Therefore because of steric hindrance we believe that for every one biotin molecule on the micelle surface, one molecule of CD47-SA will bind. Therefore, the amount of biotin molecules on the micelle surface will be equal to the amount of CD47-SA bound on the micelle surface.

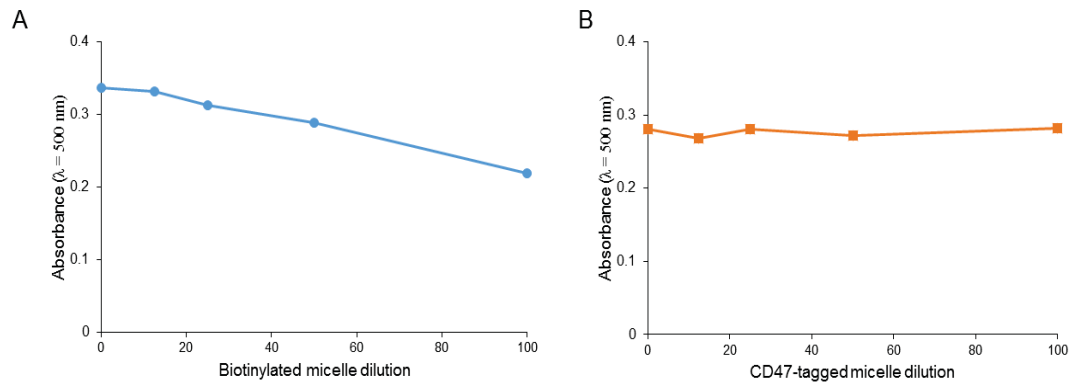


**Figure 5.4.** HABA/avidin assay. If biotin is present, HABA will be displaced from avidin resulting in a decrease of absorbance at 500 nm. (A) biotinylated micelles, and (B) CD47-tagged micelles.

#### 5.4.2. *Antiphagocytic effect*

To observe the antiphagocytic effect endowed onto micelle particles by CD47-SA, cell studies were conducted. As shown in Figure 5.5, cells treated readily phagocytized biotinylated micelle particles while CD47-tagged particles showed little uptake. While little difference was seen after 2 h of treatment (most likely due to the small size of micelle particles) (Figure 5.5 A and B), 4 h and 6 h clearly show more fluorescence in biotinylated micelles (Figure 5.5 C and E) than in CD47-tagged micelles (Figure 5.5 D and F).

The 6 h sample, which by fluorescent imaging showed the biggest difference in particle uptake by macrophages was run on flow cytometry. As can be seen from Figure 5.6, a shift in the mean fluorescent intensity of biotinylated and CD47-tagged micelles was seen. The mean fluorescence intensity of

biotinylated and CD47-tagged micelles was quite different at 3628.33 and 2325.60, respectively.

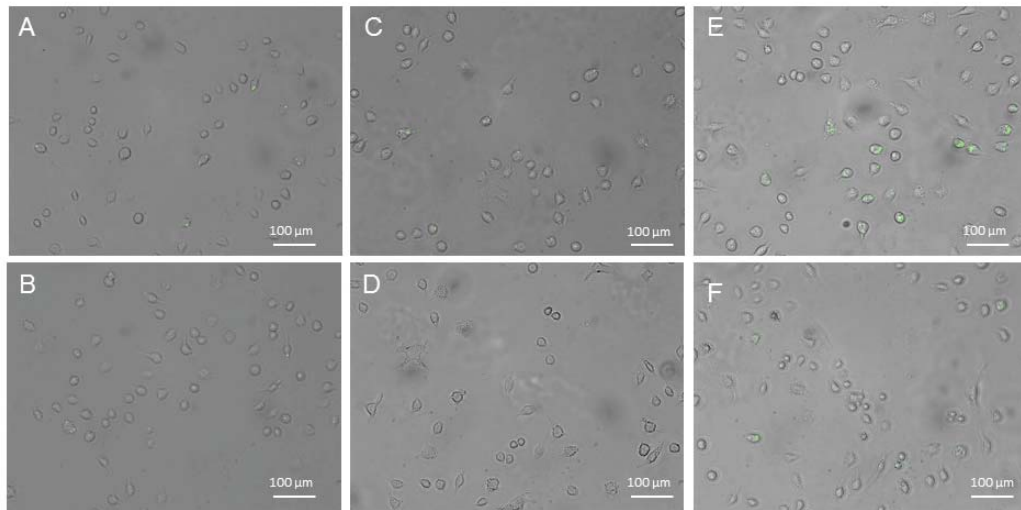


**Figure 5.5.** Effect of CD47 on micelle uptake by J774A.1 cells. (A) 2 h treatment with biotinylated micelles, (B) 2 h treatment with CD47-tagged polymeric micelles, (C) 4 h treatment with biotinylated micelles, (D) 4 h treatment with CD47-tagged polymeric micelles, (E) 6 h treatment with biotinylated micelles, and (F) 6 h treatment with CD47-tagged polymeric micelles.

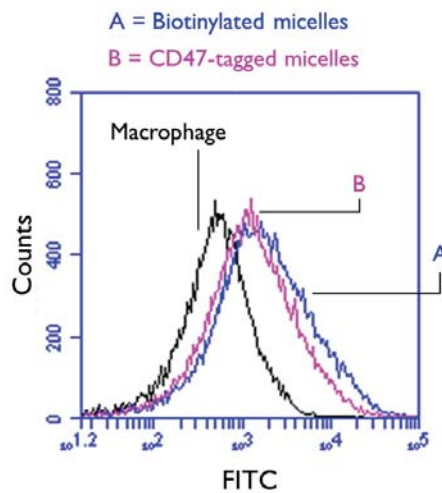


**Figure 5.6.** Flow cytometry analysis of J774A.1 macrophages after treatment with biotinylated and CD47-tagged micelles for 6 h.



### 5.4.3. Integrin targeting

Since CD47 is an integrin associated protein [5], it might be employed to target integrin  $\alpha_v\beta_3$ , which is overexpressed on tumor-activated neovascular endothelial cells and under expressed on mature quiescent ones lined in blood vessels [6]. In the previous section, we have shown that CD47 serves as an antiphagocytic ligand, to show that CD47 can also be used to target drug carriers, PC3 cells which show high levels of integrin  $\alpha_v\beta_3$  were treated with our CD47-tagged micelle carriers. As can be seen in Figure 5.7, cells with low  $\alpha_v\beta_3$  expression (BHK) despite having micelle carriers surrounding the cells (Figure 5.7 A and B) showed very little uptake of micelle carriers after trypan blue treatment (Figure 5.7 C and D). In contrast, PC3 cells showed a much higher uptake level of micelle carriers after trypan blue treatment (Figure 5.8 C and D).

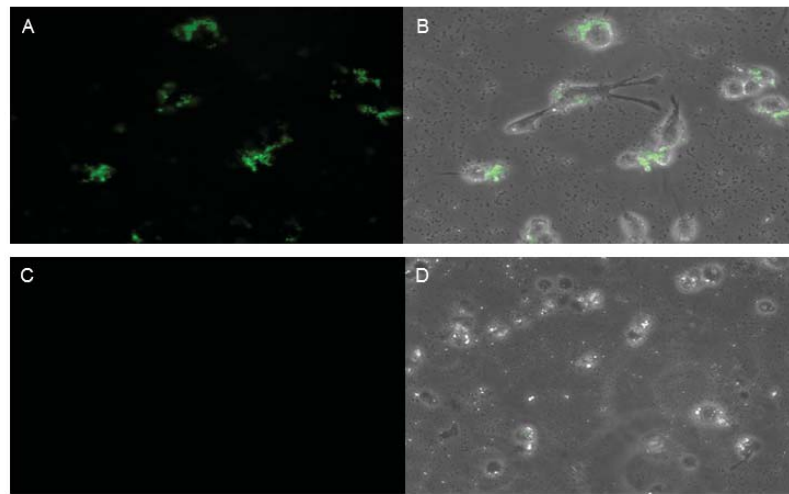


**Figure 5.7.** Integrin targeting to BHK21 cells which have low expression of  $\alpha_v\beta_3$  integrin. BHK21 cells were treated with CD47-tagged micelle carriers for 4 h. (A) Fluorescent image, (B) overlay of bright field and fluorescent image, (C) fluorescent image after trypan blue treatment to quench outside fluorescent, and (D) overlay of bright field and fluorescent image.

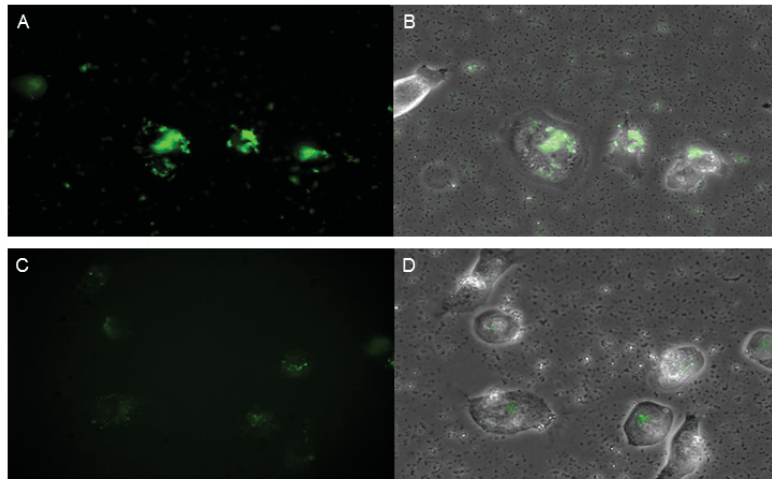


**Figure 5.8.** Integrin targeting to PC3 cells which have high expression of  $\alpha_v\beta_3$  integrin. PC3 cells were treated with CD47-tagged micelle carriers for 4 h. (A) Fluorescent image, (B) overlay of bright field and fluorescent image, (C) fluorescent image after trypan blue treatment to quench outside fluorescent, and (D) overlay of bright field and fluorescent image.

## 5.5. CONCLUSIONS

In this study, biotinylated polymeric micelles were successfully synthesized. Moreover, CD47-SA was conjugated onto the micelle surface via biotin/SA affinity. Macrophages treated with CD47-tagged micelles revealed and increased antiphagocytic effect as well as increased the uptake into cells with high  $\alpha_v\beta_3$  expression. These results indicated that CD47 can be utilized not only as an antiphagocytic ligand but also serve to target drug carriers onto abnormal endothelial cells bearing high levels of  $\alpha_v\beta_3$  and thereby block tumor angiogenesis. CD47-tagged nanocarriers could potentially be developed enhanced anticancer therapy due to their immune evasion and targeting capabilities.

## 5.6. REFERENCES

1. Evans EA. *Structure and deformation properties of red blood cells: Concepts and quantitative methods*. In: *Methods Enzymol.*, Sidney Flischer BF (Eds). Academic Press, 3-35 (1989).
2. Oldenburg PA, Zheleznyak A, Fang YF *et al.* Role of CD47 as a marker of self on red blood cells. *Science* 288(5473), 2051-2054 (2000).
3. Khandelwal S, Van Rooijen N, Saxena Rajiv k. Reduced expression of CD47 during murine red blood cell (RBC) senescence and its role in RBC clearance from the circulation. *Transfusion* 47(9), 1725-1732 (2007).
4. Hsu Y-C, Acuña M, Tahara S *et al.* Reduced phagocytosis of colloidal carriers using soluble CD47. *Pharmaceutical Research* 20(10), 1539-1542 (2003).
5. Brown EJ, Frazier WA. Integrin-associated protein (CD47) and its ligands. *Trends in Cell Biology* 11(3), 130-135 (2001).
6. Murphy EA, Majeti BK, Barnes LA *et al.* Nanoparticle-mediated drug delivery to tumor vasculature suppresses metastasis. *Proceedings of the National Academy of Sciences* 105(27), 9343-9348 (2008).
7. Sinha VR, Singla AK, Wadhawan S *et al.* Chitosan microspheres as a potential carrier for drugs. *International Journal of Pharmaceutics* 274(1-2), 1-33 (2004).
8. Dash TK, Konkimalla VB. Poly- $\epsilon$ -caprolactone based formulations for drug delivery and tissue engineering: A review. *Journal of Controlled Release* 158(1), 15-33 (2012).
9. Peng CL, Shieh MJ, Tsai MH *et al.* Self-assembled star-shaped chlorin-core poly( $\epsilon$ -caprolactone)-poly(ethylene glycol) diblock copolymer micelles for dual chemo-photodynamic therapies. *Biomaterials* 29(26), 3599-3608 (2008).
10. Ogris M, Brunner S, Schuller S *et al.* PEGylated DNA/transferrin-PEI complexes: Reduced interaction with blood components, extended circulation in blood and potential for systemic gene delivery. *Gene Therapy* 6(4), 595-605 (1999).
11. Mishra D, Kang HC, Bae YH. Reconstitutable charged polymeric (PLGA)<sub>2</sub>-b-PEI micelles for gene therapeutics delivery. *Biomaterials* 32(15), 3845-3854 (2011).
12. Shuai X, Merdan T, Unger F *et al.* Novel biodegradable ternary copolymers hy-PEI-g-PCL-b-PEG: Synthesis, characterization, and potential as efficient nonviral gene delivery vectors. *Macromolecules* 36(15), 5751-5759 (2003).
13. Green N. [74] Spectrophotometric determination of avidin and biotin. *Methods in Enzymology* 18(Part A) 418-424 (1970).

## CHAPTER 6: SUMMARY AND FUTURE DIRECTIONS

### 6.1. THESIS CONCLUSIONS AND SUMMARY OF FINDINGS

Gene-directed enzyme prodrug therapy is a promising approach. Some major problems remain to be solved before enzyme/prodrug strategies can become a routine therapeutic approach, largely due to inefficient drug/gene delivery. The findings in this thesis outlines an innovative approach for delivery of prodrug, gene and cytotoxic drug to malignant cells.

Prodrugs acyclovir (ACV), ganciclovir (GCV), and 5-doxifluridine (5'DFUR) were used as the sole initiators in the polymerization of  $\epsilon$ -caprolactone ( $\epsilon$ -CL). The prodrug-tagged poly(caprolactone) PCL was then grafted with hydrophilic polymers for form amphiphilic block copolymers. Synthesis of prodrug-tagged polymeric micelles was followed via standard analytical means including  $^1\text{H}$  NMR, FTIR, GPC, size and zeta analysis, and CMC. Our results indicate that prodrug-tagged micelles between 100-200 nm can be synthesized. Studies with ACV confirmed bioavailability of prodrug-tagged polymeric micelles up to a concentration of  $500 \text{ mg mL}^{-1}$ . Cytotoxicity studies with GCV confirmed that a one-step GDEPT process is a feasible anticancer therapy approach. It was found that  $4.5 \mu\text{g}$  of HSV-TK gene plasmid complexed onto GCV-PCL-chitosan micelles was sufficient to decrease cell viability to 52%. This was a 25% increase in cell death compared to the conventional two-step delivery of gene, followed by prodrug. Cytotoxicity studies with 5'DFUR, confirmed that suicide gene/prodrug pairs, in conjunction with treatment from other chemotherapy drugs, can substantially increase cell toxicity.

Furthermore, in an effort to develop multifunctional polymeric micelle carriers which can evade the immune system and target to tumor cells, CD47-SA was tagged onto the micelle surface via biotin/SA affinity. Our studies indicate that CD47-tagged micelle carrier can evade macrophage phagocytosis for up to

6 h. In addition, when targeted to cells which unregulated integrin  $\alpha_v\beta_3$ , micelle uptake was increased considerably.

## 6.2. FUTURE DIRECTIONS

This thesis has shown the feasibility of polymeric micelle carriers for the delivery of prodrug/gene and prodrug/cytotoxic drugs to tumor cells. Further work can be conducted to deliver all three (prodrug, gene and cytotoxic drug) simultaneously to malignant cells. Based on the results established here, anticancer therapy would be enhanced by a GDEPT system optimized for one-step delivery.

Moreover, this thesis has shown that extracellular targeting and antiphagocytosis can be achieved by binding CD47-SA onto the micellar surface. It would be of interest, especially in the case of one-step delivery, to use a nuclear localization sequence (NLS) to target the micelle carrier or DNA to the nucleus. A NLS is an amino acid sequence that tags a protein for import into the cell nucleus by nuclear transport [1]. For our proposed one-step delivery method, the DNA bound onto chitosan is delivered through passive diffusion. The application of NLS peptides for nonviral gene transfer has been widely investigated [2-4]. Therefore, the addition of an NLS onto the DNA or micelle carrier would allow for active targeting which should enhance gene efficiency greatly.

The work conducted in this thesis also has the potential to be applied to other GDEPT systems, including but not limited to, cytosine deaminase (CD)/5-fluorocytosine (5-FC). 5-FC is one of the main anticancer drugs used to treat colon, pancreatic and breast cancers. Similar to 5'DFUR, 5-FC is converted to 5-FU by CD. CD, unlike TP, has little cellular activity in humans and therefore increasing tumor cell proliferation is not a fear. Moreover, CD/5-FC has one of the strongest bystander effects demonstrated [5] and has shown more effective than the HSV-TK/GCV system in the treatment of renal and colorectal cancers [6, 7]. In addition to enhanced anticancer effectiveness, ring-opening

polymerization of  $\epsilon$ -CL by 5-FC would be initiated by an amine group, rather than a hydroxyl group as shown in the currently discussed prodrugs. Amine initiation has several advantages because the prodrug will not be cleaved as easily from the micelle carrier therefore allowing for extended release of the drug (see Figure 6.1) and increased activation time of the gene in a one-step delivery system. Oledzka et al. previously showed that amino acids can be used as initiators of  $\epsilon$ -CL and L,L-lactide polymerization [8]. Therefore, it is reasonable that 5-FC can be used to create prodrug-tagged polymeric micelles. Based on the drug release profile for 5-FC, it can be seen that compared to the previously used gene/prodrug pairs discussed in this thesis, the release profile of 5-FC is extensively enhanced. Here, it takes up to 12 h before 50% of the prodrug is released. Moreover, if we model the release data using the Langmuir model, we get a dissociation constant ( $K_d$ ) of 7.77, this shows a much stronger association than any of the previously discussed gene/prodrug pairs.

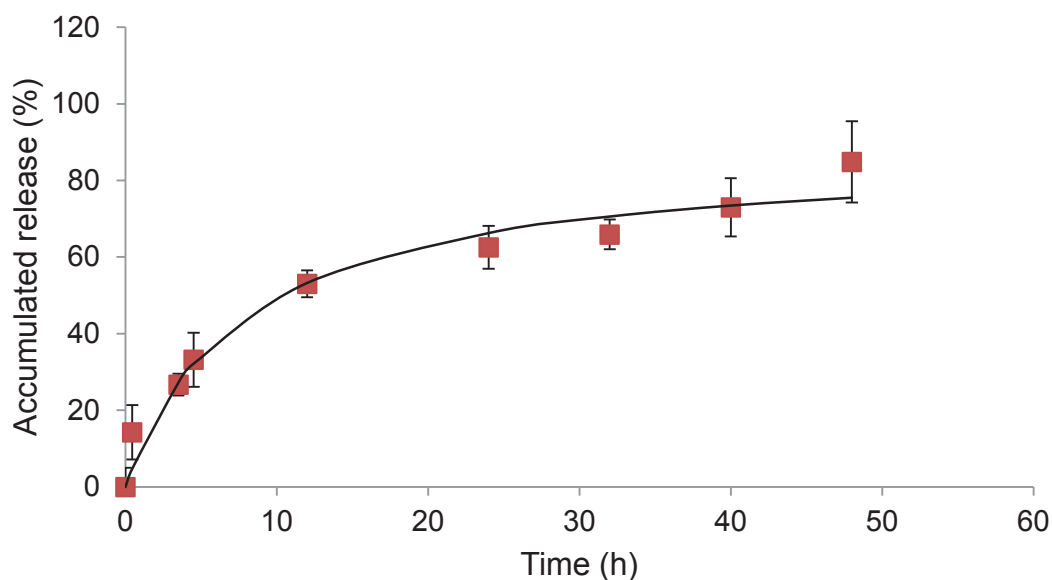


**Figure 6.1.** In vitro drug release profile of 5-FC from 5-FC-PCL-MPEG in PBS at 37°C.

### 6.3. REFERENCES

1. Zanta MA, Belguise-Valladier P, Behr JP. Gene delivery: A single nuclear localization signal peptide is sufficient to carry DNA to the cell nucleus. *Proceedings of the National Academy of Sciences* 96(1), 91-96 (1999).
2. Branden LJ, Mohamed AJ, Smith CIE. A peptide nucleic acid-nuclear localization signal fusion that mediates nuclear transport of DNA. *Nature Biotechnology* 17(8), 784-787 (1999).
3. Bremner KH, Seymour LW, Logan A *et al.* Factors Influencing the ability of nuclear localization sequence peptides to enhance nonviral gene delivery. *Bioconjugate Chemistry* 15(1), 152-161 (2003).
4. Ludtke JJ, Zhang G, Sebestyén MG *et al.* A nuclear localization signal can enhance both the nuclear transport and expression of 1 kb DNA. *Journal of Cell Science* 112(12), 2033-2041 (1999).
5. Huber BE, Austin EA, Richards CA *et al.* Metabolism of 5-fluorocytosine to 5-fluorouracil in human colorectal tumor cells transduced with the cytosine deaminase gene: significant antitumor effects when only a small percentage of tumor cells express cytosine deaminase. *Proceedings of the National Academy of Sciences* 91(17), 8302-8306 (1994).
6. Kuriyama S, Mitoro A, Yamazaki M *et al.* Comparison of gene therapy with the herpes simplex virus thymidine kinase gene and the bacterial cytosine deaminase gene for the treatment of hepatocellular carcinoma. *Scandinavian Journal of Gastroenterology* 34(10), 1033-1041 (1999).
7. Shirakawa T, Gardner TA, Ko SC *et al.* Cytotoxicity of adenoviral-mediated cytosine deaminase plus 5-fluorocytosine gene therapy is superior to thymidine kinase plus acyclovir in a human renal cell carcinoma model. *The Journal of Urology* 162(3), 949-954 (1999).
8. Oledzka E, Sokolowski K, Sobczak M *et al.*  $\alpha$ -Amino acids as initiators of  $\epsilon$ -caprolactone and L,L-lactide polymerization. *Polymer International* 60(5), 787-793 (2011).

# APPENDIX I: COPYRIGHT MATERIAL FOR CHAPTER 1

## JOHN WILEY AND SONS LICENSE TERMS AND CONDITIONS

Nov 13, 2014

---

This is a License Agreement between Alicia J Sawdon ("You") and John Wiley and Sons ("John Wiley and Sons") provided by Copyright Clearance Center ("CCC"). The license consists of your order details, the terms and conditions provided by John Wiley and Sons, and the payment terms and conditions.

**All payments must be made in full to CCC. For payment instructions, please see information listed at the bottom of this form.**

License Number	3507131155734
License date	Nov 13, 2014
Licensed content publisher	John Wiley and Sons
Licensed content publication	Wiley eBooks
Licensed content title	Multifunctional Polymeric Micelles for Drug Delivery and Therapeutics
Book title	Nanomedicine for Drug Delivery and Therapeutics
Licensed copyright line reserved.	Copyright © 2013 Scrivener Publishing LLC. All rights reserved.
Licensed content author	Alicia Sawdon, Ching-An Peng
Licensed content date	Jan 30, 2013
Start page	438
End page	469
Type of use	Dissertation/Thesis
Requestor type	Author of this Wiley chapter
Format	Print and electronic
Portion	Text extract
Number of Pages	20
Will you be translating?	No

Title of your thesis / dissertation

Design and Synthesis of Multifunctional Polymeric Micelles for Gene-Directed Enzyme Prodrug Therapy

Expected completion date Dec 2014



Expected size (number of pages)

160

Total 0.00 USD

Terms and Conditions

## JOHN WILEY AND SONS LICENSE TERMS AND CONDITIONS

Nov 13, 2014

---

This is a License Agreement between Alicia J Sawdon ("You") and John Wiley and Sons ("John Wiley and Sons") provided by Copyright Clearance Center ("CCC"). The license consists of your order details, the terms and conditions provided by John Wiley and Sons, and the payment terms and conditions.

**All payments must be made in full to CCC. For payment instructions, please see information listed at the bottom of this form.**

License Number	3507130921781
License date	Nov 13, 2014
Licensed content publisher	John Wiley and Sons
Licensed content publication	Wiley eBooks
Licensed content title	Multifunctional Polymeric Micelles for Drug Delivery and Therapeutics
Book title	Nanomedicine for Drug Delivery and Therapeutics
Licensed copyright line reserved.	Copyright © 2013 Scrivener Publishing LLC. All rights reserved.
Licensed content author	Alicia Sawdon, Ching-An Peng
Licensed content date	Jan 30, 2013
Start page	438
End page	469
Type of use	Dissertation/Thesis
Requestor type	Author of this Wiley chapter
Format	Print and electronic
Portion	Figure/table
Number of figures/tables	5

Original Wiley figure/table number(s)

Figure 15.1, Table 15.1, Figure 15.2, Figure 15.3, Figure 15.4

Will you be translating? No

Title of your thesis / dissertation

Design and Synthesis of Multifunctional Polymeric Micelles for Gene-Directed Enzyme Prodrug Therapy

Expected completion date      Dec 2014

Expected size (number of pages)

160

Total                              0.00 USD

Terms and Conditions

## Permissions

Welcome to Future Science Ltd permissions page. Written permission is required from the publisher if you wish to reproduce any of our material.

### Are you a Future Science author seeking to reuse your own material?

Once a manuscript has been accepted for publication, authors may contact Future Science Ltd for permission to use all or part of an article in other publications for non-commercial purposes. In these cases, permission should be granted free of charge.

Authors can find out more information on our [For Authors](#) page

### Do you intend to reuse material from Future Science publications in other print and/or online journal or book publications?

Reuse of material such as figures, tables, boxes or text blocks attracts a permission fee (unless the publisher is a co-signatory to the STM permission guidelines) contact [permissions@future-science.com](mailto:permissions@future-science.com) explaining which material you intend to use, the name of the publisher, in which publication and in what format.

Future Science Ltd is a signatory to the STM Permissions Guidelines produced by the International Association of Scientific, Medical and Technical Publishers (<http://www.stm-assoc.org/>). Future Science requires express permission requests to be made irrespective of whether charges apply.

If the reused material is to appear in a conventional print or electronic book or journal (only) produced by a publisher that is a co-signatory to the STM agreement may make the following use of the material without charge:

- Use up to three figures (including tables) from a journal article or book chapter, but:
  - Not more than five figures from a whole book or journal issue/edition;
  - Not more than six figures from an annual journal volume; and
  - Not more than three figures from works published by a single publisher for an article, and not more than three figures from works published by a publisher for a book chapter (and in total not more than thirty figures from a single publisher for re-publication in a book, including a multi-volume with different authors per chapter)
- Use single text extracts of less than 400 words from a journal article or book chapter, but not more than a total of 800 words from a whole book or journal issue/edition.

### Do you intend to reuse material in other media intended for commercial use, such as promotional packs or pamphlets?

If the intended publication vehicle is not a conventional print or electronic book or journal (e.g. educational information attracting commercial sponsorship) permission is not required. Please contact [permissions@future-science.com](mailto:permissions@future-science.com) in such instances or to establish whether charges apply.

### Are you planning on using our material in a Thesis/dissertation?

If you are using figure(s)/table(s), permission is granted for use in print and electronic versions of your thesis/dissertation

A full text article may be used only in print versions of a dissertation/thesis. Future Science Ltd does not permit the reproduction of full text articles in electronic versions of theses or dissertations.

### Do you wish to use the article for personal research purposes?

Permission is not required for this purpose; all articles can be purchased via our pay-per-view option. Please navigate to the article and click on the 'Full text' options for payment will launch.

### Classroom Handouts

For educational photocopies (academic course packs, classroom hand-outs, electronic classroom use) permission can be purchased on the Copyright Clearance Center website:

<http://www.copyright.com/content/cc3/en/toolbar/getPermission.html>



### Copyright Clearance Center

222 Rosewood Drive  
Danvers, MA 01923  
USA

Phone: +1-978-750-8400  
Fax: +1-978-646-8600  
E-mail: [info@copyright.com](mailto:info@copyright.com)

### How to submit a Permission Request

Before submitting a request, please make sure the material you wish to use is copyrighted by Future Science Ltd.

Take note that this form is only an initial request and it does not imply automatic permission. Future Science Ltd reserves the right to review each case individually.

If you have any questions, please direct them to [permissions@future-science.com](mailto:permissions@future-science.com)

1. Navigate to the article you wish to request permission by using the 'Advanced Search'.
2. Please click on 'Reprints & Permissions' which can be found beneath the article details.

## APPENDIX II: COPYRIGHT MATERIAL FOR CHAPTER 2

### SPRINGER LICENSE TERMS AND CONDITIONS

Nov 20, 2014

---

---

This is a License Agreement between Alicia J Sawdon ("You") and Springer ("Springer") provided by Copyright Clearance Center ("CCC"). The license consists of your order details, the terms and conditions provided by Springer, and the payment terms and conditions.

**All payments must be made in full to CCC. For payment instructions, please see information listed at the bottom of this form.**

License Number	3513251348701
License date	Nov
20, 2014	Licensed content publisher
Springer	
Licensed content publication	Macromolecular Research
Licensed content title	Guanosine-based antiviral acyclovir incorporated in ring-opening polymerization of $\epsilon$ -caprolactone
Licensed content author	Alicia J.
Sawdon	Licensed content date
Jan 1, 2012	
Volume number	21
Issue number	1
Type of Use	Book/Textbook
Requestor type	Agency acting on behalf of other industry
Portion	Full text
Format	Print and Electronic
Will you be translating?	No
Print run	1
Author of this Springer article	Yes and you are the sole author of the
new work	Order reference number
	None
Title of new book	DESIGN AND SYNTHESIS OF MULTIFUNCTIONAL POLYMERIC MICELLES FOR GENE-DIRECTED ENZYME PRODRUG THERAPY
Publisher of new book	ProQuest
Author of new book	Alicia J. Sawdon

Expected publication date of new book

Dec 2014

Estimated size of new book (pages)

150

Total 0.00 USD

Terms and Conditions

## ELSEVIER LICENSE TERMS AND CONDITIONS

Dec 06, 2014

---

---

This is a License Agreement between Alicia J Sawdon ("You") and Elsevier ("Elsevier") provided by Copyright Clearance Center ("CCC"). The license consists of your order details, the terms and conditions provided by Elsevier, and the payment terms and conditions.

**All payments must be made in full to CCC. For payment instructions, please see information listed at the bottom of this form.**

Supplier Elsevier Limited  
The Boulevard, Langford Lane  
Kidlington, Oxford, OX5  
1GB, UK

Registered Company Number  
1982084 Customer name  
Alicia J Sawdon

Customer address 1400 Townsend Dr  
HOUGHTON, MI 49931

License number 3523220755980

License date  
Dec 06, 2014 Licensed content  
publisher Elsevier

Licensed content publication Colloids and Surfaces B:  
Biointerfaces Licensed content title Polymeric  
micelles for acyclovir drug delivery Licensed content author  
None

Licensed content date 1 October 2014

Licensed content volume number

122

Licensed content issue number

n/a

Number of pages	8
Start Page	738
End Page	745
Type of Use	reuse in a thesis/dissertation
Portion	full article
Format	both print and electronic

Are you the author of this Elsevier article?

Yes

Will you be translating?	No
--------------------------	----

Title of your thesis/dissertation

Design and Synthesis of Multifunctional Polymeric Micelles for Gene- Directed Enzyme Prodrug Therapy

Expected completion date	Dec 2014
--------------------------	----------



## ELSEVIER LICENSE TERMS AND CONDITIONS

Dec 06, 2014

---

This is a License Agreement between Alicia J Sawdon ("You") and Elsevier ("Elsevier") provided by Copyright Clearance Center ("CCC"). The license consists of your order details, the terms and conditions provided by Elsevier, and the payment terms and conditions.

**All payments must be made in full to CCC. For payment instructions, please see information listed at the bottom of this form.**

Supplier Elsevier Limited  
The Boulevard, Langford Lane  
Kidlington, Oxford, OX5  
1GB, UK

Registered Company Number

1982084 Customer name

Alicia J Sawdon

Customer address

1400 Townsend Dr

HOUGHTON, MI

49931

License number

3523220919286

License date

Dec 06, 2014 Licensed content

publisher Elsevier

Licensed content publication Colloids and Surfaces B:

Biointerfaces Licensed content title Polymeric

micelles for acyclovir drug delivery Licensed content author

None

Licensed content date 1 October 2014

Licensed content volume number

122

Licensed content issue number

n/a

Number of pages 8

Start Page 738

End Page 745

Type of Use reuse in a thesis/dissertation

Intended publisher of new work

other

Portion figures/tables/illustrations

Number of figures/tables/illustrations 7

Format both print and electronic

Are you the author of this Elsevier article?

Yes

Will you be translating? No

Title of your thesis/dissertation

Design and Synthesis of Multifunctional Polymeric Micelles for Gene- Directed Enzyme Prodrug Therapy

Expected completion date Dec 2014

Estimated size (number of pages)

160

Elsevier VAT number

GB 494 6272 12 Permissions

price 0.00 USD

VAT/Local Sales Tax 0.00 USD / 0.00 GBP

Total 0.00 USD

Terms and Conditions